ESTIMATION OF VELOCITY DISTRIBUTION AND SUSPENDED SEDIMENT DISCHARGE IN OPEN CHANNELS USING ENTROPY

A Thesis

by

HUIJUAN CUI

Submitted to the Office of Graduate Studies of
Texas A&M University
in partial fulfillment of the requirements for the degree of

MASTER OF SCIENCE

May 2011

Major Subject: Water Management and Hydrological Science

Estimation of Velocity Distribution and Suspended Sediment Discharge in Open Channels Using Entropy

ESTIMATION OF VELOCITY DISTRIBUTION AND SUSPENDED SEDIMENT DISCHARGE IN OPEN CHANNELS USING ENTROPY

A Thesis

by

HUIJUAN CUI

Submitted to the Office of Graduate Studies of
Texas A&M University
in partial fulfillment of the requirements for the degree of

MASTER OF SCIENCE

Approved by:

Chair of Committee,	Vijay P. Singh
Committee Members,	Ralph A. Wurbs
	Daren B.H. Cline
Intercollegiate Faculty Chair,	Ronald A. Kaiser

May 2011

Major Subject: Water Management and Hydrological Science

ABSTRACT

Estimation of Velocity Distribution and Suspended Sediment Discharge in Open Channels Using Entropy. (May 2011)

Huijuan Cui, B.En., Tsinghua University

Chair of Advisory Committee: Dr. Vijay P. Singh

In hydraulics, velocity distribution is needed to determine flow characteristics, like discharge, sediment discharge, head loss, energy coefficient, moment coefficient, and scour. However, the complicated interaction between water and sediment causes great difficulties in the measurement of flow and sediment discharge. Thus, the development of a method which can simulate the velocity distribution and sediment discharge in open channels is designable.

Traditional methods for the estimation of velocity distribution, such as the Prandtl-von Karman logarithmic velocity and of sediment concentration distribution, such as the Rouse equation, are generally invalid at or near the channel bed and are inaccurate at the water surface. Considering the limitations of traditional methods, entropy based models have been applied, yet the assumption on the cumulative distribution function made in these methods limits their application.

The objective of this research is to develop an efficient method to estimate velocity distribution and suspended sediment discharge in open channels using the Tsallis entropy. This research focuses on a better-organized hypothesis on the

cumulative probability distribution function under more applicable coordinates, which should be transformable in different dimensions.

Velocity distribution and sediment distribution are derived using the Tsallis entropy under the hypothesis that the cumulative probability distribution follows a non-linear function, in which the value of the exponent is shown to be related to the width-depth ratio of channel cross-section. Three different combinations of entropy and empirical methods for velocity and sediment concentration distribution are applied to compute suspended sediment discharge. Advantages and disadvantages of each method are discussed.

The velocity distribution derived using the Tsallis entropy is expected to be easy to apply and valid throughout the whole cross-section of the open channel. This research contributes to the application of entropy theory and shows its advantages in hydraulic engineering.

ACKNOWLEDGEMENTS

First of all, I would like to thank my committee chair, Dr. Singh, for his guidance, encouragement and support since I entered Texas A&M University. I appreciate his vast knowledge and diligence and have learned a great deal from him. I would like to express my appreciation to my committee members, Dr. Wurbs and Dr. Cline, for their guidance throughout my research.

Thanks also go to my friends and colleagues in our group. I would like to extend my gratitude to people in the water program and Department of Biological and Agriculture Engineering, who offered me a great experience at Texas A&M.

In the end special thanks to my parents for their support and my husband for his constant love and understanding over the years.

TABLE OF CONTENTS

Page

LIST OF FIGURES

Page

Page

Page

LIST OF TABLES

Page

1. INTRODUCTION

1.1 Background

Velocity distribution is fundamental to modeling of hydraulic processes in open channels, such as flow discharge, erosion, sediment transport, pollutant transport, and watershed runoff. For instance, the energy and momentum coefficients can be evaluated if velocity is determined; the shear stress, which is the main factor for sediment concentration, also depends on the velocity distribution. Thus, velocity distribution must be investigated and determined prior to solving hydraulic problems in open channels.

In natural rivers, velocity distribution is affected by channel geometry, vegetation, roughness and the presence of bends in natural rivers. In wide open channels, velocity increases monotonically from 0 at the channel bed to the maximum value at the water surface, and can be approximately considered as one-dimensional (1-D). For the channels which are not very "wide", besides changes in the vertical direction, the velocity also changes in the transverse direction, thus velocity distribution needs to be considered in two dimensions (2-D). In such a case, velocity increases from 0 at the channel boundary to the maximum at or below the water surface near the channel center. The phenomenon in which the velocity reaches the maximum value below the water surface is called dip-phenomenon.

This thesis follows the style of *Journal of Hydrologic Engineering*.

Several classical laws have been developed to describe the velocity distribution, such as the power law and the Prandtl-von Karman universal velocity distribution law. These laws have been widely used to determine the 1-D velocity distribution and have proved sufficient for very wide channels. Unfortunately, natural channels are not always wide enough for the one-dimensional assumption to be applicable, as the velocity varies in both vertical and transverse directions.

The Prandtl-von Karman equation is invalid at or near the channel bed and is inaccurate near the water surface, especially for cases where the maximum velocity does not occur at the surface. The power law is simple to apply but its accuracy is limited. Thus, the universal velocity laws are no longer appropriate.

Considering the limitations of classical methods, Chiu (1987) derived the velocity distribution using the Shannon entropy, assuming time-averaged velocity as a random variable. Named after Chiu, this velocity distribution is called Chiu's velocity distribution and has been employed in many different flow cases by Chiu and his associates (Chiu,1987, 1989; Chiu and Murray, 1992; Chiu and Said, 1995; Chiu and Tung 2002), Barbe (1990) and Barbe et al. (1991). Chiu's velocity distribution has been expanded and applied to 2-D velocity distribution and the variation of velocity has been described in both vertical and transverse directions (Chiu, 1988; Chiu and Hsu, 2006; Marini et al., 2010). Though Chiu's method can predict the velocity distribution reasonably well, the assumption on the cumulative distribution function of velocity, which is based on the coordinates defined by Chiu (1988), is not easy to follow and limited by many parameters it contains. A mathematically sound coordinate system was

developed by Marini et al. (2010) who obtained the 2-D entropy-based velocity distribution with convenience, but the velocity distribution did not capture velocities near lower velocity areas or boundary.

The Tsallis entropy, a generalization of the Shannon entropy, can also be used for velocity distributions and leads to explicit expressions for 1-D and 2-D velocity distribution (Singh and Luo, 2009, 2011; Luo and Singh, 2011). The Tsallis entropy based velocity distribution has an advantage over the Shannon entropy-based distribution, but the cumulative probability distribution function used in these studies is the same as Chiu's, hence their practical usefulness is limited by the many parameters they contain.

In this thesis, a more realistic hypothesis on the cumulative distribution function (CDF) will be formulated and velocity distribution using the Tsallis entropy will be derived. The formulation of the cumulative distribution function will be based on the Cartesian coordinate system, so that the CDF can be straightforward when going from one dimension to two dimensions and will also be available when going backward. Different expressions on the cumulative distribution function will be verified with observed values and their inherent relations with the width-depth ratio of the channel cross-section will be discussed. Considering the time-averaged velocity as a random variable, the Tsallis entropy will be applied for deriving the velocity distribution for the whole channel.

Another main issue that will be discussed is sediment discharge: Flow in natural channels often contains sediment, which is one of the most important environmental

issues in hydraulics. There are 13 large rivers in the world that transport sediment more than 10^8 tons per year (Chien and Wan 2003). Rivers with such high sediment content may complicate flood control and aggravate the reservoir sedimentation. Since contaminants are always transported by sediment, one needs to pay close attention to sediment transport.

Einstein (1950) divided the total sediment discharge into bed-load discharge and suspended-sediment discharge based on the position and characteristics of particle movement and summed the two parts to estimate the total sediment discharge. It is widely known that the majority of rivers throughout the world transport more suspended sediment than bed load. Too much suspended sediment may lead to reservoir deposition, scouring and siltation in the downstream channel, which may destroy the balance between flow and sediment concentration. Therefore, the estimation of suspended sediment transport is especially significant in the design of hydraulic structures influencing or controlling the sediment discharge regime and in the estimation of average rate of erosion in a basin.

The suspended sediment discharge can be obtained from flow discharge and suspended sediment concentration, while flow discharge can be determined with the use of velocity distribution. Thus, the next main point is to develop an efficient method for estimating sediment concentration.

A classical method to model the sediment concentration is the Rouse equation, which is derived from the Prandtl-von Karman logarithmic velocity equation and the

linear shear stress distribution. Thus, the Rouse equation is not applicable close to the channel bed and is not accurate near the water surface.

A mathematical model, based on the Shannon entropy, has been developed by Chiu et al. (2000), which is capable of describing the sediment concentration from the channel bed to the water surface. However this entropy-based model is not reliable, since the sediment concentration derived from this model depends on Chiu's velocity equation whose limitations have been mentioned earlier. Choo (2000) derived the suspended sediment concentration distribution using the Shannon entropy, considering time-averaged sediment concentration as a random variable and it showed significant advantages over traditional Rouse equation-based methods. Combining Chiu's mean velocity and mean sediment concentration the suspended sediment discharge was also computed by Choo (2000). That was an efficient method but is still restricted by the many parameters it contains.

In the second part of the thesis, the sediment concentration distribution will be derived in the same way as velocity distribution using the Tsallis entropy. Several different hypotheses on the cumulative distribution function will be also discussed and verified. Finally, with the knowledge of mean velocity and mean sediment concentration in the cross-section, the suspended sediment discharge will be obtained. Three different combinations of entropy and empirical methods for velocity and sediment concentration distribution will be applied to compute the suspended sediment discharge. Based on the results, the advantages and disadvantage of each method will be discussed.

1.2 Objectives

The overall objective of this thesis is to develop an efficient method to compute the velocity distribution, sediment concentration distribution and suspended sediment discharge in open channels using the Tsallis entropy. The thesis will focus on a better-organized hypothesis on the cumulative distribution function, which is based on widely-used Cartesian coordinates, and may be extendable to different dimensions. The simulated velocity and sediment values will be tested using both experimental data and field data.

The specific objectives are stated below:

1) Formulate a cumulative probability distribution function for velocity distribution in open channels and compare it with that based on observed values.

2) Develop a 2-dimensional (2-D) velocity distribution for open channels using the Tsallis entropy, which can be easily transformed to a 1-dimensional case, and verify the estimated velocities with experimental data.

3) Introduce and discuss a dimensionless parameter called G, which can represent the homogeneity of the velocity distribution.

4) Discuss the location of the maximum velocity and mean velocity, and the relationship between maximum velocity and mean velocity.

5) Formulate a cumulative distribution function for suspended sediment and compare it with that based on observed values.

6) Develop the distribution of sediment concentration in open channels using the Tsallis entropy and verify with experimental data.

7) Introduce and discuss a dimensionless parameter called N which affects the homogeneity of the concentration distribution.

8) Discuss the maximum and mean sediment concentration.

9) Develop a sediment discharge model and verify it with experimental and field data.

10) Compute the suspended sediment discharge with known velocity and sediment concentration of the cross-section calculated by different methods. Compare the entropy based method and empirical method.

11) Compare the Tsallis entropy –based distributions with those based on the Shannon entropy.

2. LITERATURE REVIEW

2.1 Entropy concept and theory

Entropy, as the second law of thermodynamics, is a macroscopic property of a system which measures the microscopic disorder within the system. In informational theory, Shannon (1948) formulated the concept of entropy as a measure of information or uncertainty associated with the random variable or its probability distribution. Nearly a decade later, Jaynes (1957a, 1957b) developed the principle of maximum entropy (POME) for deriving the least-biased probability distribution of the random variable subject to given information in terms of constraints as well as the theorem of concentration for hypothesis testing. Together these concepts constitute what can now be referred to as the entropy theory.

Entropy can be regarded as a useful characteristic of any probability distribution, which makes it applicable to areas other than the initial thermodynamic field, and has since been extensively applied in environmental and water engineering, including geomorphology, hydrology, and hydraulics. Recent applications of the entropy theory in hydrology and water resources have been reviewed and discussed by Singh (1997). Chiu (1987, 1991) applied the concept of entropy to open-channel flows, including the modeling of velocity distribution, shear stress and sediment concentration. Analysis of velocity distribution in the probability domain has an advantage in determining the cross-sectional mean velocity and the momentum and energy coefficients without

dealing with the geometrical shape of cross sections, which tend to be extremely complex in natural channels (Chiu, 1991).

2.1.1 Shannon entropy

Shannon (1948) developed the entropy theory for expressing information or uncertainty in the field of communication, which is now regarded as a useful characteristic of any probability distribution. In probability theory, values of a random variable represent possible outcomes of an experiment which is uncertain. Shannon (1948) defined a quantitative measure of uncertainty associated with a probability distribution of a random variable in terms of entropy, *H*, called Shannon entropy or informational entropy, as

$$H = -\sum_i^N p_i \log p_i \tag{2-1}$$

where p_i is the probability of each random value, and *N* denotes the total number of values.

The Shannon entropy can also be extended to continuous random variables so that it may be introduced to hydraulic engineering since hydraulic processes are continuous in nature. For a random variable x, which is continuous over the range (-∞, ∞), the Shannon entropy is expressed as

$$H = -\int_{-\infty}^{\infty} p(x) \log p(x) dx \tag{2-2}$$

where, *p(x)* is the continuous probability density function of random variable *x*.

The Shannon entropy, together with the principle of maximum entropy (POME), which will be introduced in section 2.1.3, can be applied to determine the probability distribution of a given random variable.

2.1.2 Tsallis entropy

Tsallis (1988) proposed a general form of the Shannon entropy as

$$H = \frac{1}{m-1}\left\{1 - \int_{-\infty}^{+\infty}[p(x)]^m\, ds\right\} = \frac{1}{m-1}\int_{-\infty}^{+\infty} p(x)\,\{1 - [p(x)]^{m-1}\}dx \qquad (2\text{-}3)$$

where m is a real number, and when $m>0$, H becomes a convex function. For $m=1$, equation (2-3) reduces to the Shannon entropy. Thus the Tsallis entropy is defined as a generalization of the Shannon entropy or Boltzmann-Gibbs entropy. Similar to the Shannon entropy, the Tsallis entropy can be coupled with the principle of maximum entropy (POME) to achieve the probability distribution of a given random variable and may yield more accurate results than the Shannon entropy in some cases.

2.1.3 Principle of maximum entropy

The least-biased probability distribution can be obtained by the entropy theory when the entropy is maximized. To that end, Jaynes (1957a, 1957b) formulated the principle of maximum entropy (POME), according to which the probability density function can be obtained by maximizing the uncertainty expressed by entropy, subject to given information. In other words, for given information the best possible distribution fitting the data is the one with the maximum entropy. The information included through

POME is specified as constraints in the form of some statistics, including mean, variance, covariance, cross-variance, or linear combinations of these statistics.

The constraints can be specified by statistical characteristics. The first constraint can be

$$\int_{-\infty}^{+\infty} p(x)dx = 1 \tag{2-4}$$

The second constraint can represent the mean value

$$\int_{-\infty}^{+\infty} xp(x)dx = \bar{x} \tag{2-5}$$

The third constraint can represent the variance

$$\int_{-\infty}^{+\infty} x^2 p(x)dx = \overline{x^2} \tag{2-6}$$

Using POME entropy can be maximized with the constraints $g_i(x)$ imposed on the distribution using the method of Lagrange multiplier method as follows:

$$L = -\frac{1}{m-1}\int_{-\infty}^{+\infty} p(x)\{1 - [p(x)]^{m-1}\}dx + \sum_{i=1}^{n} \lambda_i g_i(x) \tag{2-7}$$

in which $g_i(x)$ is the i-th constraint function, and λ_i is the Lagrange multiplier for each constraint, reflecting its weight in the maximization of entropy. The first term on right hand side of equation (2-7) is the Tsallis entropy of the random variable and the second term is the given information in the form of constraints.

Differentiating equation (2-7) with respect to p and equating the derivative to 0, the probability density function can be obtained.

Entropy theory provides a way to introduce probability into hydraulic modeling and is useful in parameter estimation. For instance, a procedure for derivation of frequency distributions used in hydrology, which are the gamma, the log-gamma

distribution and extreme value Type I distributions also known as Frechét distributions, have been developed using POME (Singh, et al, 1986). Sonuga (1972, 1976) used POME in flood frequency analysis and rainfall-runoff relationships. In hydraulic modeling, Chiu (1987, 1988), Chiu et al. (2000) and his colleagues derived 1D and 2D velocity distributions, and shear stress and sediment concentration distributions using the Shannon entropy.

As an alternative way of assessing the goodness of fit of a distribution to experimental data, POME can lead to a simple but useful method of parameter estimation. Several advances in the application of POME were discussed by Singh and Rajagopal (1987). It is shown that the entropy method can provide a unified approach to the derivation of a number of frequency distributions, which is even applicable to the areas having limited data. Compared to other methods like methods of moments and maximum likelihood estimation, the parameters estimated through POME show connections between different distributions (Singh, et al, 1986). POME has an advantage in performing multivariate stochastic analysis, because it can be applied to derive the functional relationships between two or more variables.

2.2 Velocity distribution

There are two classical methods and two kinds of entropy based methods to obtain time averaged velocity distributions, which are the simple power law, Prandtl-von Karman logarithmic law, Shannon entropy based Chiu's velocity law and Tsallis entropy velocity law. All methods will be compared in this thesis.

2.2.1 Classical methods

For Reynolds number between 3,000 and 100,000, the velocity profile in a smooth pipe is found to be closely approximated by the depth rising to the power of 1/7 (Blasius, 1913), which is the power law also called the seventh root law (Daugherty and Franzini, 1977). The power law was expanded to open channel flow by Sarma et. al (1983), with exponent n instead of 7, which is usually in the range of 6-7 (Karim and Kennedy, 1987). Though power law is simple to apply, its accuracy is limited.

The Prandtl-von Karman logarithmic velocity distribution law was initially developed for pipe flow, which is based on the following two assumptions: The mixing length is proportional to the depth from the pipe edge and the shearing stress is constant (von Karman, 1935). Later, Vanoni (1941) showed that this equation could also be applied to wide open channels. However, the Prandtl-von Karman logarithmic law performs poorly near the bottom especially in sediment laden flows (Einstein and Chien 1955) and is shown to be inaccurate near the water surface, especially for cases where the maximum velocity does not occur at the surface, which is often the case in natural channel flows.

Furthermore, there are two constraints in the Prandtl-von Karman law; one is the universal constant κ, which is a characteristic of turbulence and the other is the characteristic of the boundary, which depends on the nature of the wall surface. The von Karman constant κ is shown independent of the amount of suspended sediment in an open channel flow (Coleman, 1981; 1986). The boundary characteristic was specified by dividing the flow region into different parts. Keulegan (1938) proposed that the flow

region can be divided into three parts corresponding to both sidewalls and the bed using the bisectors of base angles in an open-channel flow and the Prandtl-von Karman law was provided to be valid from a point near the bed to the free surface in the inner region (Yang et. al, 2004), if the shear velocity was introduced to the dimensionless distance normal to the boundary.

2.2.2 Entropy-based velocity distribution

Recognizing the drawbacks of classical methods, various studies have been dedicated to developing entropy-based methods to obtain time-averaged velocity distributions. Assuming time-averaged velocity as a random variable, both 1D and 2D velocity distributions in open channels have been derived by maximizing the Shannon entropy (Chiu 1987, 1988 and 1989) and the Tsallis entropy (Singh and Luo, 2009, 2011; Luo and Singh, 2011).

To relate the entropy-based probability distribution to the spatial distribution, an assumption on the probability distribution in the space domain is needed. In a uniform flow of depth D in a wide open channel, where velocity monotonously increases with the flow depth, Chiu (1987) assumed a linear cumulative distribution function, which stated the velocity being equal to or smaller than u was y/D, assuming that all values of y between zero and D were equally likely. The 1D velocity distribution derived in this study has an advantage over the Prandtl-von Karman velocity distribution, which is consistently found to increase with the sediment concentration. Singh and Luo (2009) developed even a better velocity distribution using the Tsallis entropy than Chiu's,

assuming the exponent value m=3/4. However, 1D velocity distribution is not enough for describing the natural channel flow in all circumstances.

To describe the velocity variation in both transverse and vertical directions, the 2D assumption on the probability distribution should be made. To that end, a new curvilinear ξ-η coordinates system was formed by isovels of primary flow and their orthogonal trajectories (Chiu and Lin, 1983; Chiu and Chiou 1986; Chiu 1988). In his coordinate system, isovels are represented by a system of ξ coordinate and η coordinate curves are their orthogonal trajectories. In this case, the time-averaged velocity u which varies from 0 to u_{max} was assigned to the ξ value varying from ξ_0 to ξ_{max}. A transforming equation from z-y coordinates to ξ-η coordinates was developed to represent different features of isovels in a cross-section, which can be estimated directly from actual velocity data or indirectly from discharge rate, slope, roughness, and cross section of the channel (Chiu and Lin, 1983; Chiu and Chiou 1986). Based on the assumption on the cumulative distribution function, the velocity distribution was derived, which described the observed data reasonably well (Chiu, 1988). Luo and Singh (2011) applied the same coordinates to develop the 2D velocity distribution using the Tsallis entropy, whose result is comparable to Chiu's. However, due to the complexity of the coordinate system and a large number of parameters used, the application of these methods is rather limited.

To reduce the many parameters in the coordinate system, Marini et. al (2010) developed a new method for deriving 2D velocity distribution. In their study, CDF was hypothesized under the x-y coordinates. The CDF is required to be between 0 and 1, which is continuous and differential, and it must have value of 0 on the borders and

reaches 1 at only one point where the maximum velocity occurs. They developed the CDF in an exponential form to obtain such properties, in which the exponent on the *x* direction is raised to the power *D/B*, where *D* is the channel depth, *B* is the channel width. Under such a hypothesis, the 2D velocity distribution was developed and has shown advantage over Chiu's velocity distribution. However, the velocity with lower values is not captured accurately.

In Chiu's (1987, 1989) derivation of velocity distribution, only two constraints are used which are the same as the first and second equations mentioned in section 2.1.3, Barbe et. al (1991) applied the entropy-based velocity distribution with three constraints in which the conservation of momentum was added, in addition to the conservation of mass and energy. Comparison from their work shows that the profile presented with three constraints did not offer a significant improvement to fit the overall profile in any case, while the greatest improvement was near the channel bed.

A dimensionless parameter of entropy function *M* was introduced in the entropy-based derivation (Chiu, 1988; Chiu and Said, 1995; Chiu and Tung 2002; Singh and Luo, 2009, 2011; Luo, 2009; Luo and Singh, 2011) with which the entropy-based velocity equation can be simplified. This parameter has proved to be useful for characterizing and comparing various patterns of velocity distributions and the status of open-channel flow system, which can be expressed by the location of mean and maximum velocity and their relationships. The mean velocity value, the location of the mean velocity (Chiu and Said, 1995; Chiu and Tung, 2002) and the energy coefficient (Chiu, 1992) can be obtained

from *M*. The use of the entropy parameter predetermined for a channel section can greatly ease discharge estimation, especially in unsteady flow (Chiu, 1992).

According to Chiu's (1988) study, when M=0, the proportional probability $p(u/umax)$ is a constant equal to unity, which represents a uniform distribution corresponding to the maximum value of entropy; when M equals ∞, the probability $p(u/umax)$=0 except at $u=u_{max}$, $p(u/u_{max})=\infty$, which corresponds to the minimum entropy situation. From data, the entropy is found significantly greater than 0 only when M is between 6 to 9, which has a relatively large width-depth ratio and roughness. By Relating u/u_* to u/u_{max}, Chiu (1988) found that the M value greater than 8 should mean the flow is in a turbulent state, and 7-8 represents the transitional range between the laminar and turbulent flows. However, it is not certain whether this is also true for sediment-laden flow as the data used were from clear-water flows.

According to the maximum entropy concept, there should be a natural tendency for the turbulent, open-channel flow to achieve and maintain an M value between 7 and 8 as the entropy in this range gets to be maximum for turbulent flow. For an erodible channel, this may be accomplished by adjusting the cross section, slope, roughness, alignment, velocity distribution and perhaps sediment transport. M=8 represents channels of greater values of width to depth ratio and roughness and smaller slopes (Chiu, 1988). For a nonerodible channel this can only be accomplished by adjusting the water depth and the pattern of velocity distribution. Thus flows in artificial channels of rigid boundaries tend to have a relatively wide range of possible values of M.

2.2.3 Maximum and mean velocity

The maximum velocity conveys an important message about channel flow as it defines the range of velocity distribution. The location of maximum velocity is of interest, as the maximum velocity does not always occur at the water surface, but some distance below it, which is called as the dip phenomenon. The dip phenomenon was reported more than a century ago by Stearns (1883) and Murphy (1904), which attracted a lot of interest. It is stated that the dip phenomenon is caused by the secondary currents (Nezu and Nakagawa 1993), which is the circulation in a transverse channel cross section as the longitudinal flow component is called primary flow. Because the secondary motion will transport the low momentum fluids from the near bank to the center and the high-momentum fluids from the free surface toward the bed.

Yang et. al (2004) investigated the mechanism of dip phenomenon in relation to the secondary currents in open-channel flow. In their study, a dip-modified log law for the velocity distribution in smooth uniform open channel was developed and its result was good. This modified velocity distribution is capable of describing the dip phenomenon and is applicable to the velocity profile in the region from the near bed to just below the free surface, and transversely from the center line to the near-wall region of the channel. From their experiments, the location of the maximum velocity was shown to be related to the lateral portion of the measured velocity profile. It is concluded that the dip may even occur in a very wide channel, not in the centerline but in the sidewall region.

Chiu and Tung (2002) states that the location of maximum velocity is linked to the ratio of the mean and maximum velocities, velocity distribution parameter, location of mean velocity, energy and momentum coefficients, and probability density function underpinning a velocity distribution equation derived by entropy. A scale parameter h_ξ called metric coefficient, introduced by Chiu (1989), needed for coordinate transformation between the y and ξ systems. Compared with Einstein and Chien's (1955) result, an appreciable difference can be seen in the lower region.

The mean velocity is another main characteristic of channel flow. With the known mean velocity value, the flow discharge, sediment transport and pollutant transport can be obtained. It is found that the mean value of the ratio of mean and maximum velocities at a given section is stable and constant, and invariant with time and discharge (Chiu and Said, 1995). Chiu and Tung (2002) linked this ratio with parameter M, which is also shown to be consistent with experimental data. A linear relation between mean and maximum velocities was discovered by collecting the velocity data in some cross-sections of the Mississippi River (Xia, 1997). It is found that the relation was perfectly linear along both straight reaches and river bends where M was constant and equal to 2.45 to 5, respectively. Based on Chiu's velocity distribution, Moramarco et. al. (2004) developed a simple method for estimating the mean velocity which is quite accurate also for new river sites without knowning M.

2.2.4 Other related research

More research on velocity and discharge of open-channel flow has been undertaken by Chiu and his associates. Analysis of velocity distribution in the probability domain made it possible to determine the cross-sectional mean velocity and the momentum and energy coefficients without dealing with the geometrical shape of the cross-section, which is always complex in natural channels. Thus, the entropy based velocity distribution is applicable in the nonuniform open-channel flow (Chiu and Murray, 1992). For more applications, the velocity equation can also represent the velocity distribution in the entire flow field in a pipe, regardless of whether the flow is laminar or turbulent, and whether the pipe is smooth or rough (Chiu, et.al, 1993), in which study the relationship of friction factor and entropy was established.

Chiu and Said (1995) developed a technique to determine discharge from a velocity profile on a single vertical passing through the point of maximum velocity in a channel cross section. The technique is an efficient way to estimate discharge in streams and rivers that can be used to continuously update the flow resistance during unsteady flow to enhance a filtering scheme designed to reduce uncertainties in flow forecasting. The use of a constant value of entropy parameter predetermined for a channel section can simplify discharge estimation.

2.3 Suspended sediment discharge in open channels

Suspended sediment discharge and bed-load sediment discharge together form the total sediment discharge in open channels (Einstein, 1950). The bed-load is the

portion of the sediment carried near the bed by the physical processes of intermittent rolling, sliding, and saltation of individual grains at various random locations in the bed. On the contrary, the suspended load is composed of sediment particles that are lifted into the body of flow by turbulence. In other words, the bed-load sediment remains in contact with bed most of the time, while the suspended sediment is away from the bed.

Suspended sediment transport always occurs in steady, uniform turbulent flow, where turbulent velocity fluctuations in vertical direction can transport sediment upward. As a result of balance between turbulent diffusion of the grains upward and gravitational settling of the grains downward, an equilibrium distribution of suspended sediment concentration is developed and thus, there are no vertical changes in the sediment concentration profile in the flow direction (Sturm, 2010). The equation describing the turbulent flux to the gravitational settling flux results in the following differential equation that governs the sediment concentration distribution:

$$-\varepsilon_s \frac{dC}{dy} = \omega_s C \tag{2-8}$$

where ε_s= the diffusion coefficient for sediment transfer, C= sediment concentration at a given point y, y= vertical distance measured from the channel bed, and ω_s= settling velocity of sediment particle.

The diffusion coefficient is not constant in alluvial channel flow, particularly near the bed, where turbulence characteristics change with distance above the bed. Thus, ε_s is often estimated as $\beta\varepsilon$, where β is a coefficient of proportionality and ε is the turbulent eddy viscosity.

The fall velocity, also called the settling velocity, ω_s, plays an important role in distinguishing between suspended sediment load, and bed load. It is related to particle size, shape, submerged specific weight, water viscosity, sediment concentration, etc. In the laminar settling region, where the Reynolds number is smaller than 1, Stokes (1851) derived the drag force on a spherical particle by solving the Navier-Stokes equations without inertia terms, which lead to the well-known Stokes' law for the settling velocity of spherical particles. However, the sediment particles in natural rivers are usually irregular shaped and have rough surfaces, which exhibit differences in settling velocity in comparison with spherical particles. A new formula for settling velocity of natural sediment particles was derived by Rubey (1933). However, Van Rijin (1984) suggested using the Stokes law for computing the velocity of sediment particles smaller than 0.1mm and using Zanke's (1977) formula for particles of size from 0.1 to 1mm; he also derived a formula for the particles larger than 1mm.

Differential equation (2-8) should be integrated so that the sediment concentration can be reached. A classical possible model derived from that equation using the Prandtl-von Karman logarithmic velocity equation and linear shear stress distribution assumption is the Rouse equation (Rouse, 1937). The ratio in the exponent is called the Rouse parameter and is a measure of the relative size of settling velocity and turbulent stress. The reference concentration is defined in the Rouse equation that is a comparison of concentration with that at some reference level so that the bed-load transport is not accounted for. The Rouse solution has been compared favorably with

observed suspended sediment concentration distribution but not valid for the sediment concentration near the channel bed or the water surface.

As an alternative velocity distribution, Chiu's (1988, 1989) velocity distribution can be used to integrate differential equation (2-8) (Chiu, 2000). In this study, using Chiu's velocity distribution, instead of the logarithmic velocity distribution, exempted from the weaknesses and limitations of the Rouse equation, the efficient model derived in this study was capable of describing the sediment concentration from the channel bed to the water surface. As a disadvantage, Chiu's sediment concentration contains a large number of parameters and its practical use is therefore limited.

Rather than using differential equation (2-8), a full entropy-based method for modeling sediment concentration was developed by Choo (2000). In his study, time-averaged sediment concentration was considered to be a random variable. Similar to the derivation of Chiu's velocity, the Shannon entropy was maximized to obtain the least-biased probability distribution of sediment concentration. Choo's work showed significant advantages over the traditional methods: the entropy based equation was capable of describing the concentration distribution in the vertical direction. The mean sediment concentration equation was effective for evaluating the cross-sectional mean concentration in open channels. However, the cumulative distribution function, the key hypothesis in the entropy method, is yet to be identified, which limits its application.

Einstein (1950) determined the suspended sediment discharge by integrating the product of local sediment concentration and flow velocity over the suspended zone. Choo's (2000) entropy-based method can also be used to estimate the suspended

sediment discharge as a product of the mean sediment concentration and mean velocity. However, he did not show any results of computed suspended sediment discharge, thus the validity of this method is yet to be examined.

3. EXPERIMENTAL AND FIELD DATA

To evaluate the accuracy of the entropy-based velocity distribution derived in this thesis, several experimental and field data were used. Velocity data from four gauged sections in the upper Tiber River basin in Central Italy (shown in Figure 3.1) was used for evaluating the 2D velocity distribution, which were collected from seven flood events from 1984 to 1997. The mean velocity data collected during a period of 20 years at the four gauges were used to evaluate the mean velocity computation using entropy. The discharge values for different events varied between 1.5m^3/s and 537m^3/s with the mean velocity ranging between 0.12m/s to 2.42m/s and the maximum water depth between 0.8m and 6.7m. The flow characteristics of each station are shown in Table 3.1.

Figure 3.1 Upper Tiber River basin with location of river gauging stations (Moramarco et al., 2004)

Table 3.1 Flow characteristics: Discharge Q and maximum water depth D of available velocity measurements N for four gauges

Location	N	Q(m^3/s)	D (m)
S. Lucia	42	1.5-215	0.9-5.2
P. Felcino	34	2.3-412	0.8-6.2
P. Nuovo	51	5.4-537	1.1-6.7
Rosciano	38	3-160	1.3-3.3

The field data are collected in Appendix A, whose main characteristics of the selected events are shown in Table 3.2.

Table 3.2 Main characteristics of selected events: Maximum velocity u_{max}, mean velocity u_m, discharge Q, flow area A and water depth along the vertical where u_{max} occurs, D

Location	Date	u_{max} (m/s)	u_m (m/s)	Q (m^3/s)	A (m^2)	D (m)
P. Nuovo	Nov. 15, 1982	2.023	1.085	159.19	146.74	2.9
P. Nuovo	Nov. 18, 1996	2.597	1.736	541.58	311.91	6.64
P. Nuovo	Jun. 03, 1997	2.719	1.820	506.39	278.16	6.07
Rosciano	May 28, 1984	2.583	1.784	156.24	87.60	3.2
Rosciano	Nov. 20, 1996	2.447	1.525	131.20	86.03	3.11
P. Felcino	Apr. 21, 1997	3.365	2.120	399.16	188.26	6.15
S. Lucia	May 28, 1984	2.437	1.873	96.53	51.53	2.93

35 Data sets as shown in Appendix B were used to evaluate 2D velocity profiles from 8 straight reaches of Ghamasiab River in western Iran. Data was collected from wide rectangular channels during periods of constant and low-flow discharge. The aspect ratios of selected sites was in the range from 1.62 to 2.5, the Froude number was in the range from 0.46 to 0.77, and the Reynolds number was between 1.5×10^5 and 7.3×10^5(Afzalimehr and Anctil, 1999, 2000; Afzalimehr and Rennie, 2009).

The laboratory data collected by Einstein and Chien (1955) were used to evaluate the 1D velocity distribution and suspended sediment concentration distribution. A total of 29 runs were collected, 13 of them with clear water and the 16 with sediment-laden flow. Table 3.3 is a summary of the most important and useful data, detailed description of each run data can be found in Appendix C. The experiments were conducted in a painted steel flume 1.006 ft wide by 1.17 ft deep and 40 ft long. The slope was adjustable by means of an especially designed jack and varied from 0.0185 to 0.025, and the discharge was variable from 2.6 to 3.0cfs by changing the speed of the pump. The water depth ranged from 0.36 to 0.49 ft and the average velocity of different runs changed from 6.1 fps to 8.7 fps. Three different sands were used in their experiment labeled as coarse (D_{50}=1.3mm), medium (D_{50}=0.94mm), and fine (D_{50}=1.14mm).

Table 3.3 Summary of data, discharge Q, average depth of flow h, bed slop s_B, the hydraulic radius of bed R_B and von Karman constant κ

Run no.	sand	Q (cfs)	h (ft)	s (10^{-3})	R_B (ft)	κ
C-1	c	2.8	0.460	14.5	0.328	0.387
S-1	c	2.78	0.451	13.9	0.314	0.305
C-2	c	2.8	0.452	14.1	0.315	0.379
C-3	c	2.62	0.404	20.6	0.306	0.403
S-2	c	2.64	0.392	19.4	0.285	0.247
S-3	c	2.62	0.381	20.9	0.282	0.231
S-4	c	2.61	0.378	23.6	0.287	0.210
S-5	c	2.62	0.364	25.5	0.277	0.173
C-4	c	2.62	0.397	18.4	0.289	0.350
C-5	c	2.62	0.582	5.5	0.341	0.350
C-6	m	3.00	0.488	14.7	0.347	0.398
S-6	m	2.93	0.470	14.3	0.327	0.295

Table 3.3 continued

Run no.	sand	Q (cfs)	h (ft)	s (10^{-3})	R_B (ft)	κ
S-7	m	2.94	0.467	14.3	0.325	0.281
S-8	m	2.91	0.470	15.0	0.317	0.263
S-9	m	2.85	0.455	17.3	0.311	0.247
S-10	m	2.88	0.447	15.4	0.311	0.248
C-7	m	2.85	0.432	20.2	0.317	0.395
C-8	m	2.83	0.449	19.3	0.296	0.391
C-9	m	2.67	0.399	12.7	0.291	0.410
C-10	f	2.62	0.398	12.7	0.284	0.400
C-11	f	2.77	0.437	13.1	0.287	0.406
S-11	f	2.75	0.439	12.2	0.286	0.398
S-12	f	2.77	0.435	13.2	0.277	0.274
C-12	f	2.76	0.433	12.6	0.286	0.391
S-13	f	2.74	0.433	17.4	0.289	0.237
S-14	f	2.75	0.440	16.9	0.285	0.218
S-15	f	2.73	0.404	18.6	0.287	0.168
S-16	f	2.73	0.408	18.9	0.279	0.182
C-13	f	2.65	0.39	18.9	0.27	0.427

Coleman's (1986) experiment data was also used to evaluate the 1D velocity distribution and the sediment concentration distribution as shown in Appendix D. Experiments were performed in a recirculating flume with a rectangular Plexiglas channel 356 mm wide and 15 m long, with slope adjustment capability for maintaining uniform flow. 40 velocity profiles and sediment concentration were measured at a vertical located on the flume channel centerline 12 m downstream from the entrance. The experiment was to establish a uniform flow at constant discharge, depth, and energy

gradient, to establish the clear-water velocity profile by local velocity measurement at standard elevations, and then to monitor changes in the velocity profile resulting from systematic increases in suspended sediment concentration while holding other flow conditions constant. Velocity and concentration profiles were established by averaging two replications of each local measurement. Experiments were repeated with three sands, with nominal diameters of 0.105, 0.210 and 0.420mm. The discharge was held at 0.064 m^3 /s, while the flow depth was held to an average of 169 mm.

Furthermore, 10 sets of experimental data for rectangular flume with nonuniform flow were also used, which is observed in a channel with 2ft width and 0.6ft depth.

4. HYPOTHESIS ON THE CUMULATIVE DISTRIBUTION FUNCTION

Through the principle of maximum entropy, the least biased probability of the velocity can be obtained, which will be fully discussed in Chapter 5. As a fundamental to this entropy based process, a hypothesis on the cumulative distribution function should be formulated so that the entropy based probability can be relate to the natural process in space and time domains.

4.1 2D velocity distribution

As a first step, the coordinate system used in this thesis should be defined, on which the cumulative distribution function is based.

4.1.1 Setting up a coordinate system

Natural channel sections are often u-shaped or v-shaped. For simplicity, a channel cross-section is idealized as a rectangle with a depth of D and a width of $2B$, as shown in Figure 4.1. It is assumed that the velocity distribution is symmetric on either side of the center vertical line, where the maximum velocity always occurs in the regular cross-section.

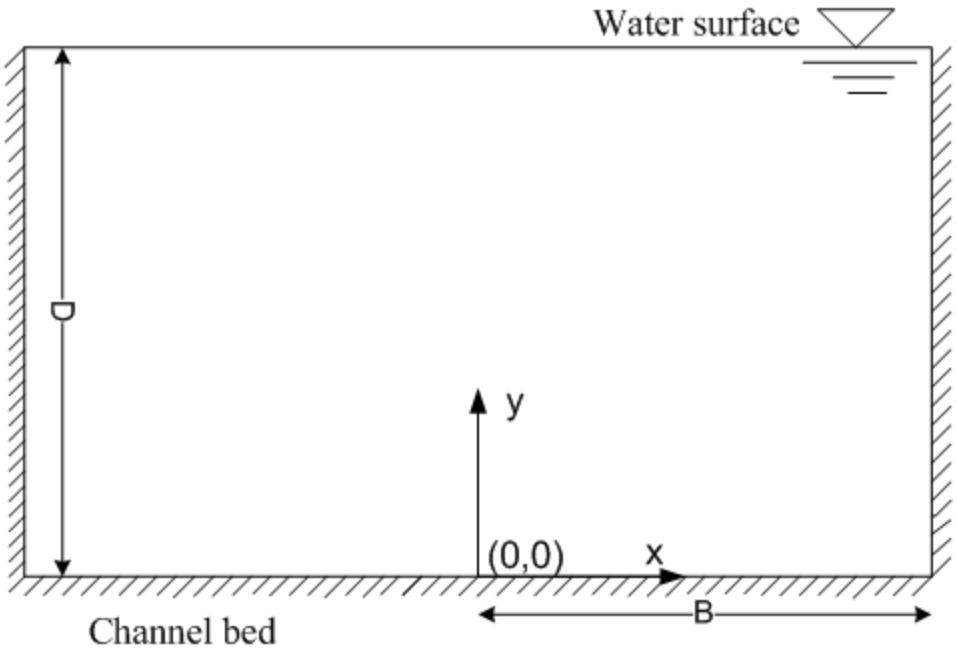

Figure 4.1 Idealized rectangular cross-section

Thus, the coordinates are set at the center of the channel bottom where *y* represents the vertical coordinate and *x* the horizontal coordinate (in the transverse direction) perpendicular to *y*. As shown in Figure 3.1, the point represented by *y= 0* and *x= 0*, denoted as (*0, 0*), corresponds to the center of the channel bed. Under this coordinate system, *x* has a positive value at the right side of the cross-section and a negative value at the left, while *y* is always positive in the cross-section.

4.1.2 Velocity isovels

The velocity isovel is defined by the curve on which the velocity shares the same value. Thus the isovels *I(u)* have the one-to one relationship with the velocity value *u*. In spatial domain, the velocity isovels can be obtained from an assemble of *x* and *y*, where

the velocity is equal to u, which can be written as $I(u)=\{(x, y), \text{ for all } u_{(x, y)}=u\}$, where $u_{(x,y)}$ is the velocity at the point (x, y) .

Since the velocity is assumed to be 0 at the boundary, $I(0) = \{x=D \text{ or } y=0\}$. For the maximum velocity which is assumed to occur at the center of the water surface, $I(u_{max})= \{x=0$ and $y=D\}$. For rest of the points, velocity isovels is monotonically increasing from 0 to u_{max}.

4.1.3 Cumulative distribution function

In natural channels, the velocity varies not only in the vertical direction but also transversely. In the vertical direction the velocity increases from the channel bed to or near the water surface and in the transverse direction velocity decreases from the center to the edge.

The velocity is shown to be monotonically increasing from the isovel $I(0)$ to $I(u_{max})$. Thus the cumulative distribution function will get the value of 0 at $I(0)$ and get to 1 at $I(u_{max})$. With the relation between coordinates x and y with isovesl $I(u)$, the cumulative distribution function can be expressed in the space domain. Thus, CDF needs to be 0 at $x=D$ or $y=0$, which corresponds to $I(0)$, and needs to be 1 at x=0 and y=D, which corresponds to $I(u_{max})$.

The cumulative distribution function (CDF) should be hypothesized such that it is capable of maintaining the above characteristics. It also should be continuous and can be derived in both x and y. Hence, the following cumulative distribution function can be

established as,

$$F(u) = \left[1 - \left(\frac{x}{B}\right)^2\right]^b \left(\frac{y}{D}\right)^a \text{ for all } (x, y) in\ I(u) \quad (4\text{-}1)$$

where the values of exponents a and b in equation (4-1) can be determined from observations. The values are shown to be related to the width-depth ratio of the channel, which will be discussed in Section 4.1.3.

Figure 4.2 shows a half part of the CDF with a=0.5, b=0.2 in the idealized cross-section. Figure 4.3 is the CDF contour map, which is also of a half cross-section. In both figures, the CDF reaches 1 at x=0 and y=D and reaches 0 at x=B or y=0, which means the maximum velocity is at the center of the cross-section and no velocity occurs at the boundary. It can also be seen from figures that the CDF increases smoothly from the boundary to the center and the rate of increase depends on the values of exponents a and b.

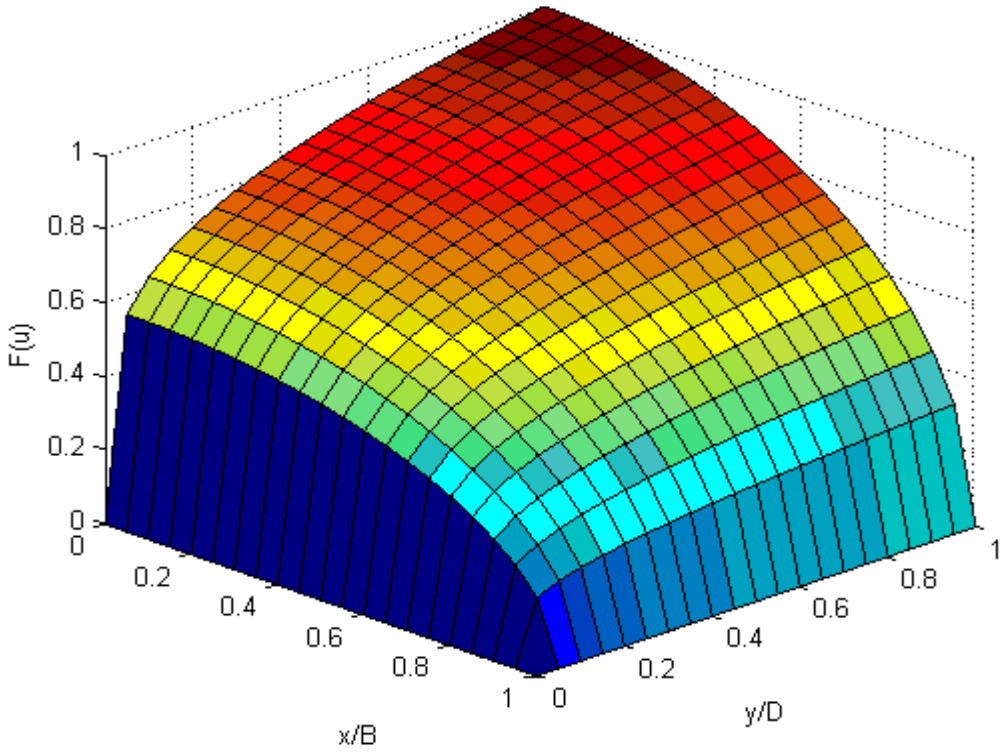

Figure 4.2 CDF of 2D velocity distribution

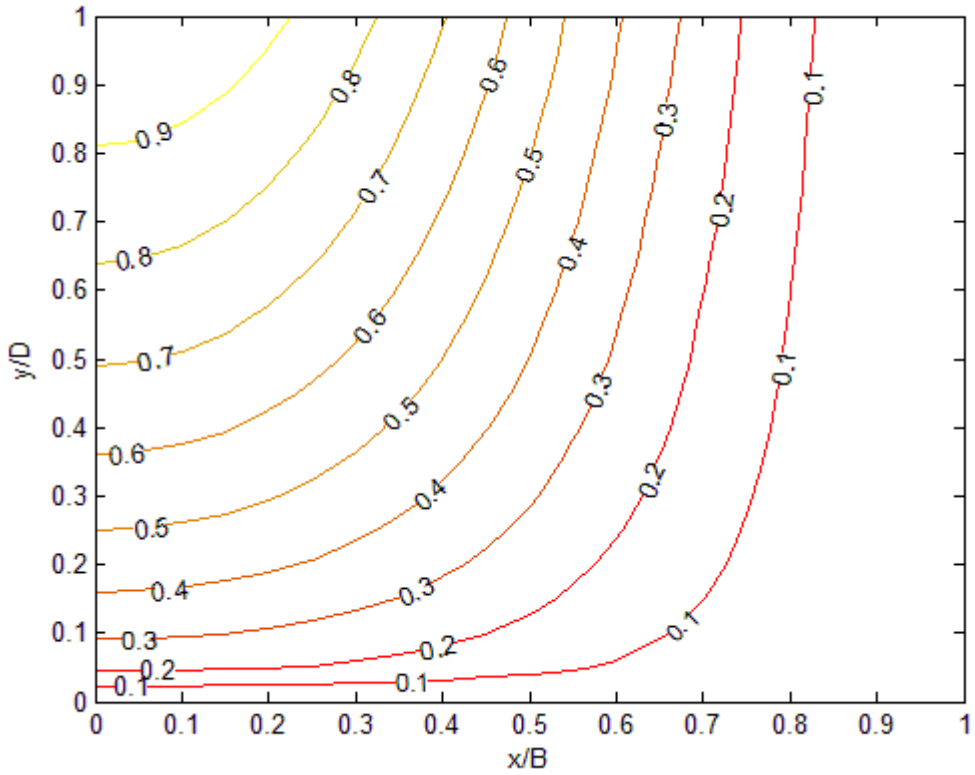

Figure 4.3 Contours of CDF for 2D velocity distribution

The effect of the exponent values *a* and *b* can be analyzed from Figure 4.4, which is a set of figures with different combinations of *a* and *b* values.

Comparing Figures 4.4 (a) and (b) with (c) and (d), the change in the *a* value leads to a slower decrease in the vertical coordinate: for a=1, the CDF contour decreases from the water surface to the channel bed linearly to the depth, while for a= 0.5, the CDF decreases slowly first, then rapidly drops from the depth about 0.1y/D to the channel bed. From this feature it seems that Figures 4.4 (a) and (d) are more likely to be shallower rivers than Figures 4.4 (b) and (c), since the impact of channel is less spread in Figures 4.4 (b) and (c) than in Figures 4.4 (a) and (d).

The difference between Figures 4.4 (a) and (d) or between Figures 4.4 (b) and (c) shows the effect of the *b* value. Similarly, for a smaller *b* value, the CDF decreases from the channel center to the wall slower than for a bigger *b* value. From the comparison of Figures 4.4 (a) and (b), one can find that the CDF is distributed more uniformly in Figure 4.4 (a) than in Figure 4.4 (b). It may be concluded that the channels described in Figures 4.4 (b) and (d) are wider than the channels in Figures 4.4 (a) and (c).

Figures 4.4 (e) and (f) show two extreme circumstances which are $a = 0$ or $b = 0$. In Figure 4.4 (e) when $a = 0$, the CDF decreases only in the transverse direction, which is from the center line to the channel wall. However, this circumstance is the least probable in natural channels. In Figure 4.4 (f), the velocity changes only in the vertical direction, which is monotonically decreasing from the water surface to the channel bed. This might result in very wide channels, where the velocity distribution is ideally one-dimensional.

To sum up, different *a* and *b* values result in different forms of CDF in a channel section, which may reflect the characteristics of the channel section. A bigger *a* value or a smaller *b* value tends to imply a higher value of the width-depth ratio. Further discussion with observed values will be discussed in the Section 4.1.3.

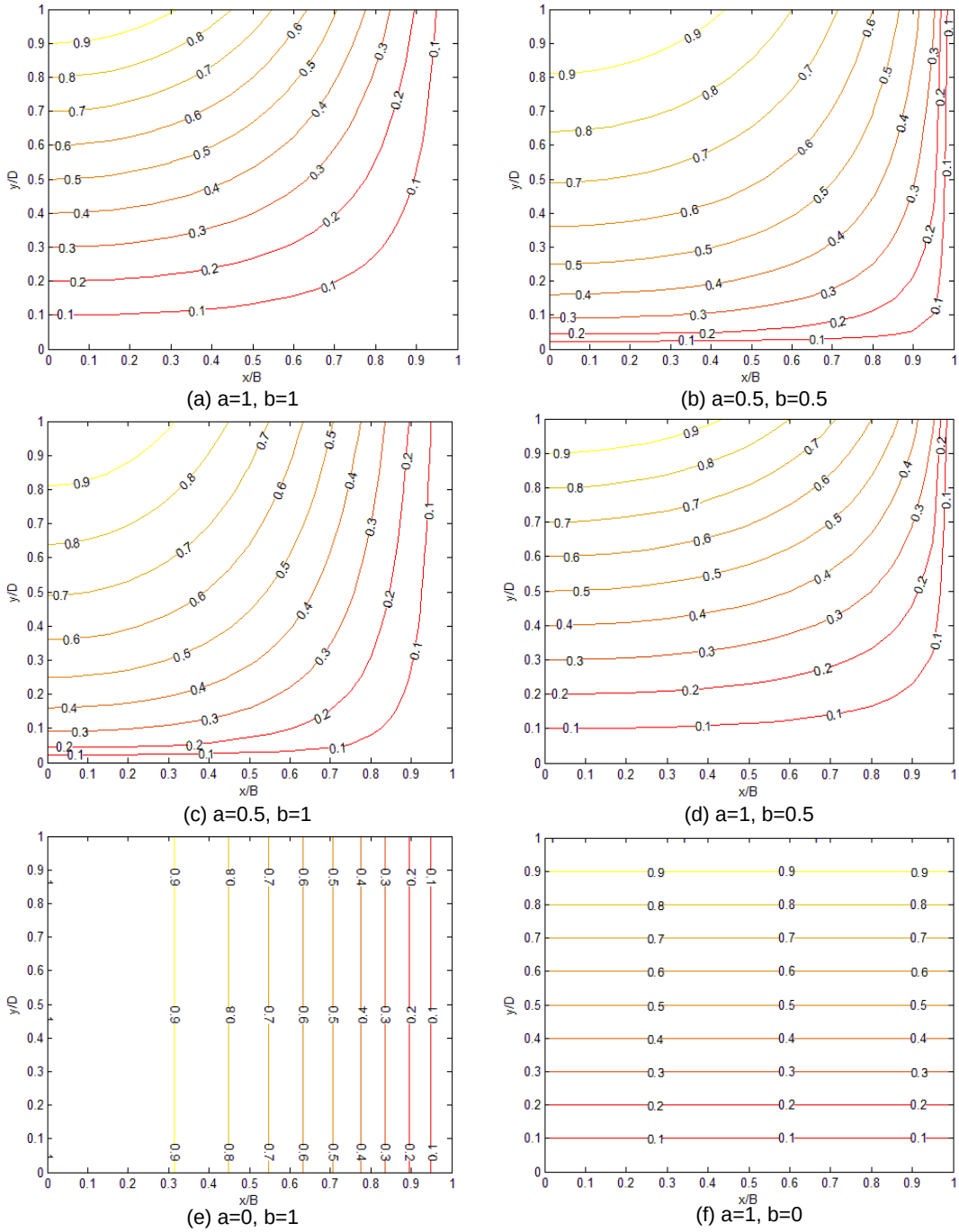

Figure 4.4 Contours of CDF for various *a* and *b* values

4.1.4 Verification of cumulative distribution function

The assumed cumulative distribution function (CDF) plays an important role in predicting the velocity distribution and its accuracy directly affects the validity of the velocity distribution. Thus the cumulative distribution function should be satisfactorily defined to maintain the validity of the velocity distribution.

Natural channels are always u-shaped or v shaped, or may not be even symmetric at all, thus the rectangular assumption is not valid for most natural channels and need to be modified. The following adjustment can therefore be made to deal with an irregular cross-section: change the fixed water depth *D* to *D(x)*, which means that for different locations, the water depth is different, and becomes a function of *x*. Then, equation (4-1) becomes

$$F(u) = \left(1 - \left(\frac{x}{B}\right)^2\right)^b \left(\frac{y}{D(x)}\right)^a \text{ for all } (x, y) in\ I(u) \tag{4-2}$$

Another parameter should be introduced to investigate the dip-phenomenon. Define a new parameter $h_{y,}$ which can be used as a proportional coefficient redistributing the probability in the vertical direction, so that the CDF may reach 1 not at the water surface, but at some distance below. With the use of h_y, the CDF can be recast in the vertical direction as

$$F(u) = \left(1 - \left(\frac{x}{B}\right)^2\right)^b \left(\frac{y}{D(x)} h_y\right)^a \text{ for all } (x, y) in\ I(u) \tag{4-3}$$

The h_y value should be determined in such a way that for a fixed value of *x* the CDF increases from the channel bottom to the possible maximum value at the point where the maximum velocity occurs and then reduces to the water surface. Here, the

least squared method will be used to determine h_y, however, more details about the method to derive the analytical solution will be discussed in Section 5.3.1.

Inputting equation (4-3) instead of equation (4-1), the limitations on the channel shape can be alleviated and the velocity distribution can be applied to any channel cross-section by fitting the observed cumulative probability through the least squared method. Figure 4.5 shows the simulation of cumulative probability on chosen vertical lines, x from -18.86m to 10.49m including the center line x=0. According to observations, a=0.2 and b=1.8 lead to the best fit of $F(u)$ for the left side of the channel and a=0.2 and b=1 yield the best fit for the right side.

From Figure 4.5, the CDF increases from 0 at the channel boundary to the water surface and reaches 1 near the water surface at x=0m, which is the center line of the channel section. It is seen from the details of each vertical line that the CDF increases from the channel bed to some amount less than or equal to 1 and decreases to the water surface, which exactly represents the shape of velocity distribution. Since the cumulative distribution is considered for the whole cross-section, the CDF can only get to 1 at one point, where the maximum velocity occurs. That's why in the vertical lines other than x=0m the CDF grows up to less than 1.

Though the a and b values are selected differently for left and right sides, the simulation of the CDF still cannot capture every observed value, which limits the accuracy. On the left side of bank [Figure 4.5(a)], the estimated curve at line x= -18.86m shows the best result and the closer to the center line, the lower the accuracy it shows. The right hand side is just opposite, the farther apart from the center the worse the

simulation. However, the overall estimation of the probability distribution can roughly reflect the pattern of the velocity distribution and seems reasonable.

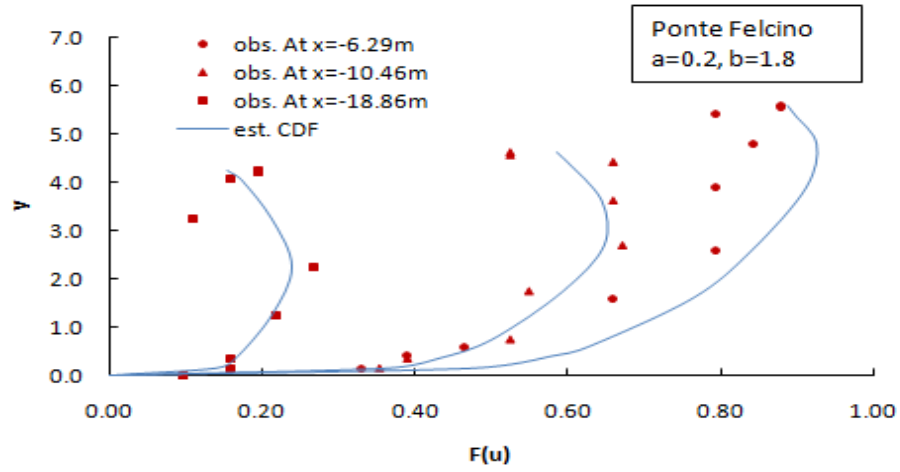

(a)

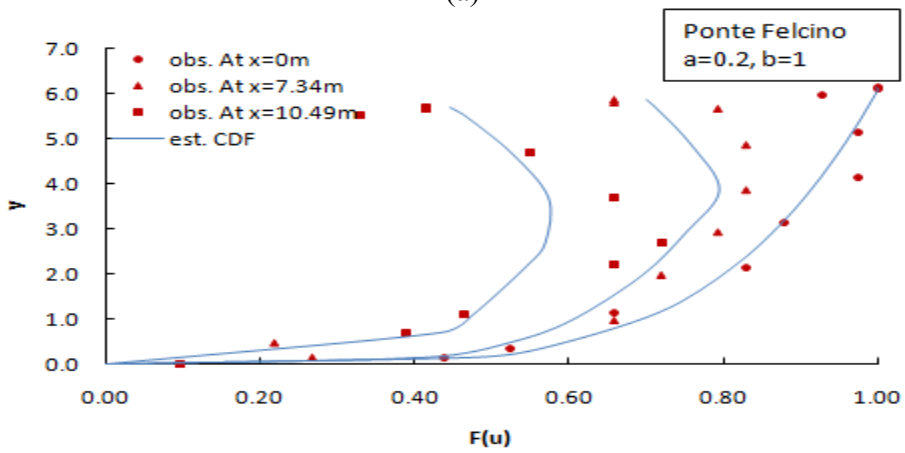

(b)

Figure 4.5 Estimated CDF of Italian data at Ponte Felcino. (a) CDF at the left side of cross-section, and (b) CDF at the right side of the cross-section

The accuracy of the estimated cumulative probability (est. CDF) can also be seen from Table 4.1, as well as observations (obs. CDF). Here, the error is computed as *error*=(est.-obs.)/obs. It is noted that here *y'* differs from *y*, which denotes the depth

from water surface ($y'=D-y$). The cross-sectional root mean square error is 0.049, and it has a root mean square error 0.013 at the left bank and 0.048 at the right side.

Table 4.1 Estimation of cumulative distribution for Italian data

x (m)	*y'* (m)	*obs. CDF*	*est. CDF*	*error*	*x* (m)	*y'* (m)	*obs. CDF*	*est. CDF*	*error*
-18.86	0	0.195	0.155	-0.208	10.49	0	0.415	0.446	0.075
-18.86	0.06	0.195	0.161	-0.173	10.49	0.06	0.415	0.452	0.091
-18.86	0.2	0.159	0.174	0.097	10.49	1	0.549	0.525	-0.044
-18.86	1	0.110	0.213	0.943	10.49	2	0.659	0.573	-0.130
-18.86	2	0.268	0.240	-0.106	10.49	3	0.720	0.569	-0.209
-18.86	3	0.220	0.213	-0.029	10.49	3.5	0.659	0.546	-0.171
-18.86	3.9	0.159	0.165	0.043	10.49	4.6	0.463	0.475	0.026
-18.86	4.1	0.159	0.140	-0.120	10.49	5	0.390	0.434	0.113
-18.86	4.25	0.098	0.000	-1.000	10.49	5.7	0.098	0.000	-1.000
-10.46	0	0.524	0.585	0.116	7.34	0	0.659	0.699	0.062
-10.46	0.06	0.524	0.590	0.125	7.34	0.2	0.793	0.713	-0.101
-10.46	0.2	0.659	0.599	-0.090	7.34	1	0.829	0.757	-0.087
-10.46	1	0.659	0.644	-0.022	7.34	2	0.829	0.793	-0.043
-10.46	1.93	0.671	0.648	-0.034	7.34	2.93	0.793	0.751	-0.053
-10.46	2.88	0.549	0.594	0.082	7.34	3.88	0.720	0.694	-0.036
-10.46	3.88	0.524	0.501	-0.044	7.34	4.88	0.659	0.602	-0.085
-10.46	4.28	0.390	0.430	0.103	7.34	5.38	0.220	0.521	1.373
-10.46	4.48	0.354	0.363	0.027	7.34	5.7	0.268	0.415	0.545
-10.46	4.63	0.098	0.000	-1.000	7.34	5.85	0.098	0.000	-1.000
-6.29	0	0.878	0.886	0.009	0.00	0	1.000	0.998	-0.002
-6.29	0.06	0.878	0.889	0.013	0.00	0.06	1.000	1.000	0.000
-6.29	0.2	0.793	0.897	0.131	0.00	0.2	0.927	0.995	0.074
-6.29	0.8	0.841	0.925	0.099	0.00	1	0.976	0.967	-0.009
-6.29	1.71	0.793	0.911	0.149	0.00	2	0.976	0.926	-0.051
-6.29	3	0.793	0.840	0.060	0.00	3	0.878	0.876	-0.002
-6.29	4	0.659	0.762	0.158	0.00	4	0.829	0.812	-0.021
-6.29	5	0.463	0.627	0.352	0.00	5	0.659	0.716	0.088
-6.29	5.2	0.390	0.578	0.480	0.00	5.8	0.524	0.565	0.077
-6.29	5.45	0.329	0.475	0.442	0.00	6	0.439	0.477	0.086
-6.29	5.60	0.098	0.000	-1.000	0.00	6.15	0.098	0.000	-1.000

Figure 4.6 compares contour maps of observed and estimated CDFs for the whole cross-section of Ponte Felcino River. It is seen from Figure 4.6 that the boundary of the channel cross-section is simulated exactly as the observation with the help of using *D(x)* for different locations. By using different values of *a* and *b* for left and right sides, contours on the right side are much looser than those on the left side, which is more likely distributed as observations. It is seen from the figure that the CDF is estimated a little larger than the observation at the boundary; however, the overall estimation in the whole cross-section seems reasonable.

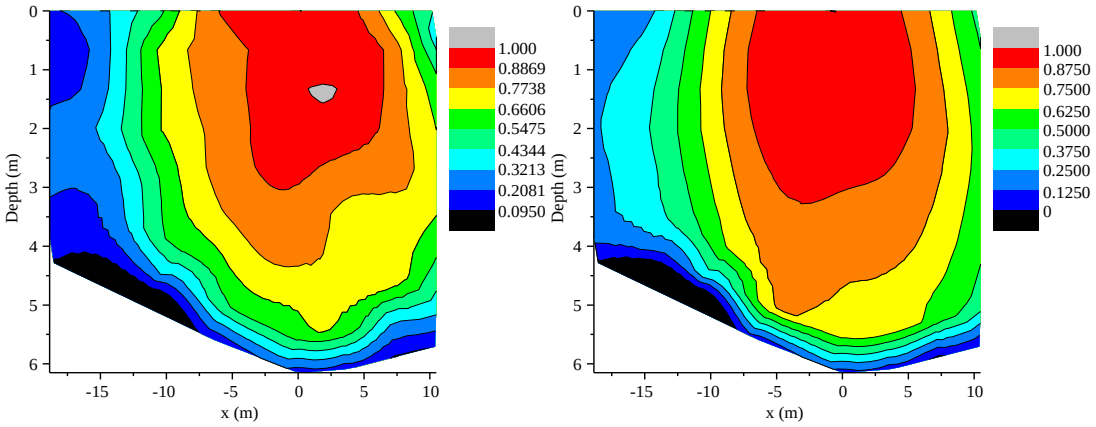

(a) (b)

Figure 4.6 Contours of CDF for Italian data at Ponte Felcino: (a) The observed CDF, and (b) The estimated CDF

More CDFs have been computed for Italian rivers and Iranian rivers and those results are presented in Appendix E.

For different river data, the *a* and *b* values are different and they are shown to be related to the width-depth ratio of the river. Table 4.2 is a summary of the *a* and *b* values

for different rivers in Italy, from which it can be observed that the *a* value increases with the width-depth ratio (*B/D*), while *b* decreases. Comparing the change with the width-depth ratio, the *a* value is more sensitive to the ratio than *b* is.

Table 4.2 Values of *a* and *b* with the width-depth rate

B/D	2.68	3.17	4.06	4.16	5.25	6.29	Average
a	0.18	0.21	0.23	0.20	0.25	0.28	0.23
b	1.10	1.00	0.90	0.90	0.80	0.80	0.92

The CDF for the Iranian data was also computed and the value of *a* and *b* are shown in Figure 4.7, where the width-depth ratio is much smaller than the Italian rivers. It is seen from Figure 4.7 that the value of *a* increases and the value of *b* slightly decreases with increasing width-depth ratio, which supports the results obtained from the Italian data.

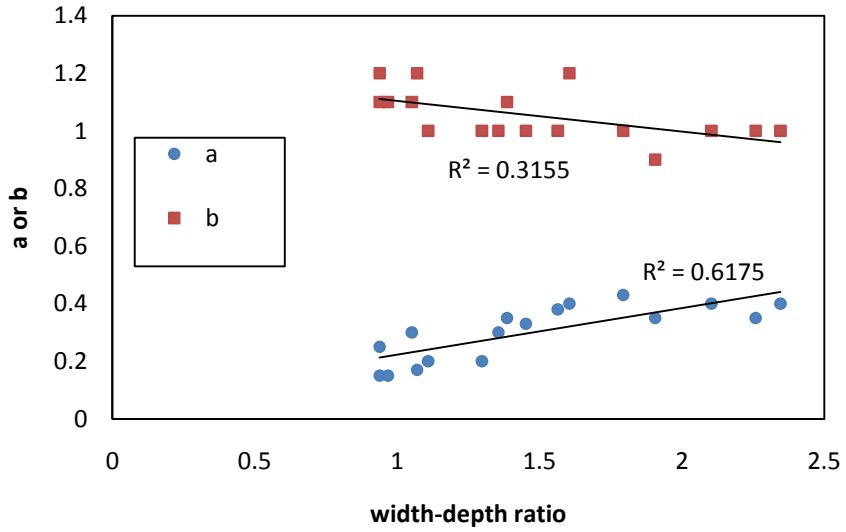

Figure 4.7 Values of *a* and *b* varying with the width-depth ratio of an Iranian river

4.2 1D velocity distribution

4.2.1 Setting a coordinate system

For 1D velocity distribution, the coordinate system is simpler than in the 2D case, since the velocity distribution is only studied in the vertical direction. Thus, the coordinate system is set at the channel bottom. Let *y* represent the vertical, omitting the *x* coordinate as shown in Figure 4.8.

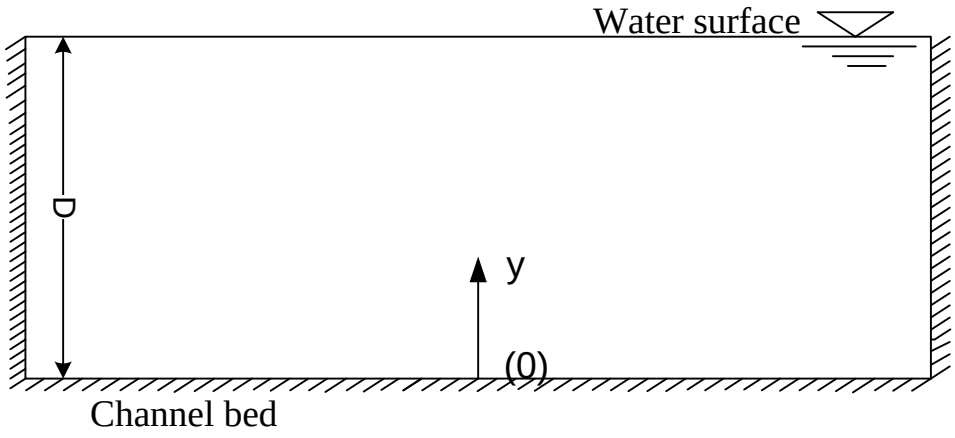

Figure 4.8 Idealized rectangular cross-section

4.2.2 Cumulative distribution function

The velocity is known to be monotonically increasing from the bottom of the channel to the water surface. In such case, the velocity isovels form a set of straight lines parallel to the channel bed. At the channel bed, y=0 corresponds to $I(0)$, whose CDF needs to be 0, while at the surface, $y=D$ corresponds to $I(u_{max})$, whose CDF needs to be 1. Similar to the 2D CDF, the CDF is hypothesized as

$$F(u) = (\frac{y}{D})^a \text{ for all } (y) in\ I(u) \quad (4\text{-}4)$$

Equation (4-4) can also be explained in another way: in the 1D case, where the channel is very wide, which has a much bigger value of *B/D*, which leads to a smaller value of b in Equation (4-1), ultimately b=0 as shown in Figure 3.4. Thus, the first term on the right side of Equation (4-1) becomes:

$$\left(1 - \left(\frac{x}{B}\right)^2\right)^b = 1 \quad (4\text{-}5)$$

which can be omitted and only the second term remains in equation (4-4).

For generalization, the cumulative distribution function containing above characteristics can be written in following forms:

$$F(u) = a_0 + a_1(\frac{y}{D})^{a_2} \text{ for all } (y) in\ I(u) \quad (4\text{-}6)$$

$$F(u) = a_0 + a_1(a_3 + \frac{y}{D})^{a_2} \text{ for all } (y) in\ I(u) \quad (4\text{-}7)$$

where a_0 to a_3 are different parameters. In this way, Equation (4-4) can be considered as the simplification of Equation (4-6) and (4-7).

4.2.3 Verification of cumulative distribution function

The value of a can be determined by fitting the observed cumulative distribution just as was done in the 2D case. From fitting experimental data, the a value ranges from 0.3 to 0.5 seen in Table 4.3, which is much bigger than in the 2D case. For the data of Run C1 of Einstein and Chien's (1955) as an example, a is set as 0.33 which is shown in Figure 4.9

Table 4.3 Estimation of cumulative distribution of Einstein and Chien's (1955) 1D data

y (ft)	*obs. F(u)*	*est. F(u)*	*error*
0.006	0.174	0.308	0.770
0.006	0.043	0.308	6.163
0.007	0.087	0.325	2.736
0.008	0.217	0.339	0.562
0.008	0.130	0.339	1.608
0.009	0.261	0.353	0.352
0.010	0.304	0.365	0.201
0.012	0.348	0.388	0.115
0.014	0.391	0.408	0.043
0.020	0.435	0.459	0.055
0.024	0.478	0.487	0.019
0.028	0.522	0.513	-0.017
0.038	0.565	0.567	0.004
0.044	0.609	0.595	-0.023
0.053	0.652	0.633	-0.029
0.074	0.696	0.707	0.016
0.084	0.739	0.737	-0.003
0.099	0.783	0.778	-0.006
0.114	0.826	0.816	-0.012
0.139	0.870	0.870	0.000
0.163	0.913	0.917	0.004
0.214	0.957	1.004	0.049

It is seen from Table 4.3 that the root mean square error is 0.252, which means the estimation is close to the observation. It can be seen from Figure 4.9 that the CDF increases from the channel bottom monotonically to 1 at the water surface. It grows slowly first from the channel bed up to 0.05mm, then faster for higher region, which might be caused by the effect of heavy sediments concentrated near the channel bed. The estimated curve fit the observation at most points but not all, for example, at the part near the channel bed, the estimation is smaller than the observed CDF. The assumption on the one-dimensional CDF shows the overall trend of prediction.

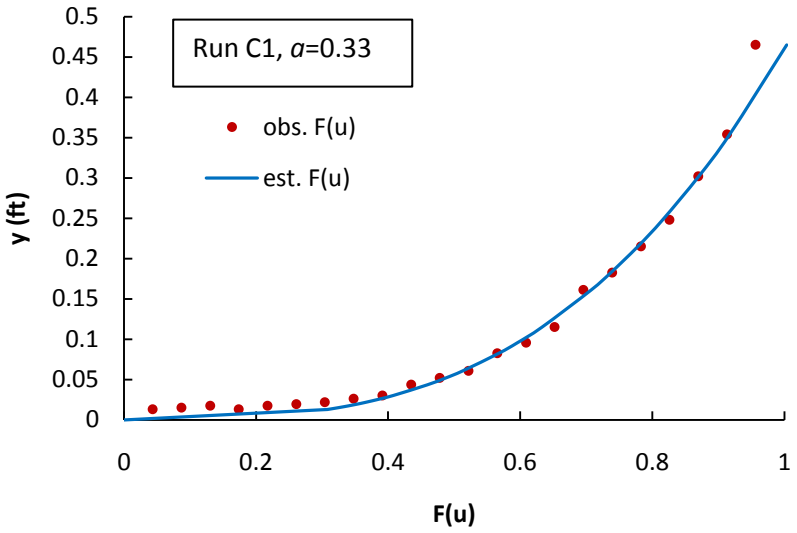

Figure 4.9 CDF of 1D velocity distribution for Einstein and Chien's data (Run C1)

The CDF has also been computed using equations (4-5) and (4-6) with the least square method comparing to equation (4-4) in Figure 4.10. It is seen from the figure that the most general equation (4-6) fit the observation slightly better than equations (4-5) and (4-4). However, the high accuracy of equation (4-6) cost too many parameters and it is not recommended for application. Thus, equation (4-4), which also can be considered as the simplification of equation (4-6) is reasonable.

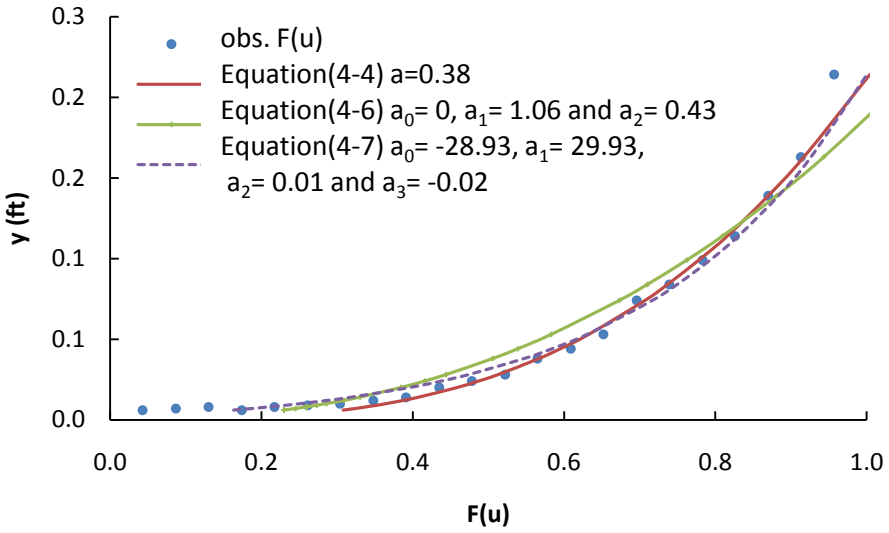

Figure 4.10 Comparison of hypotheses on the cumulative distribution function

5. DERIVATION OF VELOCITY DISTRIBUTION

The methodology used in this thesis is based on the principle of maximum entropy (POME). By maximizing the Tsallis entropy subject to the moment constraints, the least-biased probability distribution of random velocity can be obtained. When combined with pre-assumed flux-concentration relation, the space or time distribution of the random variable can be derived.

5.1 Entropy based velocity distribution

5.1.1 Tsallis entropy of velocity distribution

To apply the entropy theory, consider the time-averaged velocity *U* in a channel cross-section as a random variable and let *U* vary from 0 to u_{max}. According to the definition of Tsallis entropy [equation (2-3)], the entropy of velocity distribution can be written as:

$$H = \frac{1}{m-1}\left\{1 - \int_0^{u_{max}} [f(u)]^m \, du\right\} = \frac{1}{m-1}\int_0^{u_{max}} f(u)\{1 - [f(u)]^{m-1}\}du \quad (5\text{-}1)$$

where *u* = velocity value at a specified point, u_{max} = the maximum velocity of the cross-section, *f(u)* = the probability density function, and *m* = a real number, and for *m*>0 *H(u)* becomes a convex function.

Equation (5-1) expresses the relative Tsallis entropy for continuous velocity distribution, which is a measure for uncertainty of spatial distribution of *U* in a cross section associated with $f(u)$.

The objective is to determine the probability density function *f(u)*, which can be accomplished by maximizing the Tsallis entropy. In order to maximize the entropy *H(u)*, certain constraints need to be specified.

5.1.2 Specification of constraints

The first constraint comes from the satisfaction of the probability density function, which is

$$C_1 = \int_0^{u_{max}} f(u)du = 1 \tag{5-2}$$

To be more precise, this is not actually a constraint, for *f(u)* must always sum up to 1 in the whole range of *U*. For convenience of expression, it is often treated as a constraint if there are more than one constraint.

Additional constraints can be obtained from the laws of conservation of mass, momentum and energy which flow in open channels must satisfy. The constraint obtained from the conservation of mass in flow can be expressed as

$$\mathrm{C_2} = \int_0^{\mathrm{u_{max}}} \mathrm{uf(u)du} = \bar{\mathrm{u}} \tag{5-3}$$

where $\bar{u}$ is the cross-sectional mean velocity equal to *Q/A*. Here *Q* is the discharge rate and *A* is the cross-sectional area. Equation (5-3) is equivalent to satisfying the condition that *u* must be distributed over the cross-sectional area so that $\bar{u}A = Q$.

The third constraint can be obtained from the conservation of momentum equation, which can be written as

$$C_3 = \int_0^{u_{max}} u^2 f(u)du = \overline{u^2} = \beta\bar{u}^2 \tag{5-4}$$

in which β is the momentum distribution coefficient equal to $u^2/\bar{u}^2$, often referred to as the Boussinesq coefficient.

The last constraint, which is obtained from the conservation of energy equation, is expressed as

$$C_4 = \int_0^{u_{max}} u^3 f(u)du = \overline{u^3} = \alpha \bar{u}^3 \quad (5\text{-}5)$$

where α is the energy distribution coefficient referred to as the Coriolis coefficient.

According to Barbe et al. (1991), two constraints are considered enough to describe the velocity distribution accurately. Hence in this study, equations (5-2) and (5-3) will be applied as constraints.

5.1.3 Maximization of entropy

To maximize the entropy given by equation (5-1), subject to the specified constraint equations (5-2 and 5-3), the Lagrange multiplier method is employed. The Lagrangean function L can be expressed as:

$$L = \int_0^{u_{max}} \frac{f(u)}{m-1}\{1 - [f(u)]^{m-1}\}du + \lambda_0\left[\int_0^{u_{max}} f(u)du - 1\right] + \lambda_1\left[\int_0^{u_{max}} uf(u)du - \bar{u}\right] \quad (5\text{-}6)$$

in which λ_0 and λ_1 are the Lagrange multipliers.

Equation (5-6) can be maximized by letting $\frac{\partial L}{\partial f(u)} = 0$. Hence $f(u)$ is obtained:

$$f(u) = \left[\frac{m-1}{m}\left(\frac{1}{m-1} + \lambda_0 + \lambda_1 u\right)\right]^{\frac{1}{m-1}} \quad (5\text{-}7)$$

Equation (5-7) is the entropy-based probability density function (PDF) of velocity containing the Lagrange multipliers λ_0 and λ_1 as parameters.

To simplify equation (5-7), let $\lambda_* = \lambda_0 + \frac{1}{m-1}$, and replace $\lambda_0 + \frac{1}{m-1}$ with λ_*. Then one obtains

$$f(u) = \left[\frac{m-1}{m}(\lambda_* + \lambda_1 u)\right]^{\frac{1}{m-1}} \tag{5-8}$$

Substituting equation (5-8) in equation (5-1), the maximum entropy is achieved as:

$$H = \frac{1}{m-1} - \frac{1}{m}(\lambda_* + \lambda_1 \bar{u}) \tag{5-9}$$

Equation (5-9) is the entropy of velocity distribution expressed in terms of given information.

5.1.4 Determination of Lagrange multipliers

The probability density function, derived above, has two parameters λ_1 and λ_*, which can be computed from a non-linear system containing the two constraints. Substituting the entropy-based probability density function $f(u)$, equation (5-8), into equations (5-2) and (5-3) and integrating them from u=0 to u_{max}, the following two equations are obtained:

$$(\lambda_* + \lambda_1 u_{max})^{\frac{m}{m-1}} = \lambda_1 (\frac{m}{m-1})^{\frac{m}{m-1}} + (\lambda_*)^{\frac{m}{m-1}} \tag{5-10}$$

$$u_{max}(\lambda_* + \lambda_1 u_{max})^{\frac{m}{m-1}} + \frac{m-1}{2m-1}\frac{1}{\lambda_1}(\lambda_* + \lambda_1 u_{max})^{\frac{2m-1}{m-1}} - \frac{m-1}{2m-1}\frac{1}{\lambda_1}(\lambda_*)^{\frac{2m-1}{m-1}} = \lambda_1 \bar{u}\left(\frac{m}{m-1}\right)^{\frac{m}{m-1}} \tag{5-11}$$

These two equations should be solved simultaneously to compute λ_1 and λ_* for a given m value. Computation of these Lagrange multipliers will be discussed in Section 5.2.1.1.

5.1.5 General velocity distribution

With the hypothesis on the cumulative distribution function the next step is to compute velocity profiles using the entropy-based probability density function. To derive a general case, consider the density function in 2-D domain as (*x, y*), where *y* represents the depth from the channel bed and *x* represents the transverse distance from the center line. Since *u* is a function of *x* and *y*, $f(u)$ can be written as $f(u(x,y))$.

Since $f(u)$ is the derivative of the cumulative distribution function *F(u)*, taking the partial derivatives of *F(u)* with respect to *x* and *y*, the following two equations are obtained:

$$\frac{\partial F(u)}{\partial x} = \frac{\partial F(u)}{\partial u}\frac{\partial u}{\partial x} = f(u)\frac{\partial u}{\partial x} = \left[\frac{m-1}{m}(\lambda_* + \lambda_1 u)\right]^{\frac{1}{m-1}}\frac{\partial u}{\partial x} \tag{5-12}$$

$$\frac{\partial F(u)}{\partial y} = \frac{\partial F(u)}{\partial u}\frac{\partial u}{\partial y} = f(u)\frac{\partial u}{\partial y} = \left[\frac{m-1}{m}(\lambda_* + \lambda_1 u)\right]^{\frac{1}{m-1}}\frac{\partial u}{\partial y} \tag{5-13}$$

$$\text{Now define a new variable w} = \left[\frac{m-1}{m}(\lambda_* + \lambda_1 u)\right]^{\frac{m}{m-1}}. \tag{5-14}$$

Compute partial derivatives of w with respect to *x* and *y*,

$$\frac{\partial w}{\partial x} = \frac{\partial w}{\partial u}\frac{\partial u}{\partial x} = \lambda_1\left[\frac{m-1}{m}(\lambda_* + \lambda_1 u)\right]^{\frac{1}{m-1}}\frac{\partial u}{\partial x} \tag{5-15}$$

$$\frac{\partial w}{\partial y} = \frac{\partial w}{\partial u}\frac{\partial u}{\partial y} = \lambda_1\left[\frac{m-1}{m}(\lambda_* + \lambda_1 u)\right]^{\frac{1}{m-1}}\frac{\partial u}{\partial y} \tag{5-16}$$

Comparing equations (5-15) and (5-16) with equations (5-12) and (5-13), the relationship between *F(u)* and *w* can be formed as:

$$\frac{\partial w}{\partial x} = \lambda_1\frac{\partial F(u)}{\partial x} \tag{5-17}$$

$$\frac{\partial w}{\partial y} = \lambda_1 \frac{\partial F(u)}{\partial y} \tag{5-18}$$

Equations (5-17) and (5-18) can be seen as a system of linear differential equations, which can be solved using the Leibnitz rule:

$$\int_{(0,0)}^{(x,y)} \frac{\partial w}{\partial x} dx + \frac{\partial w}{\partial y} dy = w(x,y) - w(0,0) \tag{5-19}$$

Since the point with coordinates (0, 0) lies on the channel floor, which has the velocity u= 0, w(0,0) on the right hand side of equation (5-19) equals $\left[\frac{\mathrm{m}-1}{\mathrm{m}}(\lambda_*)\right]^{\frac{\mathrm{m}}{\mathrm{m}-1}}$ from equation (5-14). Hence the right hand side of equation (5-19) now becomes

$$w(x,y) - w(0,0) = w(x,y) - \left[\frac{m-1}{m}(\lambda_*)\right]^{\frac{m}{m-1}} \tag{5-20}$$

The definite integral on the left hand side of equation (5-19) can be calculated at a generic point of coordinate $(\bar{x}, \bar{y})$ which is identified by means of a polygonal curve that starts from the origin of axes (0, 0), passing through the point $(\bar{x}, 0)$ and ends at $(\bar{x}, \bar{y})$. The cumulative distribution function *F(u)* is constantly 0 at point (0, 0) to $(\bar{x}, 0)$. Thus using equations (5-17) and (5-18), the integral of equation (5-19) yields:

$$\int_{(0,0)}^{(\bar{x},\bar{y})} \lambda_1 \frac{\partial F(u)}{\partial x} dx + \lambda_1 \frac{\partial F(u)}{\partial y} dy = \int_0^{\bar{y}} \lambda_1 \frac{\partial F(u)}{\partial y} dy = \lambda_1 F(u) \tag{5-21}$$

Combining equation (5-21) with equation (5-20),

$$\int_{(0,0)}^{(x,y)} \frac{\partial w}{\partial x} dx + \frac{\partial w}{\partial y} dy = \int_{(0,0)}^{(\bar{x},\bar{y})} \lambda_1 \frac{\partial F(u)}{\partial x} dx + \lambda_1 \frac{\partial F(u)}{\partial y} dy \tag{5-22}$$

Hence, *w(x, y)* can be obtained as:

$$w(x,y) = \lambda_1 F(u) + \left[\frac{m-1}{m}(\lambda_*)\right]^{\frac{m}{m-1}} \tag{5-23}$$

Substituting the definition of *w* from equation (5-23) into equation (5-14), the velocity distribution function is obtained as:

$$u = -\frac{\lambda_*}{\lambda_1} + \frac{1}{\lambda_1}\frac{m}{m-1}\left[\lambda_1 F(u) + \left(\frac{m-1}{m}\lambda_*\right)^{\frac{m}{m-1}}\right]^{\frac{m-1}{m}} \tag{5-24}$$

Hence, the general velocity distribution is derived using the Tsallis entropy. With equation (5-24), the velocity distribution in both 1D and 2D can be obtained, according to whether the 1D or 2D cumulative distribution function *F(u)* is used.

5.1.6 Dimensionless parameter *G*

The method of computing the Lagrange multipliers, λ_1 and λ_*, is difficult, because equations (5-10) and (5-11) form a set of non-linear equations. In Chiu's velocity method, there's a dimensionless parameter *M* defined by $\lambda_1 u_{max}$ to reduce the computational difficulty, which can also act as an index for characterizing and comparing various patterns of the velocity distribution (Chiu, 1988). In a similar manner, a dimensionless parameter *G* can be defined in the following way:

$$G = \frac{\lambda_1 u_{max}}{\lambda_1 u_{max} + \lambda_*} \tag{5-25}$$

Inputting *F(u)*=1, the u_{max} can be obtained from equation (5-24), which is

$$u_{max} = -\frac{\lambda_*}{\lambda_1} + \frac{1}{\lambda_1}\frac{m}{m-1}\left[\lambda_1 + \left(\frac{m-1}{m}\lambda_*\right)^{\frac{m}{m-1}}\right]^{\frac{m-1}{m}} \tag{5-26}$$

Dividing equation (5-24) by equation (5-26) with *G* instead of λ_1 and λ_*, the following equation is obtained:

$$\frac{u}{u_{max}} = 1 - \frac{1}{G}\left(1 - \left(\left(\frac{m}{m-1}\right)^{\frac{m}{m-1}}\frac{G}{u_{max}}(F(u)-1) + 1\right)^{\frac{m-1}{m}}\right) \tag{5-27}$$

Substituting u_0=0, the velocity distribution in equation (5-27) can be simplified as:

$$\frac{u}{u_{max}} = 1 - \frac{1}{G}\left(1 - \left((1-G)^{\frac{m}{m-1}} + \left(1 - (1-G)^{\frac{m}{m-1}}\right)F(u)\right)^{\frac{m-1}{m}}\right) \qquad (5\text{-}28)$$

With the known CDF in equation (4-1), the velocity distribution can now be obtained with a single parameter *G*. Assume *m*= 3, when *x*= 0 the density function *F(u)* is determined by *a* only, thus the velocity distribution varies with different *a* and *G* values, as shown in Figure 5.1. It is seen from the figure that a bigger *G* value tends to slow the growth of the velocity from the channel bed to the water surface, while *a* plays the opposite role. Comparing the effect of the two parameters, the velocity distribution is more sensitive to *a* than *G*. The method to compute the dimensionless parameter *G* and the importance of this parameter will be discussed in a Sections5.2.1.1 and 5.3.

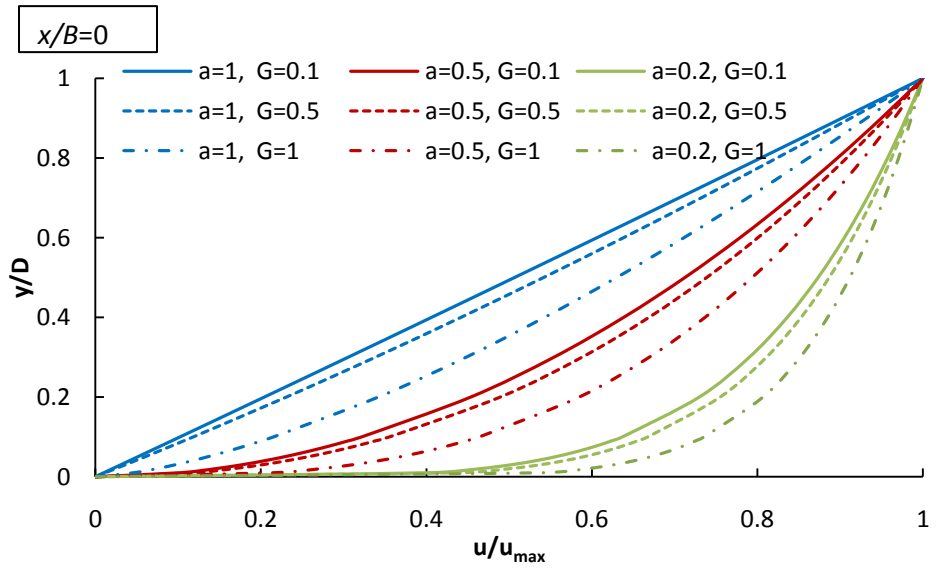

Figure 5.1 The velocity distribution for various *a* and *G* values

5.2 Application of velocity distribution

5.2.1 Computation methods

There are two methods to compute velocity profiles: one is the original method which directly solves the set of non-linear equations; and the other makes use of the dimensionless parameter *G*. Either method is feasible, while the second is more convenient.

5.2.1.1 Use of Lagrange multipliers

Equations (5-10) and (5-11) can be solved simultaneously to obtain the Lagrange multipliers λ_1 and λ_* for a given *m* value. According to the definition of the Tsallis entropy, entropy becomes a convex function when $m>0$. Thus, *m* should keep positive to maintain the entropy function convex, so that the maximum entropy can be achieved. Table 5.1 shows the results of solving λ_1 and λ_* for different *m* values in several rivers. It can be observed that the λ value tends to decrease with increasing *m* value. A bigger *m* value leads to more difficulty in solving the equations and the solutions of λ values for bigger *m* values are not as stable as smaller ones. To that end, it seems inappropriate for *m* to exceed a value of 3 or 4.

Table 5.1 Computation of λ values for different *m* values for Italian River data

River	*m*	1.5	2	3	4	5
Ponte Felcino	λ_1	0.101	0.055	0.016	0.005	0.001
	λ_*	0.464	0.503	0.106	0.027	0.001
Roscinano	λ_1	0.194	0.123	0.050	0.020	0.001
	λ_*	0.676	0.667	0.191	0.067	0.249
Santa Lucia	λ_1	0.863	0.608	0.319	0.172	0.051
	λ_*	1.388	0.543	0.177	0.076	0.018

Table 5.1 continued

River	m	1.5	2	3	4	5
	λ_1	0.450	0.331	0.182	0.100	0.031
Pontelagoscuro1	λ_*	1.816	0.811	0.302	0.141	0.037
	λ_1	0.442	0.335	0.194	0.113	0.038
Pontelagoscuro2	λ_*	1.906	0.883	0.352	0.174	0.051

Table 5.2 and Figure 5.2 show the impact of m on predicting the velocity distribution. It is seen from the computed coefficient of determination (R^2) between estimated and observed values in Table 5.2 that the bigger m values result in better R^2, which means a bigger m leads to a more accurate prediction.

Table 5.2 R^2 values for different m values

m	1.5	2	3	4	5
Ponte Felcino	0.943	0.959	0.977	0.980	0.989
Roscinano	0.940	0.956	0.982	0.985	0.990
Santa Lucica	0.938	0.952	0.978	0.980	0.988
Pontelagoscuro1	0.952	0.963	0.982	0.983	0.985
Pontelagoscuro2	0.934	0.957	0.979	0.987	0.988

It is seen from the Figure 5.2 that the dimensionless velocity distribution was computed for various m values with CDF with a=0.2, b=1. Compared to the data from Ponte Felcino River, it is seen that m=3, 4 and 5 curves fit the observations better than others, and with increasing m value, the velocity curves have less difference than those when m is small. For velocity near the surface, observations are more likely to fit the curve for m=5, while for the velocity close to the channel bed, the observations tend to be close to the curve for m=3. To sum up, considering the difficulties in solving the equations, m=3 seems to be the best choice, which leads to a reasonably accurate velocity distribution.

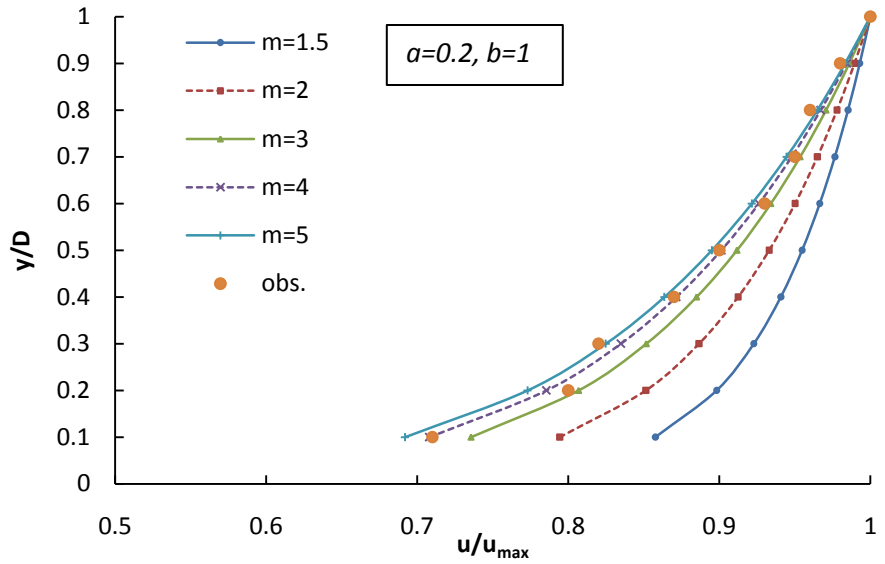

Figure 5.2 Dimensionless velocity distribution for various *m* values (data from Ponte Felcino River, Italy)

5.2.1.2 Use of dimensionless parameter G

If *m*=3 is defined, equation (5-28) can be further simplified as:

$$\frac{u}{u_{max}} = 1 - \frac{1}{G}\left(1 - \left((1 + 0.5\ln G)F(u) - 0.5\ln G\right)^{\frac{2}{3}}\right) \tag{5-29}$$

The key step is to determine the value of dimensionless parameter *G*. According to the experience with Chiu's (1988) method of determining parameter *M*, the relationship between the mean velocity and the maximum velocity is the key. To obtain the analytical solution of the mean velocity, equation (5-29) can be integrated over the whole cross-section:

$$\bar{u} = \frac{1}{A}\int u dA = \frac{1}{A}\int u_{max}\left[1 - \frac{1}{G}\left(1 - \left((1 + 0.5\ln G)F(u) - 0.5\ln G\right)^{\frac{2}{3}}\right)\right] dA \tag{5-30}$$

The mean velocity now can be written as some function of *G* multiplied by u_{max}, which is $\bar{u} = \psi(G)u_{max}$. If the function $\psi(G)$ is known, the value of *G* can be easily

obtained through $\bar{u}/u_{max}$. However, an analytical solution of equation (5-30) is difficult to obtain, hence the numerical methods are applied.

For the data from the Iranian and the Italian rivers, according to the definition of parameter G [equation (5-25)], the value of G can be computed using the Lagrange multipliers method described in the previous section. Results can be found in Appendix E. Then, its relation with the mean and maximum velocity data is simulated in Figure 5.3. The trend line can be simulated with a second order polynomial function which has a coefficient of determination as high as 0.997.

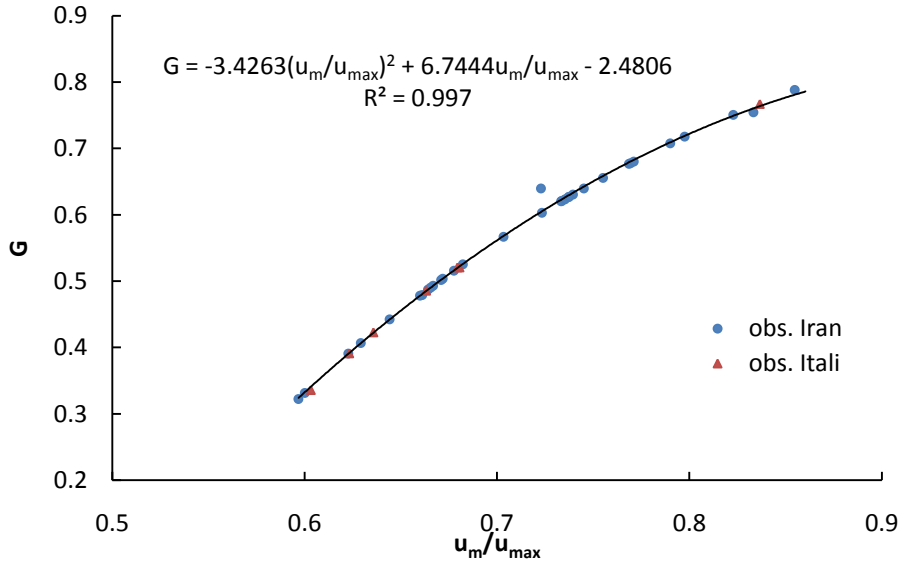

Figure 5.3 The relationship between G and u_m/u_{max}

Thus, Equation (5-30) can be simulated from observed data as

$$\frac{\bar{u}}{u_{max}} = 0.554G^2 - 0.077G + 0.568 \qquad (5\text{-}31)$$

Equation (5-31) can be used to determine the value of G with given mean and maximum velocity at a cross-section. Table 5.3 shows the difference between two

methods in computation of the *G* values. *G1* is the computation from the definition [Equation (5-25)], and *G2* is the result from equation (5-31). It is seen from the difference, which has a mean value about 0.003. Thus, it is safe to use Equation (5-31) instead of the Lagrange multiplier method.

Table 5.3 The difference in computation of G values

u_{max}	u_{mean}	*G1*	*G2*	*Difference (G1-G2)*
0.524	0.348	0.487	0.488	0.000
0.491	0.335	0.525	0.526	-0.001
0.582	0.421	0.603	0.606	-0.003
0.578	0.424	0.621	0.624	-0.003
0.575	0.345	0.331	0.333	-0.002
0.607	0.378	0.391	0.391	0.000
1.071	0.708	0.479	0.481	-0.002
0.885	0.584	0.478	0.478	0.000
0.774	0.516	0.493	0.493	0.000
0.682	0.493	0.639	0.605	0.035
0.824	0.614	0.640	0.643	-0.003
0.778	0.598	0.677	0.680	-0.003
0.746	0.574	0.678	0.681	-0.003
0.642	0.435	0.516	0.517	-0.001
0.585	0.393	0.504	0.504	-0.001
0.502	0.370	0.626	0.630	-0.003
0.450	0.347	0.680	0.683	-0.003
0.469	0.374	0.718	0.719	-0.002
0.657	0.519	0.707	0.710	-0.002
0.743	0.561	0.656	0.659	-0.003
0.735	0.539	0.620	0.623	-0.003
0.660	0.543	0.751	0.749	0.001
0.660	0.488	0.630	0.633	-0.003
0.550	0.366	0.490	0.491	0.000
0.480	0.302	0.407	0.407	0.000
0.635	0.426	0.502	0.502	-0.001
0.710	0.522	0.623	0.626	-0.003
0.739	0.441	0.323	0.324	-0.002
0.592	0.506	0.788	0.781	0.007
0.899	0.579	0.442	0.442	0.000
0.971	0.683	0.567	0.569	-0.002

Table 5.3 continued

u_{max}	u_{mean}	*G1*	*G2*	*Difference (G1-G2)*
0.810	0.675	0.755	0.761	-0.006
0.899	0.663	0.627	0.630	-0.003

5.2.2 2D Velocity distribution

Now the velocity distribution can be computed. Either equation (5-24) with the Lagrange multiplier method or equation (5-29) with the dimensionless parameter *G* can be applied with the assumed CDF. In this study the second method with parameter *G* is preferred.

Table 5.4 shows the computed velocity distribution of Ponte Felcino River in Italy, which has a *G* value of 0.336. The relative error is computed as (est.-obs.)/obs. The root mean square error for the whole cross section is 0.927. The computed errors were plotted in Figure 5.4, which shows that the error is normally distributed around 0.

Table 5.4 Computed velocity at Ponte Felcino River, Italy

x (m)	y′ (m)	obs. u (m/s)	est. u (m/s)	relative error	x (m)	y′ (m)	obs. u (m/s)	est. u (m/s)	relative error
-18.860	0.000	0.830	0.746	-0.101	10.490	0.000	1.780	1.269	-0.287
-18.860	0.060	0.830	0.779	-0.061	10.490	0.060	1.780	1.355	-0.239
-18.860	0.200	0.740	0.840	0.135	10.490	1.000	2.150	2.042	-0.050
-18.860	1.000	0.640	1.031	0.610	10.490	2.000	2.320	2.416	0.041
-18.860	2.000	1.150	1.158	0.007	10.490	3.000	2.570	2.546	-0.009
-18.860	3.000	0.960	1.031	0.074	10.490	3.500	2.320	2.404	0.036
-18.860	3.900	0.740	0.799	0.079	10.490	4.600	1.950	1.974	0.012
-18.860	4.100	0.710	0.672	-0.053	10.490	5.000	1.610	1.733	0.077
-18.860	4.250	0.000	0.000	0.000	10.490	5.700	0.000	0.000	0.000
-10.460	0.000	2.060	1.937	-0.060	7.340	0.000	2.360	2.504	0.061
-10.460	0.060	2.060	1.965	-0.046	7.340	0.200	2.610	2.536	-0.028
-10.460	0.200	2.340	2.025	-0.135	7.340	1.000	2.700	2.640	-0.022

Table 5.4 continued

x (m)	y′ (m)	obs. u (m/s)	est. u (m/s)	relative error	x (m)	y′ (m)	obs. u (m/s)	est. u (m/s)	relative error
-10.460	1.000	2.310	2.269	-0.018	7.340	2.000	2.740	2.738	-0.001
-10.460	1.930	2.440	2.457	0.007	7.340	2.930	2.610	2.647	0.014
-10.460	2.880	2.190	2.264	0.034	7.340	3.880	2.530	2.523	-0.003
-10.460	3.880	2.060	1.928	-0.064	7.340	4.880	2.320	2.314	-0.003
-10.460	4.280	1.650	1.665	0.009	7.340	5.380	0.980	2.117	1.160
-10.460	4.480	1.590	1.413	-0.111	7.340	5.700	1.190	1.837	0.544
-10.460	4.630	0.000	0.000	0.000	7.340	5.850	0.000	0.000	0.000
-6.290	0.000	2.990	2.980	-0.003	0.000	0.000	3.360	3.360	0.000
-6.290	0.060	2.990	2.974	-0.005	0.000	0.060	3.360	3.354	-0.002
-6.290	0.200	2.660	2.960	0.113	0.000	0.200	3.160	3.340	0.057
-6.290	0.800	2.820	2.896	0.027	0.000	1.000	3.200	3.252	0.016
-6.290	1.710	2.660	2.785	0.047	0.000	2.000	3.280	3.125	-0.047
-6.290	3.000	2.610	2.583	-0.010	0.000	3.000	2.910	2.970	0.021
-6.290	4.000	2.360	2.358	-0.001	0.000	4.000	2.780	2.766	-0.005
-6.290	5.000	1.950	1.958	0.004	0.000	5.000	2.320	2.461	0.061
-6.290	5.200	1.600	1.812	0.132	0.000	5.800	2.030	1.964	-0.032
-6.290	5.450	1.460	1.499	0.027	0.000	6.000	1.860	1.670	-0.102
-6.290	5.600	0.000	0.000	0.000	0.000	6.150	0.000	0.000	0.000

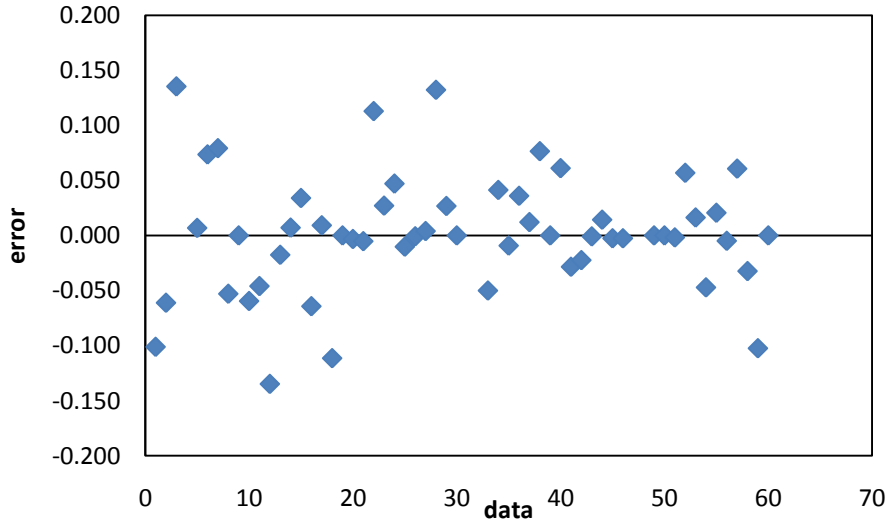

Figure 5.4 Distribution of relative errors computed for velocity distribution of Italian data at Ponte Felcino

Figure 5.5 shows plots of simulated velocity profiles which can be divided into three portions. In the first region from the channel bed to some depth about 0.2m, the velocity distribution on each vertical line increases slowly. Then it starts to grow faster to the maximum velocity, which is the second region. At last the velocity decreases from the maximum to some value at the water surface, where the decreasing rate is similar to the increasing rate in the second region. It can be concluded that the slow increase in the first region is caused by the resistance due to the bed shear stress, so that beyond the bed effective region the velocity grows faster. In the third portion, it is the secondary current which retards the velocity from growing to the water surface.

The highlighted point is the maximum velocity observed from each vertical line. The estimation can capture these points well. Comparing the curves in Figure 5.5, it is found that the farther from the center line the lower the location of the maximum velocity occurring, which exactly meets the analysis of Yang et. al (2004). Overall, the estimated values fit the observed values reasonably well with the coefficient of determination between the estimation and observation as high as 0.977.

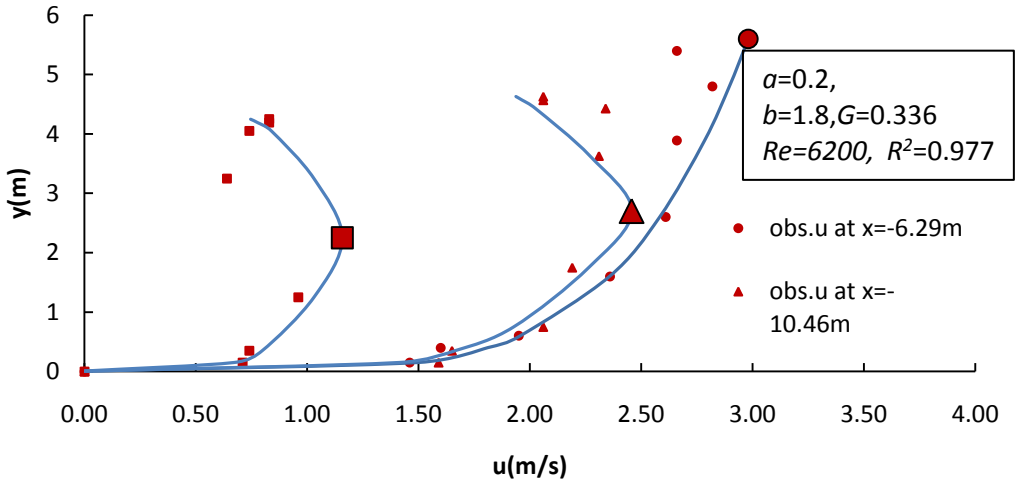

(a)

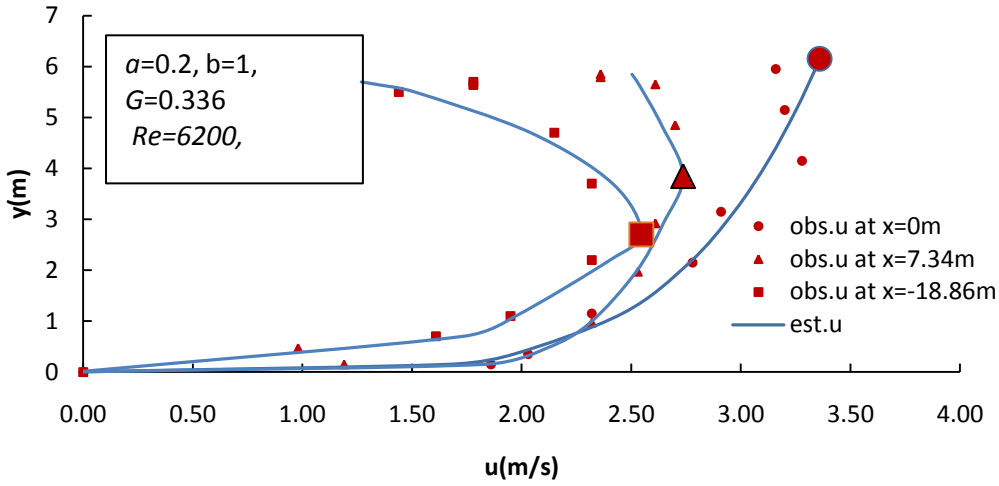

(b)

Figure 5.5 Simulation of velocity distribution of Italian data at Ponte Felcino: (a) The velocity at left ride of cross-section, and (b) the velocity at right side

The estimated velocity distribution for the whole cross-section can be observed from the Isovels in Figure 5.6. Though the velocity is not estimated point to point, the overall trend of isovels provides a reasonable idea. Compared to the observation, the

estimated isovels are shown to be more uniformly distributed than observation. It is because the velocity distribution reached through POME is meaningful to seek the distribution with the maximum entropy, which turns out as the most uniform model under the given constraints. Similar to the contours of CDF, the velocity estimated around the channel boundary is generally acceptable in this method.

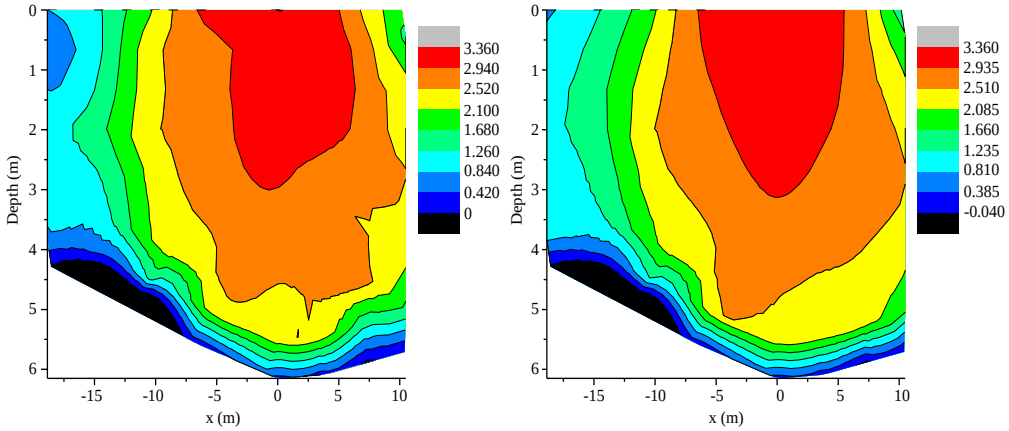

Figure 5.6 Isovels of Italian data at Ponte Felcino: (a) Isovels of observed value, and (b) Isovels of estimated value

For further verification, 4 more sets of Italian data and 20 sets of Iranian data are computed. Results can be found in Appendix E. Figure 5.7 shows results of 4 sets computations, which shows the validity of the entropy-based.

It is seen from Figures 5.7, the maximum velocities were captured correctly for each vertical line. The velocity distribution in Figures 5.7 (a) and (b) are similar with that discussed in Figure 5.5, in which the velocity increases to maximum and decreases to some value up to the water surface. The location of the maximum velocity is also

decreasing with the distance from the center. However, the velocity distribution collected from the Iranian River shown in Figure 5.7 (c) and (d) shows different patterns. Without knowing the location of each profile, it is hard to determine whether the profile is obtained from a line near the center or the boundary. It is seen from Figure 5.7(c) that profile 4 has the largest velocity value, which is supposed to be the nearest to the center line, while the location of the maximum velocity in this profile is the lowest. Similar patterns can be found in profiles 1 and 5 of Figure 5.7 (d). But overall, the estimation of the velocity was reasonable.

It can be concluded from the above analysis that the entropy-based method employed in this thesis performs well in predicting two-dimensional velocity profiles in open channels. Other than previous models, this method cannot only describe the overall trend of the velocity accurately, but also can capture the lower value of velocity near the channel bed. More comparison will be processed in later chapters.

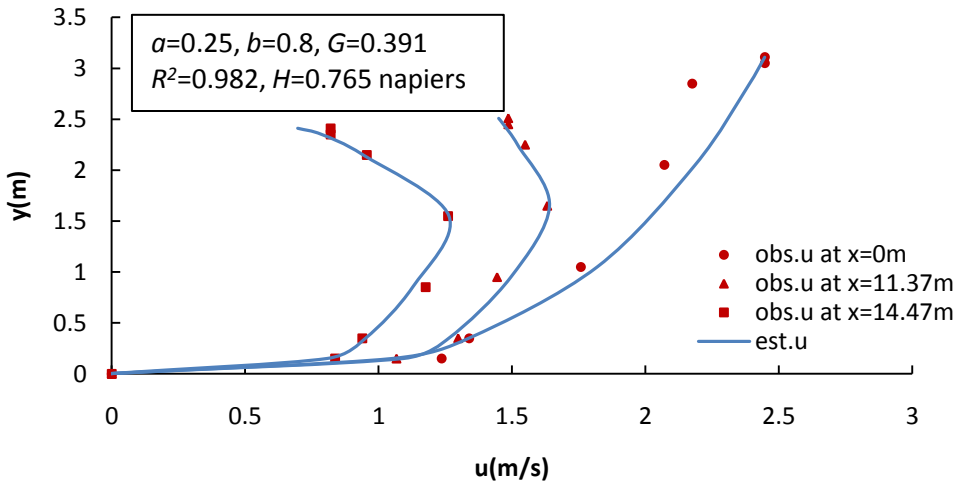

(a)

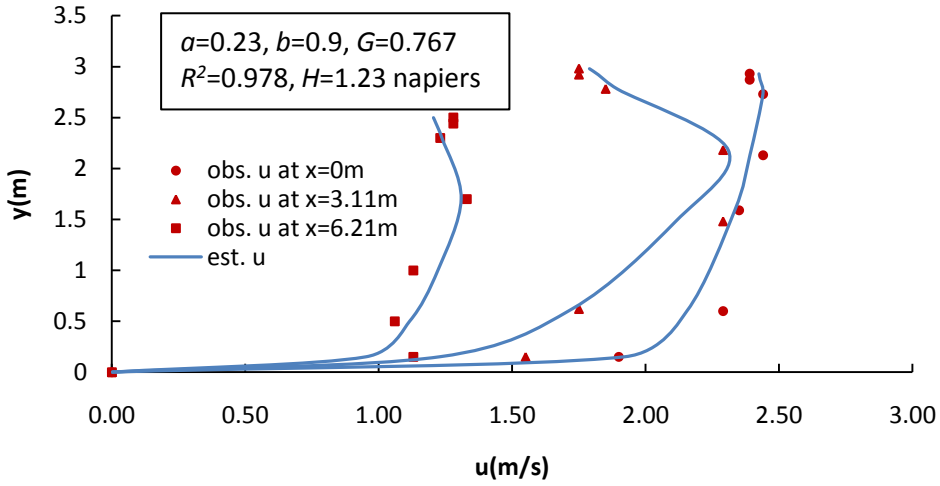

(b)

Figure 5.7 2D velocity distributions: (a) Velocity distribution at Rosciano (Italy), (b) Velocity distribution at Santa Lucia (Italy), (c) Velocity distribution of Run A2-1 (Iran), and (d) Velocity distribution of Run B9-1 (Iran)

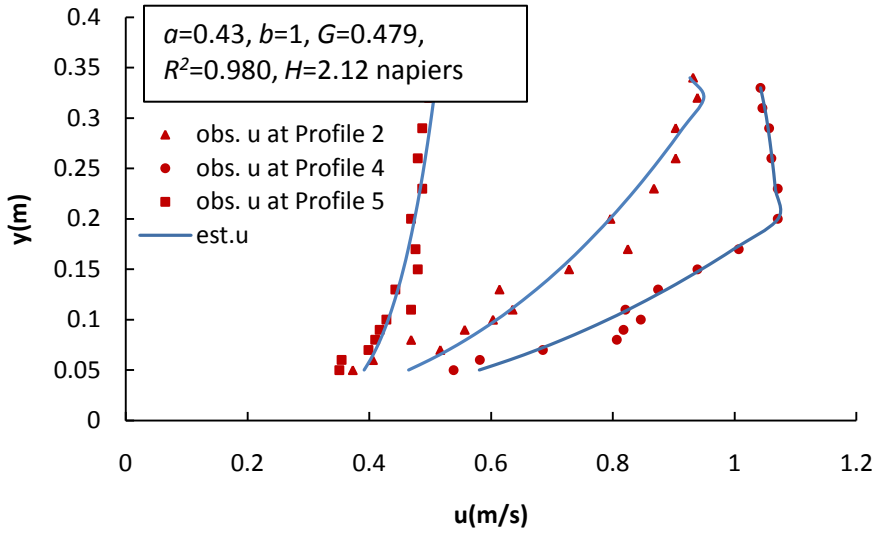

(c)

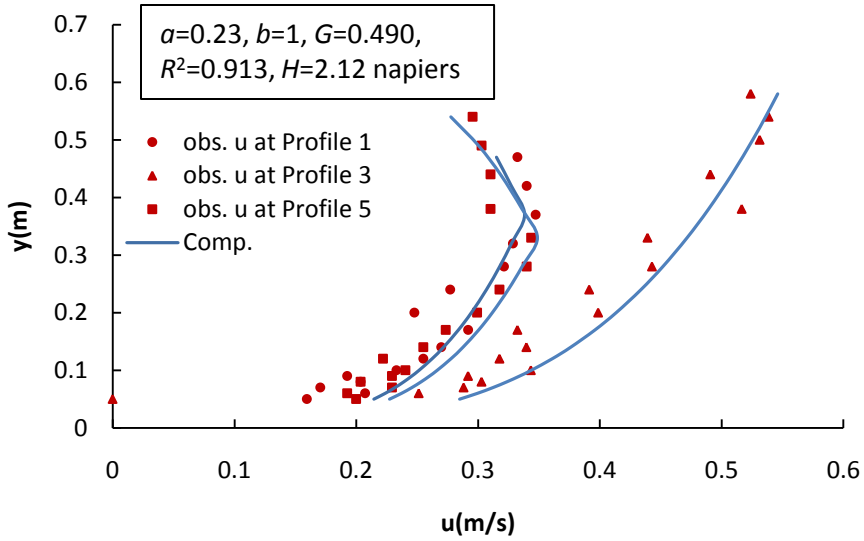

(d)

Figure 5.7 continued

In Chiu's (1988, 1989) study, the dimensionless parameter was shown as a index of the flow status, and it gives a range for laminar and turbulence flow. To analyze the possible information about the flow characteristics, the Reynolds number was computed as

$$R_e = \frac{QD_H}{\nu A} \tag{5-32}$$

where Q is the flow discharge, D_H is the hydraulic diameter, ν is the kinematic viscosity, and A is the flow area. Results are shown in Table 5.5, in which H represents the entropy computed through equation (5-9).

Table 5.5 Summary of velocity characteristics for Italian data

Location	Date	u_{max} (m/s)	Q (m^3/s)	A (m^2)	D (m)	Re	G	H (napiers)
P. Nuovo	Nov. 15, 1982	2.023	159.19	146.74	2.9	1882	0.520	0.925
P. Nuovo	Nov. 18, 1996	2.597	541.58	311.91	6.64	5992	0.485	0.882
P. Nuovo	Jun. 03, 1997	2.719	506.39	278.16	6.07	5824	0.521	0.925
Rosciano	May 28, 1984	2.583	156.24	87.6	3.2	3084	0.423	0.804
Rosciano	Nov. 20, 1996	2.447	131.2	86.03	3.11	2581	0.391	0.765
P. Felcino	Apr. 21, 1997	3.365	399.16	188.26	6.15	6201	0.336	0.696
S. Lucia	May 28, 1984	2.437	96.53	51.53	2.93	2745	0.767	1.231

It is seen from the above results that the relation between G and the Reynolds number is not as clear as found by Chiu (1988). It seems like for a higher Reynolds number, the G value tends to be smaller, while due to the lack of data it is not obvious. However, it is found that the higher G value might imply a higher entropy value, which

means more uniform distribution. It might be related that for the laminar flow with a higher *G* value whose entropy tends to be bigger, and vise versa; for the turbulent flow with a lower *G* value whose entropy should be smaller; however, it is yet to be concluded.

5.2.3 1D velocity distribution

The 1D velocity distribution can be seen as a special case of the 2D velocity distribution and can be computed in exactly the same way. However, some adjustment should be made first.

Following the same procedure as in Section 5.2.2, the velocity can be obtained with one-dimensional CDF computed as in Table 4.3. The value of G is used using the mean and maximum velocity from known observations. Table 5.6 shows the computed velocity distribution for 1D Einstein and Chien's (1955) data (Run C1). The error was computed in the same way as was done previously, which turns out to be normally distributed around 0.

Table 5.6 Computed velocity distribution of Einstein Chien's (1955) data (Run C1)

y (ft)	obs. u (ft/s)	est. u (ft/s)	error
0.006	2.745	2.641	-0.038
0.006	2.452	2.641	0.077
0.007	2.510	2.747	0.094
0.008	2.831	2.842	0.004
0.008	2.643	2.842	0.075
0.009	2.858	2.926	0.024
0.010	2.960	3.003	0.015
0.012	3.136	3.144	0.003
0.014	3.167	3.265	0.031

Table 5.6 continued

y (ft)	obs. u (ft/s)	est. u (ft/s)	error
0.020	3.566	3.566	0.000
0.024	3.871	3.728	-0.037
0.028	3.933	3.873	-0.015
0.038	4.203	4.171	-0.008
0.044	4.516	4.322	-0.043
0.053	4.583	4.519	-0.014
0.074	4.903	4.901	0.000
0.084	5.161	5.051	-0.021
0.099	5.239	5.253	0.003
0.114	5.372	5.435	0.012
0.139	5.603	5.697	0.017
0.163	5.885	5.916	0.005
0.214	6.295	6.311	0.003

The velocity distribution of this data set was obtained with a high value of *G* and got a high value of entropy, which can be seen from the Figure 5.8; it seems the data is likely to be uniformly distributed. It is seen from the figure that the bed effective region for this data set is very small only about 0.01ft, so the velocity distribution can considered as monotonically increasing from the channel bed to the water surface. Figure 5.8 shows the agreement between estimated and observed velocity values. It is clear that the agreement is reasonable, with the coefficient of determination equal to 0.97. The estimated curve increases from the channel bed to the water surface across observations. Unlike the classical method, the velocity distribution computed here can also capture lower values of velocity near the channel bed.

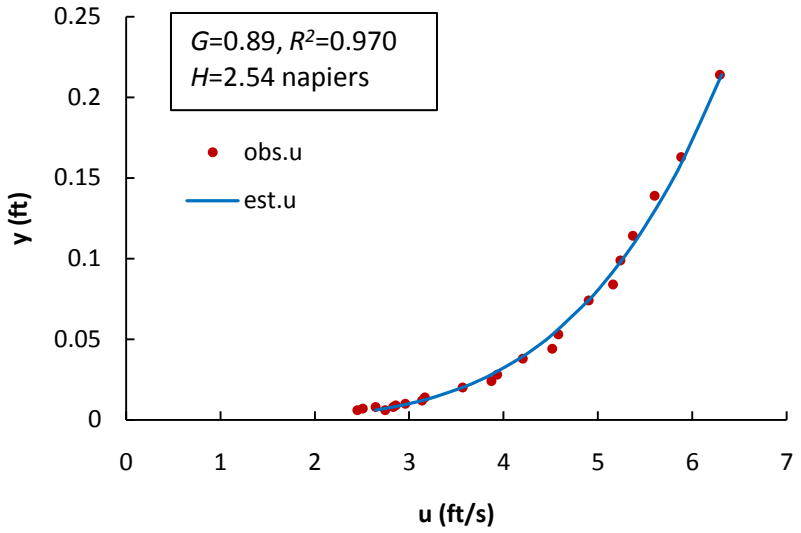

Figure 5.8 Estimate of 1D velocity distribution

To sum up, the Tsallis entropy based method derived in this study is a good predictor for both 1D and 2D velocity distributions. It can simulate the observations reasonably well in the whole cross-section and gives good results at the boundaries. More advantages will be discussed in the next chapter.

5.3 Maximum and mean velocity

The maximum velocity and mean velocity carry important information in open channel hydraulics. Most of the time, the velocity distribution in the whole cross-section is hard to obtain. However, the maximum velocity provides the range of velocity and the mean velocity is needed in the governing equations for transport of mass, momentum and energy through a channel cross-section. In the following section, the location of these velocities and their values are discussed.

5.3.1 Location of maximum velocity

It is known that in natural channels that are not wide enough, the maximum velocity occurs below the water surface (Francis 1878; Stearns 1883). Not only is the maximum velocity along the vertical in the center of the channel is located below the surface, the maximum velocity on each vertical line is also below the surface. As shown in Figure 5.6, isovels in a natural channel are convex and the location of maximum velocity in each vertical direction is not under the same depths.

The velocity distribution varies from one vertical line to another, and the flow near the wall is more affected by the boundary shear and vegetation if there is any. Also the flow near the wall is dominated by secondary flow, which transports low-momentum fluids to the center and high-momentum fluids to the bed. As a result, the depth of maximum velocity varies with location.

Yang (2004) discussed that the depth of maximum velocity is mainly related to the lateral position of velocity profiles in natural channels. It is seen from Figure 5.9 that the location of maximum velocity, h/D, is more likely below the water surface when the G value is bigger than 0.5.

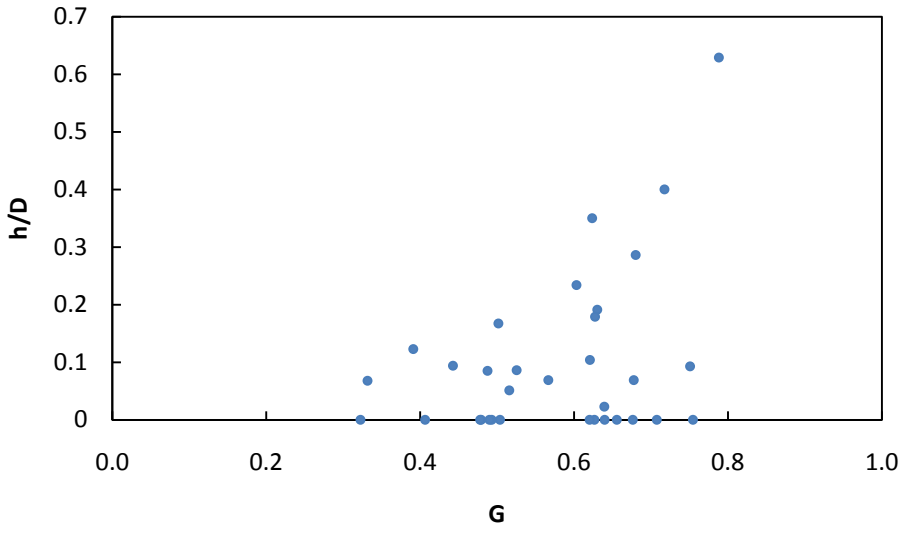

Figure 5.9 Location of maximum velocity

To determine the location of the maximum velocity below the water surface, one needs to consider the bed shear stress as

$$\tau = \rho g S_f (D - h) = \rho \varepsilon_0 \frac{du}{dy}|_{y=0} \tag{5-33}$$

where S_f= friction slope; ε_0 = momentum transfer coefficient at the channel bed, which is equal to the kinematic viscosity of the fluid; du/dy can be computed from Equation (5-29) with the modified cumulative distribution function [equation (4-3)], as mentioned in Section 4.1.4.

$$\frac{du}{dy} = u_{max} a \frac{m-1}{m} \left(1 - \left(\frac{x}{B}\right)^2\right)^{\frac{m-1}{m}} \frac{h_y}{D} \left(\frac{y}{D} h_y\right)^{\left(a\frac{m-1}{m}-1\right)} \tag{5-34}$$

According to the Darcy-Weisbach equation

$$\frac{\bar{u}}{u_*} = \sqrt{\frac{8}{f}} \tag{5-35}$$

Equation (5-33) combined with equation (4-3) yields to the following relation:

$$\left(1-\frac{h_y}{D}\right)^2=\frac{\varepsilon_0}{\nu}\frac{8}{fR_e}\frac{1}{G}\left(\frac{m-1}{m}\right)\left[\left(1-\frac{x}{B}\right)\exp\left(\frac{x}{B}\right)\right]^{\frac{m-1}{m}} \quad (5\text{-}36)$$

where R_e= Reynolds number.

Using equation (5-35) the location of the maximum velocity can be determined. Equation (5-35) gives the relation between depth and parameter *G* and transverse distance z, which shows that the previous assumption makes sense.

If h is defined as the depth from the water surface where the maximum velocity happens, where $\frac{y}{D}h_y=1$, according to the density function, then

$$h=\frac{D}{h_y}=1-\sqrt{\frac{\varepsilon_0}{\nu}\frac{8}{fR_e}\frac{1}{G}\left(\frac{m-1}{m}\right)\left[\left(1-\frac{x}{B}\right)exp\left(\frac{x}{B}\right)\right]^{\frac{m-1}{m}}} \quad (5\text{-}37)$$

For *x*=0, equation (5-37) reduces to

$$h=\frac{D}{h_y}=1-\sqrt{\frac{\varepsilon_0}{\nu}\frac{8}{fR_e}\frac{1}{G}\left(\frac{m-1}{m}\right)} \quad (5\text{-}38)$$

Figure 5.10 shows the computed location of maximum velocity *h/D* on several vertical lines of experimental data. The estimated *h/D* represents the mean value of observed values.

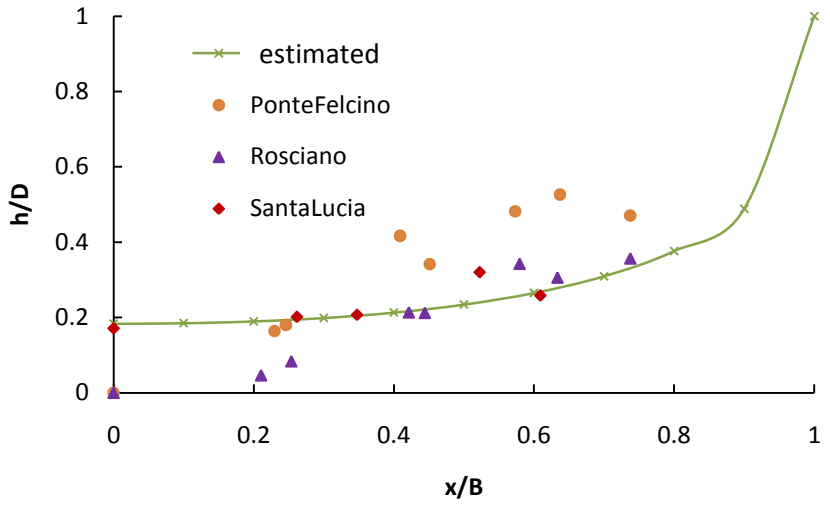

Figure 5.10 Simulated depths of maximum velocity

It can be found from Figure 5.10 that for each data set, the location of maximum velocity *h/D* increases with *x/B*, while the increment does not exactly follow the estimated curve. It is seen from the computed results that the data are distributed around the estimated curve. For the data from Santa Lucia, the data was most likely with the estimated curve, while for the data from Rosciano and Ponte Felcino, the agreements only happen in some values of *x/B*. These results are not acceptable, perhaps due to the lack of proper observation data.

5.3.2 Mean velocity

In practice, the velocity at every point in a channel section is not necessary, which is also not easy to get. More often, the mean velocity is needed to estimate sediment transport or other processes in open channels.

Equation (5-31) was used to compute the *G* value for cross-sections with known maximum and mean velocities. Vice versa, equation (5-31) can be used to compute the mean velocity with known *G* values, since *G* value is supposed to be constant for a given cross-section.

For the Ponti Felcino River, *G* was computed as 0.336 from the previous section. The mean velocity was computed for collected data from Ponti Felcino gauges for the last 20 years. Computation is shown in Table 5.7 with the root mean square error of 0.02.

Table 5.7 Estimation of mean velocity at Ponti Felcino River (Italy)

u_{max} (m/s)	obs. u_{mean} (m/s)	est. u_{mean} (m/s)	error
0.274	0.186	0.178	-0.042
0.771	0.492	0.501	0.019
0.794	0.471	0.516	0.096
1.678	1.110	1.091	-0.017
0.594	0.409	0.386	-0.056
1.130	0.820	0.735	-0.104
0.082	0.041	0.053	0.300
0.146	0.111	0.095	-0.145
1.902	1.292	1.236	-0.043
2.608	1.802	1.695	-0.059
3.362	2.296	2.185	-0.048
0.868	0.604	0.564	-0.066
1.122	0.777	0.729	-0.061
2.547	1.734	1.656	-0.045
2.924	2.025	1.901	-0.061
3.118	2.154	2.027	-0.059
1.421	1.026	0.924	-0.100
0.061	0.023	0.040	0.724
1.810	1.190	1.177	-0.011
2.079	1.373	1.351	-0.016
2.680	1.874	1.742	-0.070
1.461	0.957	0.950	-0.008
2.637	1.687	1.714	0.016
2.906	1.858	1.889	0.017

Table 5.7 continued

umax ((m/s)	obs. umean (m/s)	est. umean (m/s)	error
2.580	1.900	1.677	-0.117
1.340	0.885	0.871	-0.016
1.394	1.060	0.906	-0.145
2.405	1.594	1.563	-0.019
3.320	2.163	2.158	-0.002
3.181	2.074	2.068	-0.003
2.660	1.815	1.729	-0.047
3.365	2.120	2.187	0.032
0.206	0.123	0.134	0.089
3.410	2.097	2.217	0.057
1.102	0.726	0.716	-0.013
2.164	1.449	1.407	-0.029

The estimated mean velocity and the observation are plotted in Figure 5.11. It is seen from the figures that the data spread around the 1:1 straight line, and had a high relative coefficient as 0.99, which means the estimation has a high accuracy. More computation of the mean velocity in other rivers can be found in Appendix E.

The estimated values for the Ponte Felcino and Santa Lucia cross-sections are slightly smaller than observations, which is shown in the Figure 5.11 (a) and (b) that the points are distributed more below the 1:1 line. For the data from Ponte Nuovo, the points are plotted both up and below the line. However, it seems that the accuracy of equation (5-31) is acceptable.

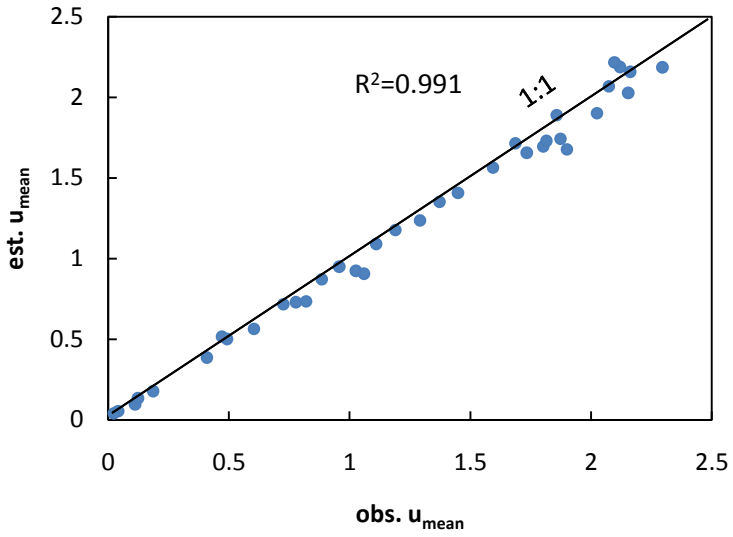

(a)

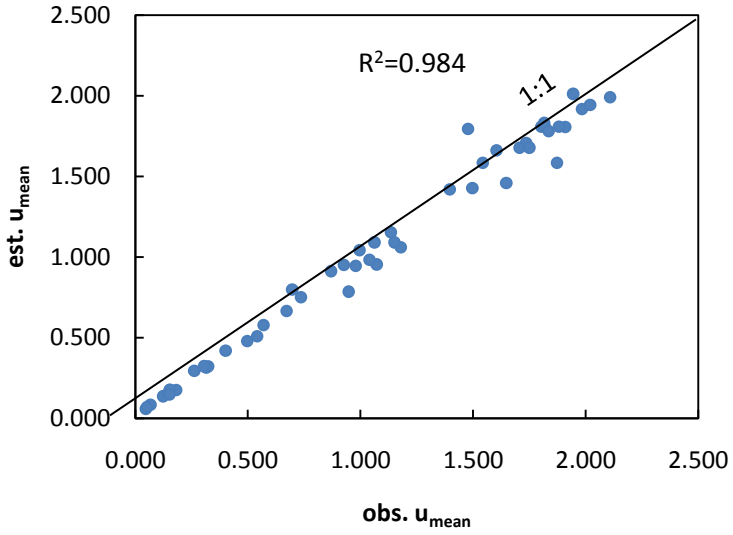

(b)

Figure 5.11 Comparison of estimated and observed mean velocities. (a) Ponte Felcino River (Italy), (b) Santa Lucia River (Italy) and (c) Ponte Nuovo (Italy)

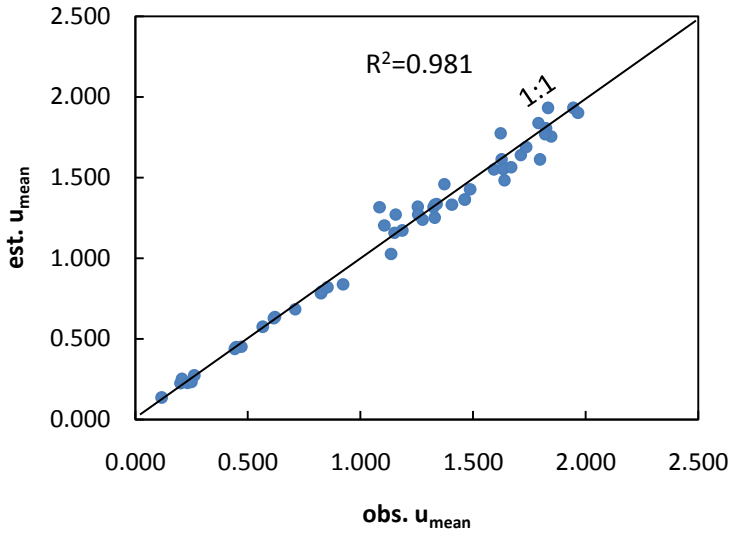

(c)

Figure 5.11 Continued

6. COMPARISON WITH OTHER VELOCITY DISTRIBUTION METHODS

The widely used methods for velocity distribution in open channels are simple power law and the Prandtl-von Karman velocity distributions. The entropy-based method which was derived by Chiu (1987, 1988) has been shown to have advantages over traditional methods. These methods are compared to the velocity distribution derived in this thesis.

6.1 Simple power law

The power law velocity distribution for flow in an open channel can be stated as:

$$\frac{u}{u_D} = \left(\frac{y}{D}\right)^{(1/n)} \tag{6-1}$$

where u is the velocity at a vertical depth y above the channel bed, u_{max} is the maximum velocity which occurs at the water surface, D is the total depth of the channel, n is a parameter which can be determined by the frictional resistance at the bed, which is usually in the range of 6-7 (Karim and Kennedy, 1987). Table 6.1 shows the results of computation using equations (4-29) and (6-1) for Run C1 from Einstein and Chien's (1955) data, which is from the clear water experiment. It is seen from the errors computed in Table 6.1 that the estimated values by power law are always bigger than observations, which values are bigger with a bigger n value.

Table 6.1 Computation of velocity profile using the Tsallis entropy and the simple power law

y (ft)	obs. u (ft/s)	est. Tsallis (ft/s)	error	est. power n=6 (ft/s)	error	est. power n=7 (ft/s)	error
0.006	2.442	2.894	0.185	3.679	0.506	3.983	0.631

Table 6.1 continued

y (ft)	obs. u (ft/s)	est. Tsallis (ft/s)	error	est. power n=6 (ft/s)	error	est. power n=7 (ft/s)	error
0.007	1.455	3.005	1.065	3.774	1.593	4.071	1.798
0.008	2.755	3.105	0.127	3.858	0.400	4.149	0.506
0.009	2.899	3.199	0.104	3.938	0.358	4.222	0.457
0.011	3.154	3.358	0.065	4.070	0.290	4.344	0.377
0.013	3.286	3.496	0.064	4.184	0.274	4.448	0.354
0.015	3.433	3.618	0.054	4.285	0.248	4.539	0.322
0.018	3.560	3.783	0.062	4.418	0.241	4.660	0.309
0.021	3.804	3.925	0.032	4.532	0.191	4.763	0.252
0.025	4.079	4.094	0.004	4.666	0.144	4.884	0.197
0.029	4.226	4.242	0.004	4.784	0.132	4.989	0.180
0.030	4.249	4.276	0.006	4.811	0.132	5.013	0.180
0.034	4.470	4.407	-0.014	4.912	0.099	5.103	0.142
0.039	4.636	4.553	-0.018	5.026	0.084	5.204	0.123
0.046	4.857	4.735	-0.025	5.166	0.064	5.328	0.097
0.054	5.039	4.920	-0.024	5.308	0.053	5.454	0.082
0.064	5.252	5.119	-0.025	5.459	0.039	5.586	0.064
0.074	5.395	5.296	-0.018	5.591	0.036	5.703	0.057
0.086	5.592	5.486	-0.019	5.734	0.025	5.827	0.042
0.099	5.712	5.666	-0.008	5.868	0.027	5.943	0.040
0.114	5.952	5.857	-0.016	6.008	0.009	6.065	0.019
0.130	6.084	6.029	-0.009	6.135	0.008	6.174	0.015
0.149	6.308	6.232	-0.012	6.283	-0.004	6.302	-0.001
0.170	6.416	6.417	0.000	6.416	0.000	6.416	0.000

The difference of these two methods is seen in Figure 6.1 which shows two velocity distributions both from clear water. The velocity distribution estimated by the Tsallis entropy fits better than the power law with either *n*=6 or 7, especially in the region near the channel bed. It seems that the *n* value range 6-7 discovered by Karim and Kennedy (1987) is not adequate in both clear water cases, while for Figure 6.1 the *n* value should be smaller than 6 in (a) and bigger than 7 in (b).

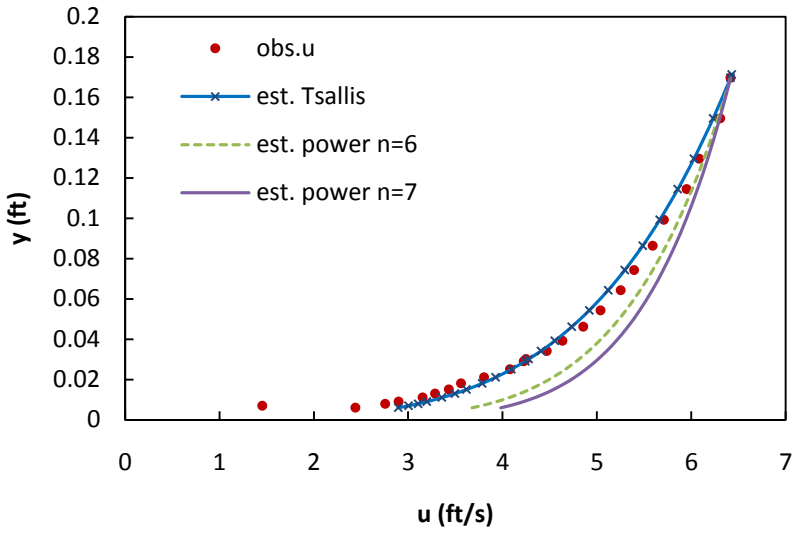

(a)

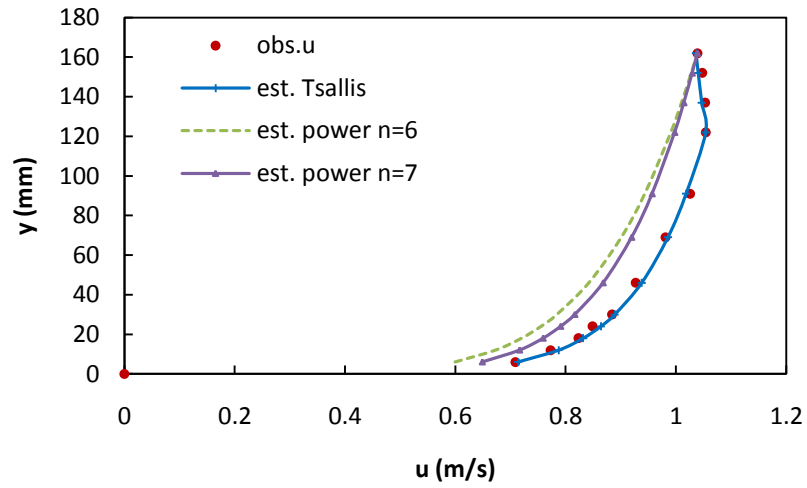

(b)

Figure 6.1 Comparison of velocity profiles by Tsallis entropy and Power law: (a) Run C1 of Einstein and Chien's (1955), and (b) Series 1 of Coleman's (1981) data

The value of *n* can be determined by the frictional resistance at the bed, while in practice, if the velocity is observed in a cross-section, *n* can also be determined using the

least square method. Using the Shannon entropy, it can also be computed from known mean and maximum velocities as follows:

$$n = \frac{1}{lnu_{max} - \overline{lnu}} \tag{6-2}$$

In Figure 6.2 the power law is applied with *n* computed with Equation (6-2), it improved the results comparing to *n*=6 or 7. With equation (6-2) *n* is computed as 8.53, for Run 15 of Coleman's (1981) data, which is heavy sediment flow. It is seen from the figure that the velocity estimated by power law is somehow close to the observation from the channel bed to 30mm, while it fails to capture the velocities higher than that, while the Tsallis entropy-based method is acceptable for the whole depth. To sum up, the power law is still not comparable to the Tsallis entropy-based velocity at all.

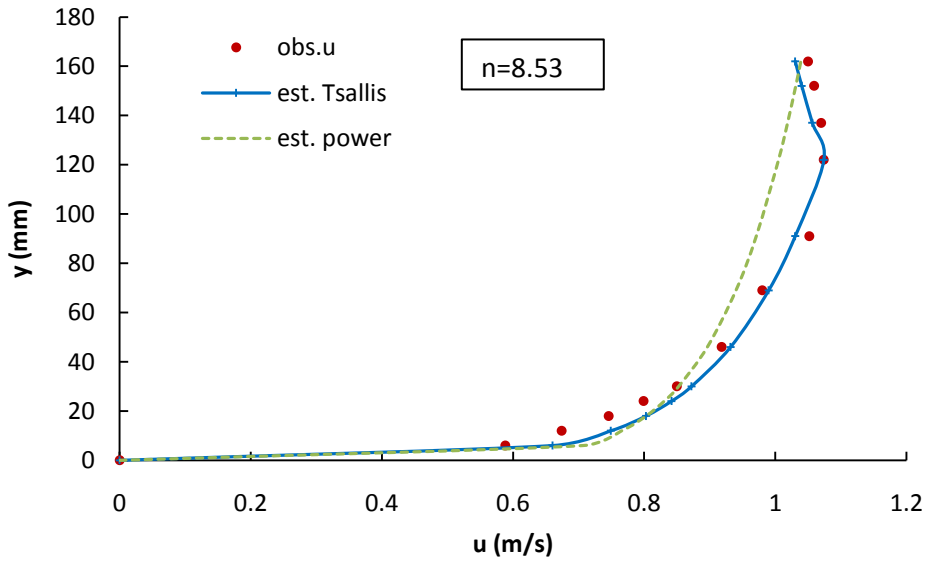

Figure 6.2 Velocity profile of power law improved by entropy [data from Run 15 Coleman (1981)]

6.2 Prandtl-von Karman universal velocity distribution

The Prandtl-von Karman universal velocity distribution was originally developed for pipe flow and has been shown to be relatively effective in wide open channels. It makes the following two assumptions:

1. The mixing length is proportional to the depth from the channel bed to the specified point.
2. The shear stress is constant.

The universal velocity distribution for open channel flow is

$$u = \frac{u_*}{\kappa} ln \frac{y}{y_0} \tag{6-3}$$

where u is the velocity at a vertical depth y above the channel bed, u_* represents the shear velocity, κ is the von-Karman universal constant, and y_0 is the depth of the shear velocity.

The shear velocity u_* can be computed with known channel characteristics from following equation:

$$u_* = \sqrt{gDS} \tag{6-4}$$

where g is the acceleration due to gravity, D is the total depth of the channel, and S is the channel slope.

The von Karman universal constant κ has a value of 0.4 for clear water and a value as low as 0.2 for heavily sediment water.

Table 6.2 gives the velocity distribution of Run S4 of Einstein and Chien's (1955) data computed by the Tsallis entropy and Prandtl-von Karman method, which are also

plotted in Figure 6.3. From both the table and figure, it is seen that the Tsallis entropy method is more accurate in describing the velocity distribution near the channel bed.

Table 6.2 Velocity distribution computed by the Tsallis entropy and Prandtl-von Karman equations for Run S4 of Einstein and Chien's (1955) data

y (ft)	obs. u (ft/s)	est. Tsallis (ft/s)	error	est. prandt (ft/s)	error
0.000	0.000	0.000	0.000	0.000	0.000
0.006	2.221	2.492	0.122	1.306	-0.412
0.009	2.497	2.821	0.130	1.964	-0.213
0.011	2.720	3.040	0.118	2.366	-0.130
0.011	2.858	3.138	0.098	2.535	-0.113
0.015	2.964	3.407	0.150	2.978	0.005
0.017	3.329	3.565	0.071	3.224	-0.032
0.019	3.573	3.776	0.057	3.535	-0.010
0.024	3.898	4.084	0.048	3.962	0.017
0.034	4.519	4.604	0.019	4.620	0.022
0.040	4.831	4.824	-0.001	4.878	0.010
0.045	5.075	5.029	-0.009	5.108	0.007
0.050	5.298	5.212	-0.016	5.307	0.002
0.054	5.522	5.383	-0.025	5.486	-0.006
0.064	5.806	5.701	-0.018	5.807	0.000
0.074	6.090	5.986	-0.017	6.081	-0.002
0.084	6.293	6.242	-0.008	6.316	0.004
0.095	6.516	6.486	-0.005	6.533	0.003
0.104	6.699	6.705	0.001	6.720	0.003
0.124	7.113	7.109	-0.001	7.054	-0.008

From the computed result shown in Table 6.2, it is found that the Prandtl-von Karman velocity is smaller than observation for lower values. For heavy sediment data from Einstein and Chien's (1955), it is seen from Figure 6.3 that the Tsallis entropy-based method works out better for the velocities near the channel bed. Though for the depth from 0.04mm to about 0.12mm, the Prandtl-von Karman velocity fits better than the Tsallis entropy velocity distribution, for the depth higher than 0.12mm up to the

water surface, the Tsallis entropy more accurately follows the natural velocity profile, where the velocity should increase smoothly to the water surface without resistance. In such cases, the Tsallis entropy-based method is recommended.

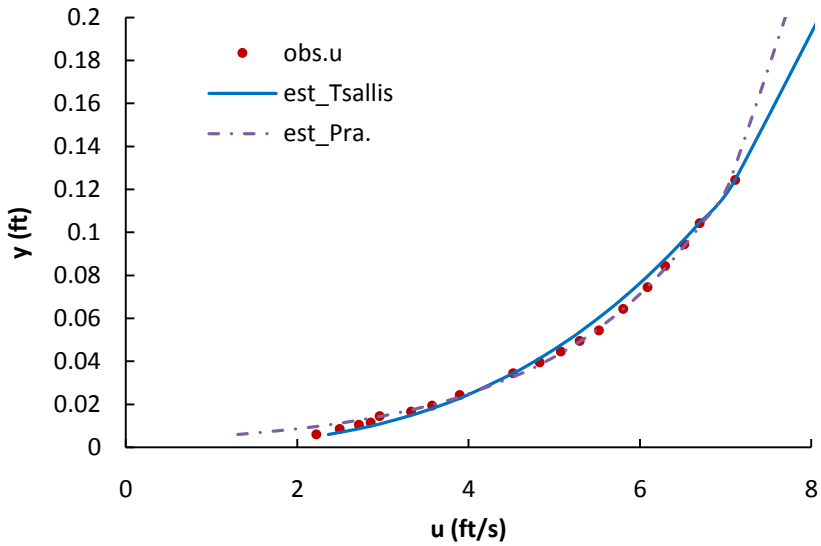

Figure 6.3 Comparison of velocity profiles computed by the Tsallis entropy and Prandt-von Karman for Run S4 of Einstein and Chien's (1955) data

6.3 Chiu's entropy method

Chiu's velocity distribution is obtained by applying POME to maximize the Shannon entropy, and the two constraints used in Chiu's velocity are the same as equations (4-2) and (4-3) used in this thesis. To develop the entropy-based velocity distribution, Chiu (1988) changed Cartesian coordinates *y*-*z* (represented as *x* in this thesis) to another system ξ-η based on the velocity isovels as shown in Figure 6.4, where ξ has a unique, one-to-one relation with a value of velocity. It is seen from Figure 6.4 that the isovels are represented by a system of ξ coordinate curves, and η curves are their

orthogonal trajectories. Once the equation of ξ as a function of y and z is determined, the equation of η can be derived from it.

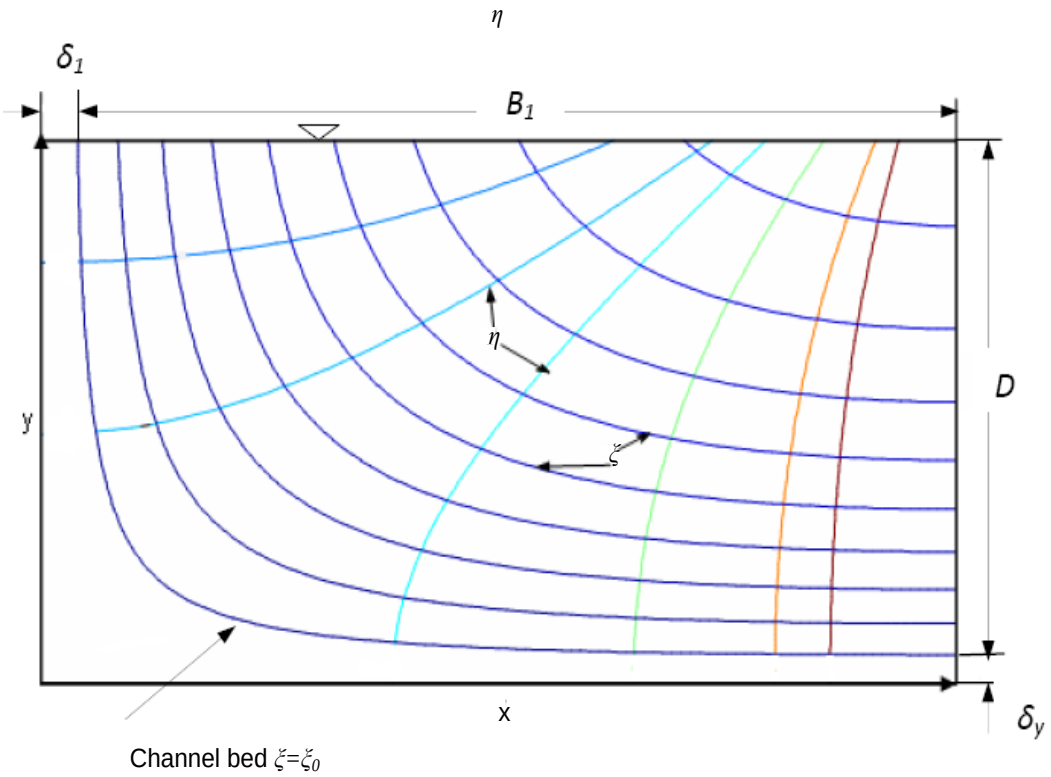

Figure 6.4 ξ-η coordinate system defined by Chiu (1988)

The idea of using the ξ-η coordinate is similar to that of using the cylindrical coordinates in studying the flow in a circular pipe. Let u be the time-averaged and, therefore, time invariant velocity on an isovel, which is assigned a value ξ. The value of u is almost 0 at ξ_0 which corresponds to the channel boundary, and u reaches u_{max} at ξ_{max}, which may occur at or below the water surface. Under such circumstances, u monotonically increases from ξ_0 to ξ_{max}. Then, at any value of the spatial coordinate less

than ξ, the velocity is less than u, which can be written in the cumulative distribution function as

$$F(u) = \frac{\xi - \xi_0}{\xi_{max} - \xi_0} \tag{6-5}$$

The Shannon entropy of velocity distribution can be written as:

$$H = -\int_0^{u_{max}} p(u) \log p(u) du \tag{6-6}$$

Through a similar procedure as stated in Section 5.1, the probability density function of the velocity distribution is obtained by maximizing the Shannon entropy equation (5-6) with the same constraint equations (5-2) and (5-3):

$$f(u) = \exp(\lambda_1 - 1 + \lambda_2 u) \tag{6-7}$$

where λ_1 and λ_2 are the Lagrange multipliers. Combining equation (6-7) with equation (6-5), Chiu's velocity distribution is obtained as

$$u = \frac{u_{max}}{M} \ln(1 + (\exp(M) - 1)F(u)) = \frac{u_{max}}{M} \ln\left(1 + (\exp(M) - 1)\frac{\xi - \xi_0}{\xi_{max} - \xi_0}\right) \tag{6-8}$$

where u_{max} is the maximum velocity which occurs at or below the water surface, M is the dimensionless entropy parameter, which equals $\lambda_1 u_{max}$.

The dimensionless parameter M is used as an index for characterizing and comparing various patterns of velocity distribution and state of flow systems. From equation (6-7), parameter M can be expressed as

$$M = \ln \frac{p(u_{max})}{p(0)} \tag{6-9}$$

which also equals

$$M = \ln \frac{p(u_{max})}{p(0)} = \ln \frac{\left(\frac{du}{d\xi}\right)_{\xi=\xi_0}}{\left(\frac{du}{d\xi}\right)_{\xi=\xi_{max}}} \tag{6-10}$$

Hence, M can be used as a measure of uniformity of probability and velocity distributions. The value of M can be determined by the mean and maximum velocity values derived from the following equation:

$$\frac{\bar{u}}{u_{max}} = e^{M}(e^{M}-1)^{-1} - \frac{1}{M} \tag{6-11}$$

With known M for a certain cross-section, the mean velocity can be estimated from Equation (6-11). With the knowledge of the value of M, the last step is to obtain the velocity distribution from equation (6-8) with the cumulative distribution function.

The Tsallis entropy [Equation (5-29)] and Chiu's entropy method [Equation (6-8)] are compared using 2D data for Ponte Felcino River as shown in Table 6.3 and Figure 6.5. It is found from Table 6.3 that the Chiu's velocity distribution has a higher root mean square error with 0.12 compared to that of Tsallis entropy-based velocity distribution with 0.07.

Table 6.3 Computation of 2D velocity profiles using the Tsallis entropy-based and Chiu's velocity distribution at Ponte Felcino River (Italy)

x (m)	*y' (m)*	*obs. u (m/s)*	*est. Tsallis (m/s)*	*error*	*est. Chiu (m/s)*	*error*
-18.860	0.000	0.830	0.746	0.000	0.811	0.000
-18.860	0.060	0.830	0.779	-0.061	0.839	0.011
-18.860	0.200	0.740	0.840	0.135	0.890	0.202
-18.860	1.000	0.640	1.031	0.610	1.039	0.624
-18.860	2.000	1.150	1.158	0.007	1.133	-0.014
-18.860	3.000	0.960	1.031	0.074	1.039	0.083
-18.860	3.900	0.740	0.799	0.079	0.856	0.156
-18.860	4.100	0.710	0.672	-0.053	0.748	0.053
-18.860	4.250	0.000	0.000	0.000	0.000	0.000
-10.460	0.000	2.060	1.937	-0.060	2.064	0.002
-10.460	0.060	2.060	1.965	-0.046	2.082	0.011
-10.460	0.200	2.340	2.025	-0.135	2.120	-0.094
-10.460	1.000	2.310	2.269	-0.018	2.267	-0.019

Table 6.3 continued

x (m)	*y'* (m)	*obs. u* (m/s)	*est. Tsallis* (m/s)	*error*	*est. Chiu* (m/s)	*error*
-10.460	1.930	2.440	2.457	0.007	2.373	-0.028
-10.460	2.880	2.190	2.264	0.034	2.264	0.034
-10.460	3.880	2.060	1.928	-0.064	2.058	-0.001
-10.460	4.280	1.650	1.665	0.009	1.882	0.140
-10.460	4.480	1.590	1.413	-0.111	1.695	0.066
-10.460	4.630	0.000	0.000	0.000	0.000	0.000
0.000	0.000	3.360	3.360	0.000	3.286	-0.022
0.000	0.060	3.360	3.354	-0.002	3.286	-0.022
0.000	0.200	3.160	3.340	0.057	3.285	0.040
0.000	1.000	3.200	3.252	0.016	3.265	0.020
0.000	2.000	3.280	3.125	-0.047	3.188	-0.028
0.000	3.000	2.910	2.970	0.021	3.028	0.041
0.000	4.000	2.780	2.766	-0.005	2.727	-0.019
0.000	5.000	2.320	2.461	0.061	2.134	-0.080
0.000	5.800	2.030	1.964	-0.032	1.069	-0.474
0.000	6.000	1.860	1.670	-0.102	0.558	-0.700
0.000	6.150	0.000	0.000	0.000	0.000	0.000

It is seen from Figure 6.5 that Chiu's velocity distribution increases more smoothly from the water bed to the water surface, which is faster than the Tsallis entropy-based velocity distribution. The Tsallis entropy-based velocity is more precise than Chiu's velocity. The Tsallis entropy-based velocity distribution increases from 0 at the channel bed up to the depth of maximum velocity and can exactly determine the maximum value, then it slowly decreases to the water surface. In the whole profile, the estimated curve detects the observation closely. However, Chiu's velocity distribution increases faster than the Tsallis entropy for determining the velocity near the center (x=0m vertical line), and slower for the vertical line x=-10.46m. The reason might be because in Chiu's method the velocity is considered for the whole channel cross-section

by using the coordinates based on isovels, in which study velocity isovels are simulated for the whole cross-section while it may not be accurate for each vertical line.

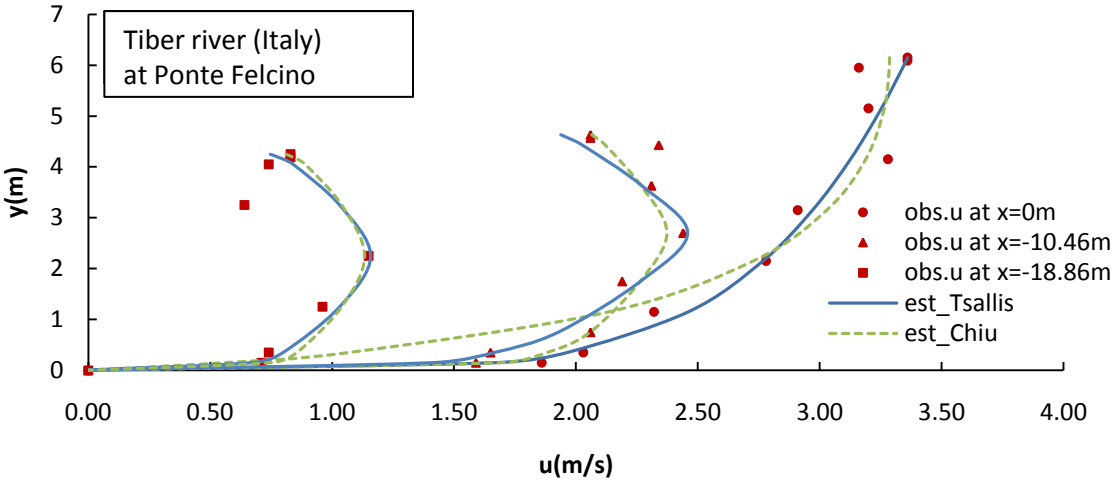

Figure 6.5 Comparison of velocity profiles computed by Tsallis entropy and Chiu's method

Figures 6.6 and 6.7 show the estimated velocity isovels for Italian rivers by two methods. Comparing these figures, Chiu's velocity isovels are smoother than those from the Tsallis entropy. This may be due to the reason that in Chiu's method, the CDF was defined on the ξ-η coordinate system. In Chiu's method, velocity is not determined at every point (x, y) in the cross-section, while the isovel curves mimic observations. However, the velocity distribution derived in this thesis based on the x-y coordinate system is determined at every point (x, y), which then shows more accuracy than Chiu's velocity.

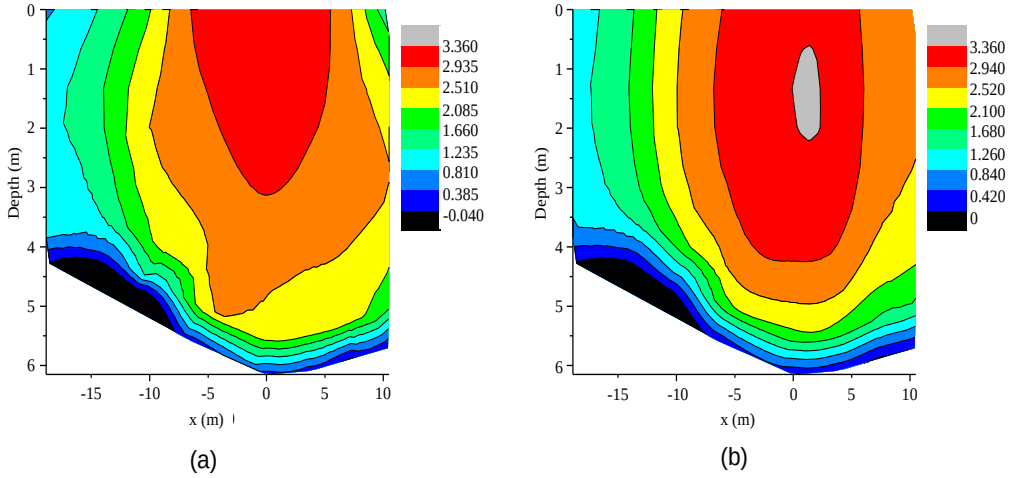

Figure 6.6 Isovels for data from Ponte Felcino (Italy) estimated. (a) by Tsallis entropy, (b) by Chiu's velocity

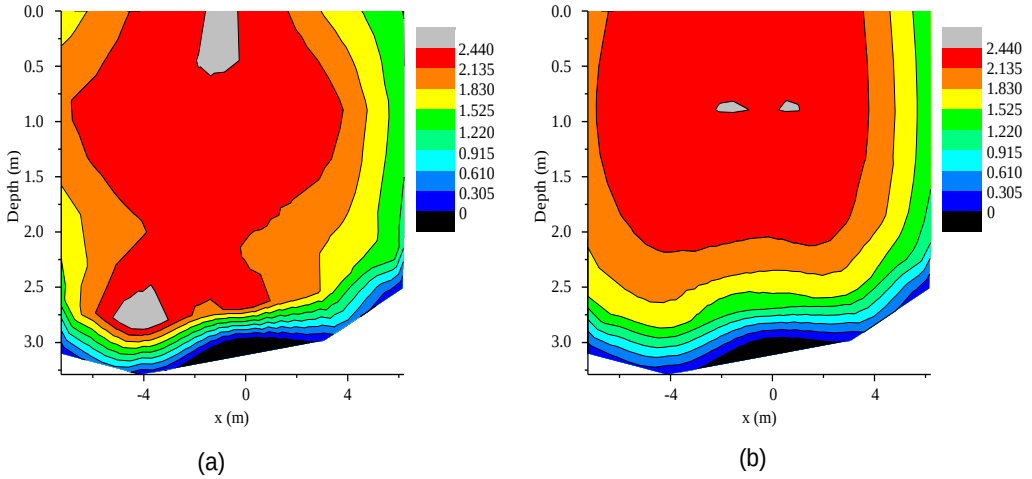

Figure 6.7 Isovels for data from Santa Lucia (Italy) estimated: (a) by Tsallis entropy, and (b) by Chiu's velocity

The 1D velocity distributions for both methods are compared as shown in Table 6.4 and Figure 6.8. The set data was from the experiment with heavy sediment flow. It is

found that the Tsallis entropy has a smaller estimation error than Chiu's velocity distribution.

Table 6.4 1D velocity distributions computed by Tsallis entropy and Chiu's method for Run 20 from Coleman's (1981) data

y *m*	*obs. u* *m/s*	*est. Tsallis* *m/s*	*error*	*est. Chiu* *m/s*	*error*
0	0	0.000	0.000	0.000	0.000
6	0.57	0.658	0.154	0.747	0.310
12	0.648	0.746	0.152	0.811	0.252
18	0.743	0.800	0.076	0.851	0.146
24	0.791	0.838	0.060	0.881	0.114
30	0.848	0.869	0.025	0.905	0.067
46	0.922	0.928	0.007	0.952	0.033
69	0.986	0.986	0.000	1.000	0.014
91	1.043	1.026	-0.016	1.033	-0.009
122	1.07	1.070	0.000	1.070	0.000
137	1.068	1.052	-0.015	1.055	-0.012
152	1.057	1.036	-0.019	1.042	-0.015
162	1.048	1.026	-0.021	1.033	-0.014

Regarding the impact of cumulative distribution function, the Tsallis entropy-based method and Chiu's method are compared for 1D velocity distribution. Figure 6.8 shows that the velocity from both methods increases slowly from the channel bed to 20mm then starts to increase faster up to the water surface. It is reasonable, since the near bed region is more affected by the shear stress than the higher region. It is seen from the figure that the two curves are close each other and both methods can predict the actual velocity reasonably well. However, the Tsallis entropy-based method is slightly more accurate than Chiu's method and its advantage is mainly shown in the lower velocity values near the channel bed.

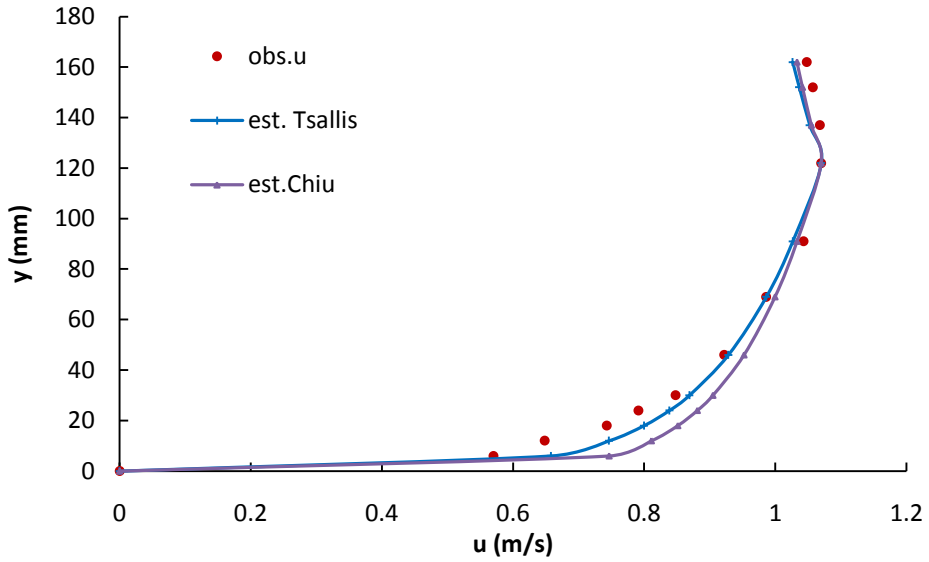

Figure 6.8 1D velocity distribution by Tsallis entropy and Chiu's method [data from Run 20 of Coleman's (1981)] data

For comparison of the above three methods with the Tsallis entropy, velocity for Einstein's data Run S16 is computed and plotted in Figure 6.9. The Tsallis and Shannon entropy based velocity distributions show an advantage over classical methods in overall estimation. The velocity distribution estimated by power law has the least accuracy than is the Prandtl-von Karman velocity distribution. The Prandtl-von Karman logarithmic law is valid from a depth of 0.03mm up to the water surface. However, all methods capture the maximum velocity exactly at the water surface in this case where the dip-phenomenon does not occur. It is seen from the figure that the Tsallis entropy shows more efficiency in determining the velocity near the boundaries over other methods.

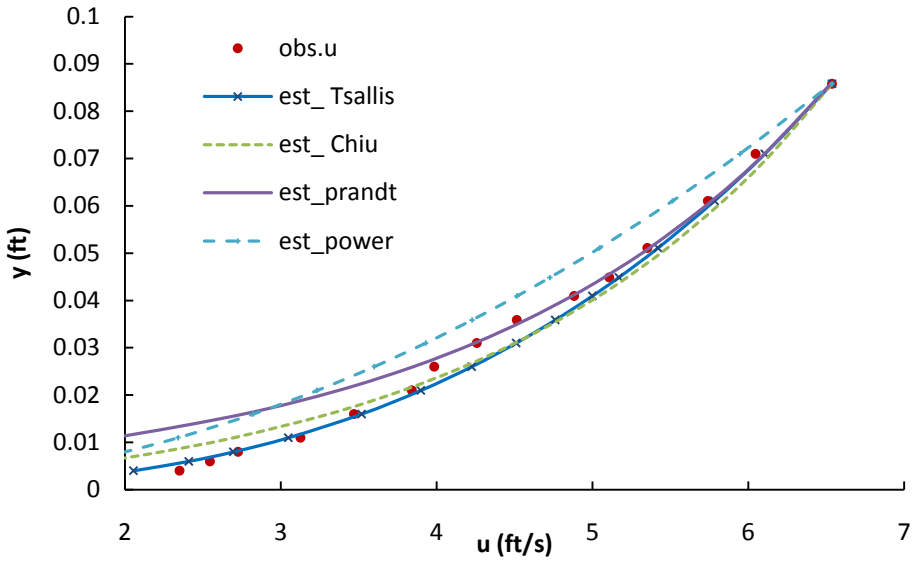

Figure 6.9 Comparison of velocity profiles by Tsallis entropy and the other three methods

7. DERIVATION OF SEDIMENT CONCENTRATION

The procedure is the same as that for the derivation of velocity distribution, while for sediment concentration the upper and lower limits of integration are changed for the reason that the sediment is mainly concentrated at the bed and decreases from the bed to the water surface.

7.1 Entropy based sediment concentration distribution

7.1.1 Tsallis entropy of sediment concentration

Consider the time-averaged sediment concentration *C* as a random variable. Unlike the velocity in open channels, the suspended sediment concentration is distributed conversely, which has the maximum value at the channel bed and decreases with increasing depth from the channel bed. If the sediment concentration is assumed 0 at the water surface, then *C* varies from c_0 to 0. According to equation (2-3), the Tsallis entropy of the sediment concentration can be written as:

$$H(c) = \frac{1}{m-1}\left\{1 - \int_{c_0}^{0} [f(c)]^m \, dc\right\} = \frac{1}{m-1}\int_{C_0}^{0} f(c)\,\{1 - [f(c)]^{m-1}\} dc \qquad (7\text{-}1)$$

where *C* is the time-averaged sediment concentration at a specified point, c_0 is the maximum sediment concentration of the cross-section, *f(c)* is the probability density function, and *m* is a real number.

Similar to the derivation of the velocity distribution, the way to obtain the probability distribution *f(c)* is by maximizing the entropy with known information from observations.

7.1.2 Specification of constraints

Two constraints will be applied here: one comes from the satisfaction of the density function and the other is obtained from the conservation of mass of sediment, which are stated as:

$$\int_{C_0}^{0} f(c)dc = 1 \tag{7-2}$$

$$\int_{C_0}^{0} cf(c)dc = \bar{c} \tag{7-3}$$

where $\bar{c}$ is the mean sediment concentration of the cross-section, which equals Q_s/Q. Here *Qs* is the suspended sediment discharge and *Q* is the flow discharge. Thus, equation (7-3) is equivalent to satisfying the condition that *C* must be distributed so that $\bar{c}Q = Q_s$.

7.1.3 Maximization of entropy

The Lagrange multiplier method is applied to maximize equation (7-1) subjected to equations (7-2) and (7-3). The Lagrangean function *L* can be written as:

$$L = \int_{c_0}^{o} \frac{f(c)}{m-1}\{1 - [f(c)]^{m-1}\}dc + \lambda_0\left[\int_{C_0}^{0} f(c)dc - 1\right] + \lambda_1\left[\int_{C_0}^{0} cf(c)dc - \bar{c}\right] \tag{7-4}$$

in which λ_0 and λ_1 are the Lagrange multipliers. Let $\frac{\partial L}{\partial f(c)} = 0$, the probability density function is obtained as:

$$f(c) = \left[\frac{m-1}{m}\left(\frac{1}{m-1} + \lambda_0 + \lambda_1 c\right)\right]^{\frac{1}{m-1}} \tag{7-5}$$

Let $\lambda_* = \lambda_0 + \frac{1}{m-1}$, and replace $\lambda_0 + \frac{1}{m-1}$ with λ_*. Then one obtains

$$f(c) = \left[\frac{m-1}{m}(\lambda_* + \lambda_1 c)\right]^{\frac{1}{m-1}} \tag{7-6}$$

Equation (7-6) is the entropy based probability density function of sediment concentration, which is used to determine the sediment concentration distribution.

7.1.4 Cumulative distribution function

Similar to the application of the velocity distribution, a hypothesis on the cumulative distribution needs to be specified first. The sediment transport is mainly in the stream wise direction of a channel, and for long-term sedimentation problem in rivers, the sediment concentration is often applied in 1D, without incorporating details over the whole cross-section. In this thesis, the suspended sediment concentration distribution is derived to predict the overall suspended sediment discharge through the cross-section; thus, it is assumed that sediment concentration is distributed in 1D, which will be verified in this research.

As used in 1D case of velocity distribution, the coordinate y is defined as in Figure 7.1. Assume that the water surface is clear at $y = D$ and $y = 0$ is the intersection of the bed-load and suspended sediment concentration, so that the suspended sediment, which is dealt with in this thesis, is distributed from $y = 0$ to D.

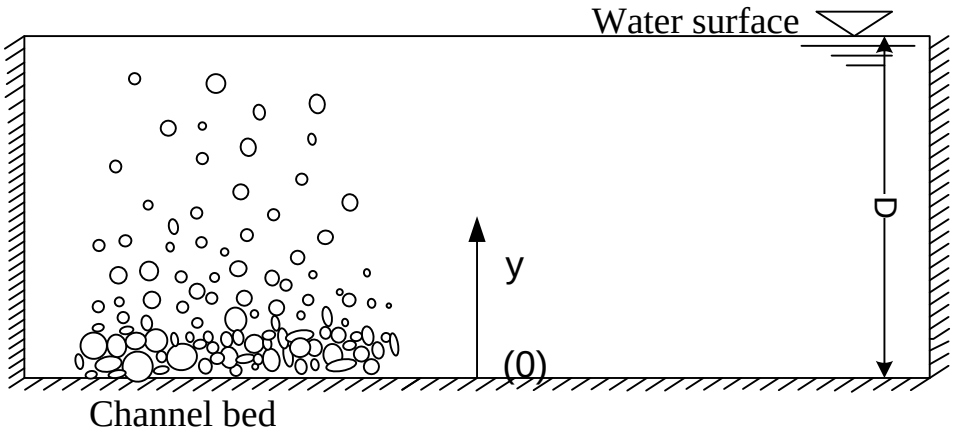

Figure 7.1 Coordinate system for sediment concentration

The cumulative distribution function should be assumed in the way that it is 1 at the channel bed, where y= 0 and 0 at the water surface, where y= D. Let the cumulative distribution function be assumed as:

$$F(c) = 1 - (\frac{y}{D})^a \quad (7\text{-}7)$$

where the value of a can be determined from observations.

As the definition suggests, the cumulative distribution function decreases from the channel bed to the water surface as shown in Figure 7.2. The change in the a value changes the rate of decline; a smaller a value causes a slower decline while a bigger value leads to a faster decline. The smaller the a value is, the less uniform the sediment concentration is distributed. For a value smaller than or equal to 0.4, the decline is simply separated as two parts: one is from the channel bed up to the depth at about 0.1y/D, and the other is from about 0.1y/D up to the water surface. The cumulative distribution decreases faster in the first part than the second part, which means the sediment concentration is distributed more near the bed area.

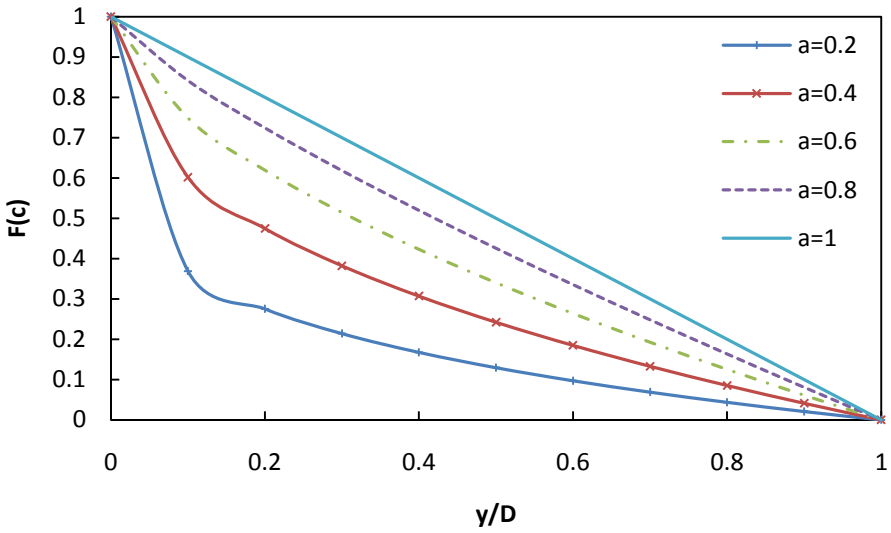

Figure 7.2 Cumulative distribution for various values of *a*

7.1.5 General sediment concentration distribution

To develop a general sediment concentration distribution, combining the entropy based probability distribution [equation (7-6)] with the cumulative distribution function [equation (7-7)],

$$F(c) = \int_{C_0}^{0} f(c)dc = \int_{C_0}^{0} \left[\frac{m-1}{m}(\lambda_* + \lambda_1 c)\right]^{\frac{1}{m-1}} dc = 1 - (\frac{y}{D})^a \tag{7-8}$$

from which one can obtain the sediment concentration distribution as

$$c = -\frac{\lambda_*}{\lambda_1} + \frac{1}{\lambda_1}\frac{m}{m-1}\left[\lambda_1 F(c) + \left(\frac{m-1}{m}\lambda_*\right)^{\frac{m}{m-1}}\right]^{\frac{m-1}{m}} \tag{7-9}$$

Thus, the sediment distribution is derived using the Tsallis entropy.

7.1.6 Dimensionless parameter *N*

In a similar manner used in the velocity distribution, a dimensionless parameter *N* is introduced to simplify computation, which also helps with an in-depth analysis:

$$N = \frac{\lambda_1 C_0}{\lambda_1 C_0 + \lambda_*} \tag{7-10}$$

Thus, the velocity distribution in equation (7-9) can be simplified by replacing the Lagrange multipliers with parameter *N* as:

$$\frac{c}{c_0} = 1 - \frac{1}{N}\left(1 - \left((1-N)^{\frac{m}{m-1}} + \left(1 - (1-N)^{\frac{m}{m-1}}\right) F(c)\right)^{\frac{m-1}{m}}\right) \tag{7-11}$$

For a fixed *m*=3, the value of N can be determined from the relationship between the mean and maximum sediment concentrations as

$$\bar{c} = \frac{1}{D}\int c_0\left[1 - \frac{1}{N}\left(1 - \left((1 + 0.5lnN)F(c) - 0.5lnN\right)^{\frac{2}{3}}\right)\right]dy \tag{7-12}$$

which is the same as that used for velocity distribution. Hence, the *N* value can be still obtained from equation (5-31). Inputting $\bar{c}$ and c_0 instead of $\bar{u}$ and u_{max} accordingly, one obtains:

$$\frac{\bar{C}}{C_0} = 0.554N^2 - 0.077N + 0.568 \tag{7-13}$$

With the *N* value obtained from equation (7-13), equation (7-11) can be applied to determine the sediment concentration. Vice versa, if the *N* value is known for a channel cross-section, the mean sediment concentration can be obtained from equation (7-13).

7.2 Application of sediment distribution

7.2.1 Verification of cumulative distribution function

The hypothesis on the cumulative distribution function needs to be verified first before computing the sediment concentration distribution. Table 7.1 shows the difference between observed and estimated cumulative distribution values for Einstein and Chien's (1955) data. For this data series the best fit *a* value is 0.5.

Table 7.1 Computation of *F(c)* of Run S1 of Einstein and Chien's (1955) data

y/D	*obs. F(c)*	*est. F(c)*
0.000	1.000	1.000
0.046	0.888	0.816
0.091	0.778	0.732
0.136	0.704	0.666
0.227	0.556	0.558
0.364	0.444	0.427
0.545	0.333	0.284
0.772	0.222	0.133
1.000	0.000	0.000

It is seen from Figure 7.3 that the estimated cumulative distribution fits observations well. Though estimated values are slightly smaller than observations except only one point at the depth *y/D*= 0.2, the biggest deviation is only 0.09. The cumulative distribution function attains a value of 1 at the channel bed and decreases to 0 at the water surface.

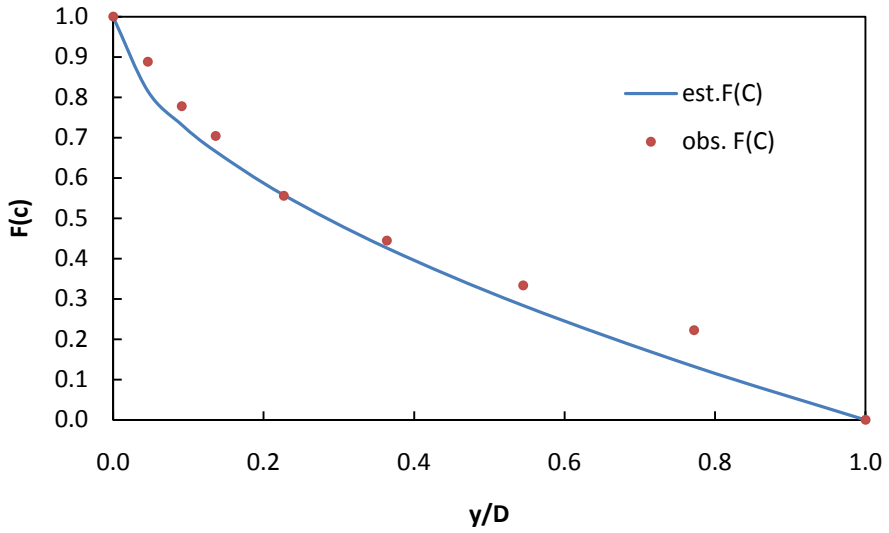

Figure 7.3 Comparison of computed and observed *F(c)* values for Run S1 of Einstein and Chien's (1955) data

More data sets from Einstein and Chien's (1955) and Coleman's (1981) have been used to verify the assumption on the cumulative distribution function. Results are shown in Figure 7.4. The distribution of the *a* value is right skewed and most values have dropped between 0.1 to 0.3, while the value of a for Coleman's (1981) data is smaller than for Einstein and Chien's (1955). Coleman's (1981) data has a mean value of *a* at 0.1 compared to that of Einstein and Chien's (1955) at 0.25.

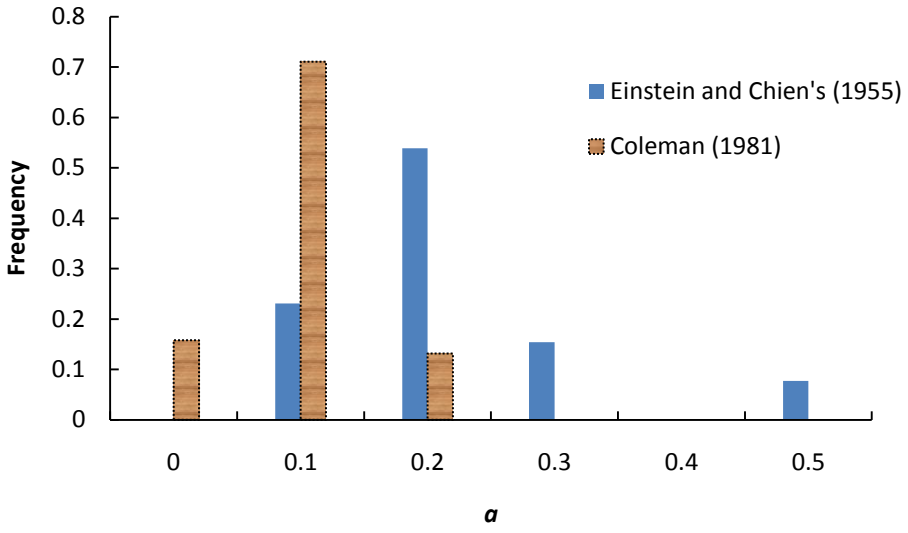

Figure 7.4 Computed values of *a*

It is found from the details of both experiments that the particle size is significantly different, which might be the reason for the difference. It is seen from the Figure 7.5 that for the same set of data, the value of *a* is big when the particle size is small. However the *a* value is much bigger for Einstein and Chien's (1955) data than for Coleman's (1981) data, which means there should be other unknown effective factors. The two points where *a*= 0.5 seems to be an outlier in both cases.

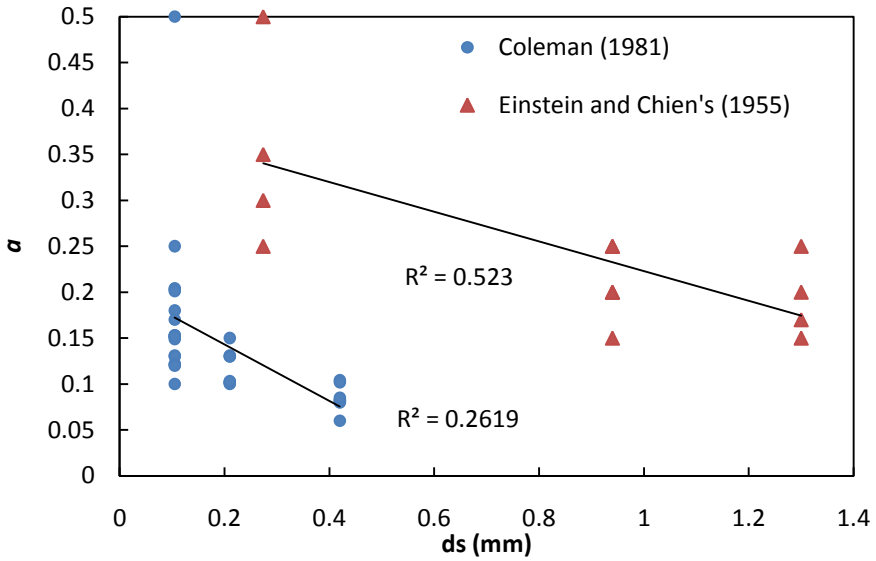

Figure 7.5 Value of *a* related to particle size

7.2.2 Computation of sediment concentration

With the CDF substituted into equation (7-11), the sediment concentration distribution is obtained for Run S1 of Einstein and Chien's (1955) data as shown in Table 7.2. The relative error is computed *as (est.-obs.)/obs.* as previously; it is seen from the table that the computed sediment concentration is close to the observed concentration. The biggest error occurs at y= 0.019m, where the water surface is assumed as clear water, which is actually not.

Table 7.2 Computed sediment concentration distribution for Run S1 of Einstein and Chien (1955) data

y m	*obs. c* g/l	*est. Tsallis* g/l	*relative error*
0.005	58.000	58.000	0.000
0.006	54.000	50.528	-0.064
0.007	49.700	44.681	-0.101
0.007	44.300	39.845	-0.101

Table 7.2 continued

y m	*obs. c* g/l	*est. Tsallis* g/l	*Relative error*
0.010	20.700	23.160	0.119
0.013	11.100	14.506	0.307
0.016	6.010	6.361	0.058
0.019	3.050	0.000	-1.000

Figure 7.6 also shows the results of equation (7-11) for both Einstein and Chien's (1955) and Coleman's (1981) data. It is seen that the Tsallis entropy based method can describe the sediment concentration distribution comparably well; the observation is distributed around the estimated curve. From comparison of two figures in Figure 7.6, the curve in (a) monotonically decreases from the channel bed to water surface with similar rate, while in (b) the sediment concentration decreases quickly for about 80% from depth 0 to 20mm, then slowly to the water surface. It can be concluded that data in (a) is more uniformly distributed than in (b) with a higher value of *a* and a higher entropy value.

The suspended sediment concentration becomes maximum near the channel bed, which is considered as the top of the bed-load sediment concentration. Then it decreases from that point up to the water surface, reaches 0 at the water surface as assumed. The sediment concentration near the water surface is estimated better in Figure 7.6 (b) than in (a). Because the flow in Coleman's (1981) experiments is much clearer than Einstein and Chien's (1955) at the water surface, the no sediment assumption on the water surface is not valid for Einstein and Chien's(1955) data.

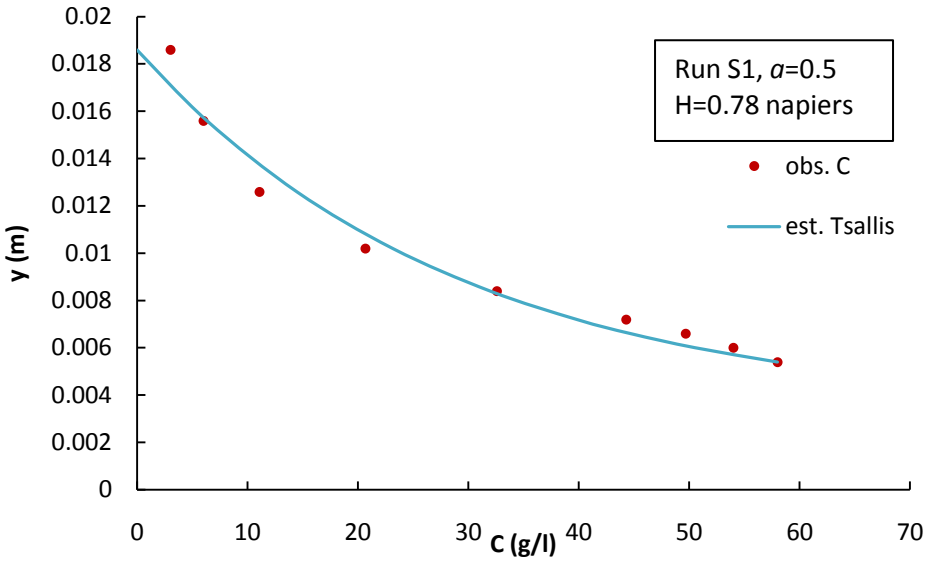

(a)

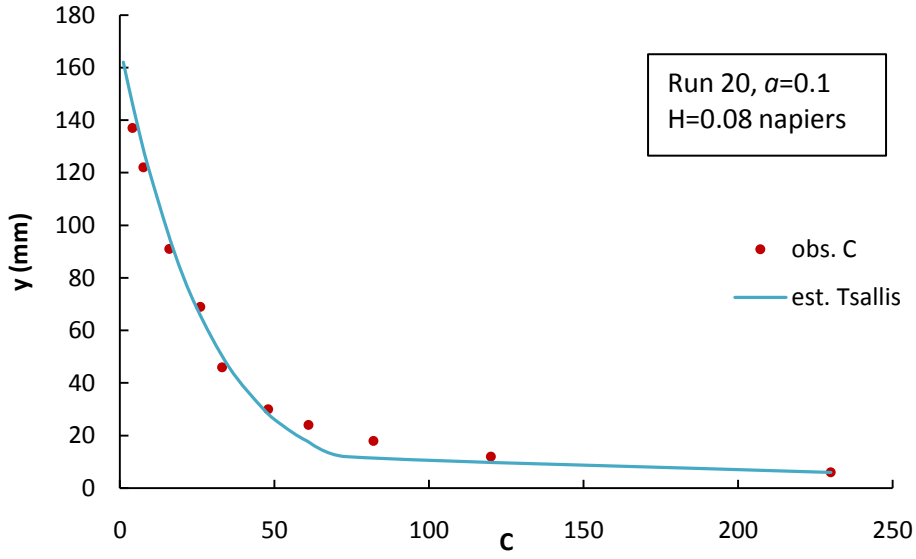

(b)

Figure 7.6 Sediment concentration distribution for (a) Run S1 of Einstein and Chien's (1955) data, and (b) Run 20 of Coleman's (1981) data

7.3 Comparison with deterministic equations

Before introducing the methods of estimating the sediment concentration, basic theories like the settling velocity of sediment particles are introduced first, which is essentially used in empirical methods.

7.3.1 Preliminaries

The settling or fall velocity is the average terminal velocity that a sediment particle attains in the settling process in quiescent, distilled water. It is related to particle size, shape, submerged specific weight, water viscosity and sediment concentration. In a clear still fluid, the particle fall velocity of a solitary sand particle smaller than about 100μm (Stokes-range) can be described as

$$\omega_s = \frac{1}{18}\frac{(s-1)gd_s^2}{\nu} \tag{7-14}$$

For suspended sand particles in the range 100-1,000 μm, van Rijin (1984) suggested to use following type of equation as proposed by Zanke (1978):

$$\omega_s = \frac{10\nu}{d_s}\left[\left(1 + \frac{0.01(s-1)gd_s^3}{\nu^2}\right)^{0.5} - 1\right] \tag{7-15}$$

For larger particles (>1,000 μm), van Rijn (1984) computed ω_s as

$$\omega_s = 1.1[(s-1)gd_s]^{0.5} \tag{7-16}$$

Cheng (1997) related the settling velocity to sediment and fluid properties but not restricted to the particle dimensions as

$$\frac{\omega_s d_s}{\nu} = (\sqrt{25 + 1.2d_*^2} - 5)^{1.5} \tag{7-17}$$

where $d_* = [\frac{(\rho_s-\rho)g}{\rho\nu^2}]^{1/3} d_s$, in which ρ is the fluid density, and ρ_s is the sediment density.

7.3.2 Rouse equation

The Rouse equation is a solution of differential equation (2-8) with the help of Prandtl-von Karman logarithmic velocity equation and linear shear stress distribution assumption. For equation (2-8), ε_s does not have a constant value, particularly near the bed. The distribution of ε_s with the vertical coordinate y is deduced based on the vertical distribution of turbulent eddy viscosity ε which is defined as

$$\tau = \rho\varepsilon\frac{du}{dy} \tag{7-18}$$

in which τ is the shear stress, and u is the time-averaged velocity at depth y above the channel bed. Let $\varepsilon_s = \beta\varepsilon$, where β is a coefficient of proportionality. From the Navier-Stokes equations, the vertical shear stress distribution in a steady, uniform flow in an open channel is linear, which can be stated as

$$\tau = \tau_0\frac{(y_0 - y)}{y_0} \tag{7-19}$$

where τ_0 is the shear stress at the bed, and y_0 is the depth of the uniform flow.

Recalling the Prandtl-von Karman velocity equation, the gradient of the velocity distribution can be written as:

$$\frac{du}{dy} = \frac{u_*}{\kappa y} \tag{7-20}$$

Substituting $\varepsilon_s = \beta\varepsilon$ into equation (7-18) along with equations (7-19) and (7-20) and solving for ε_s, one gets

$$\varepsilon_s = \beta\kappa u_*\frac{y}{y_0}(y_0 - y) \tag{7-21}$$

Equation (7-21) can be substituted into differential equation (2-8), so that it can be integrated to produce

$$\frac{c}{c_a} = \left(\frac{(y_0 - z)}{y}\frac{a}{(y_0 - a)}\right)^{R_0} \tag{7-22}$$

in which c_a is the reference concentration at the distance z=a, which is arbitrarily $0.05y_0$ above the bed and $R_0 = \omega_s/\beta\kappa u_*$, which is referred as the Rouse number.

The following table shows a comparison between equation (7-11) and Equation (7-22). It is seen that the values from the Rouse equation are always smaller than observed values, while the Tsallis entropy-based values are smaller for sediment concentration near the bed and bigger for that near the water surface.

Table 7.3 Computed sediment concentration distribution for Run S13 from Einstein and Chien (1955)

y m	*obs. c* g/l	*est. Tsallis* g/l	*error*	*est. Rouse*	*error*
0.004	352.000	352.000	0.000	352	0.000
0.005	319.000	155.208	-0.513	246.140	-0.228
0.006	248.000	127.588	-0.486	164.295	-0.338
0.008	174.000	105.214	-0.395	101.379	-0.417
0.010	117.000	86.504	-0.261	61.440	-0.475
0.013	77.900	70.290	-0.098	37.546	-0.518
0.018	43.100	52.821	0.226	21.024	-0.512
0.024	21.600	35.979	0.666	11.520	-0.467
0.031	10.200	20.155	0.976	6.2906	-0.383
0.040	4.610	5.467	0.186	3.434	-0.255

More computed values are presented in Appendix E. Figure 7.7 compares two methods for Einstein and Chien's (1955) data. Overall, the Tsallis entropy based method is more accurate than the Rouse equation. From both figures, the curve computed by the Rouse equation estimates the sediment concentration with smaller values than

observations, which shows in the figure that observation points are always above the curve. However, the minimum point in Figure 7.7 (b) is captured by the Rouse equation better than the entropy based curve, since the entropy based method has a trend to reach 0 at the water surface.

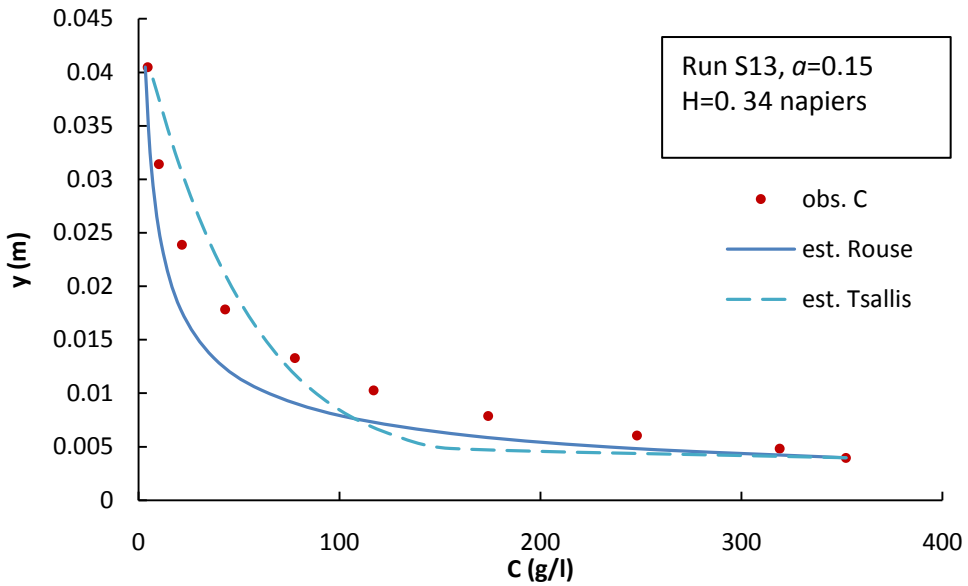

(a)

Figure 7.7 Comparison of sediment concentration distributions for the Tsallis entropy method and the Rouse equation: (a) Run S13 of Einstein and Chien (1955), and (b) Run S11 of Einstein and Chien (1955)

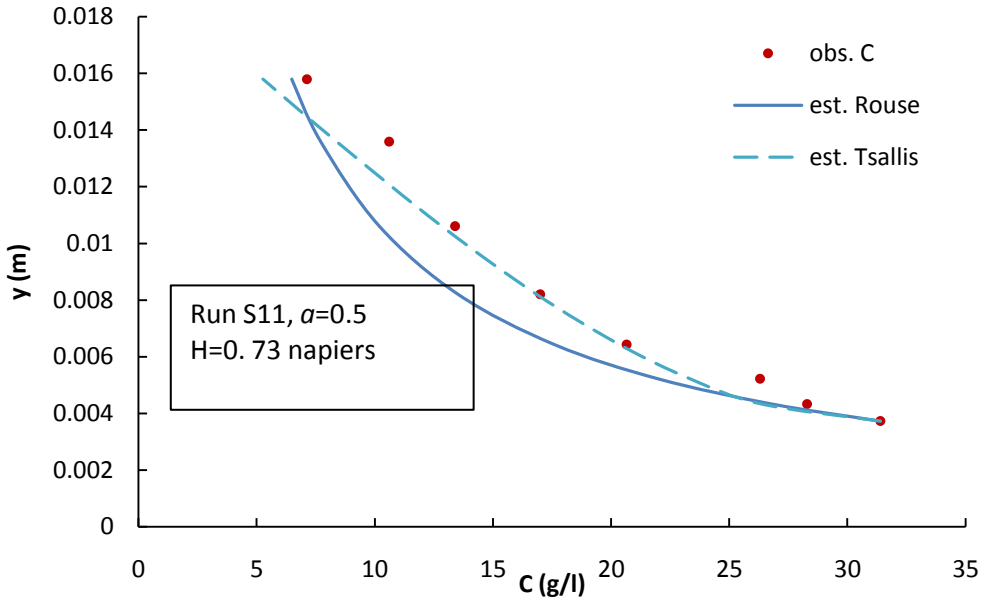

(b)

Figure 7.7 Continued

Comparing Figures 7.7 (a) and 7.7 (b), it is found that the data of Run S11 is more uniformly distributed than that of Run S13, which is shown with a higher value of a and a higher value of entropy.

7.3.3 Chiu's entropy based equation

Chiu (2000) derived another sediment distribution, with his velocity gradient instead of equation (7-16). Recall Chiu's (1987) velocity distribution [equation (6-8)], the change of velocity to the depth can be stated as:

$$\frac{du}{dy} = \frac{u_{max}}{MD}(e^M - 1)[1 + (e^M - 1)\frac{y}{D}]^{-1} \qquad (7\text{-}23)$$

Instead of equation (7-20), combining equation (7-23) with equations (7-18) and (7-19), another sediment concentration distribution can be obtained as:

$$\frac{C}{C_0} = \left(\frac{1-\frac{y}{D}}{1+(e^M-1)\frac{y}{D}}\right)^{z'} \tag{7-24}$$

where $z' = \frac{\omega_s u_{max}(1-e^{-M})}{\beta {u_*}^2 M}$.

Table 7.4 shows the comparison between equation (7-11) and equation (7-24). The overall root mean square error of estimation for the Tsallis entropy is 0.137 and that for Chiu's method is 0.269. With Chiu's method, the estimation is bigger than observation in the lower half of the depth, while smaller than observation in the upper half of the depth. However, no such trend is found for the Tsallis entropy method.

Table 7.4 Computed sediment concentration distribution for Run 33 of Coleman's (1981) data

y mm	*obs. c* 10^{-4}	*est. Tsallis* 10^{-4}	*error*	*est. Chiu* 10^{-4}	*error*
6.000	2.700	2.700	0.000	2.700	0.000
12.000	1.400	0.892	-0.363	1.521	0.087
18.000	0.860	0.740	-0.139	1.097	0.275
24.000	0.660	0.644	-0.024	0.866	0.312
30.000	0.570	0.573	0.005	0.717	0.258
46.000	0.430	0.437	0.016	0.487	0.132
69.000	0.340	0.307	-0.098	0.316	-0.071
91.000	0.230	0.215	-0.065	0.217	-0.056
122.000	0.190	0.115	-0.397	0.120	-0.368
137.000	0.160	0.074	-0.539	0.081	-0.496
152.000	0.140	0.036	-0.739	0.040	-0.713
162.000	0.120	0.013	-0.889	0.000	-1.000

It is seen from Figure 7.8 that the sediment concentration from the Tsallis entropy is closer to the observed concentration than Chiu's sediment concentration. Chiu's method fails to capture the observed point in the middle section in Figure 7.8 (a), whose disadvantage is less significant in Figure 7.8(b). Because in Chiu's method, it is

not dealt with the decreasing speed, a more accurate estimation is expected in more uniform distribution with a higher entropy value. However, in the Tsallis entropy method, the exponent *a* value will change according to different decreasing speeds, thus this method is more widely applicable than Chiu's method. Based on the clear water surface assumption, both of methods are not valid in channels where the sediment is distributed up to the water surface.

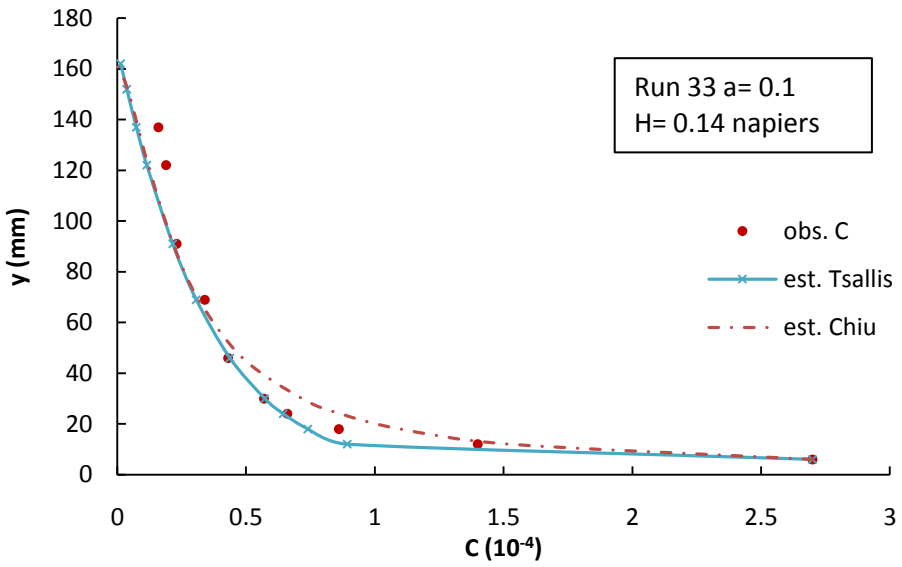

(a)

Figure 7.8 Comparison between equation (7-11) and equation (7-24) for (a) Run 33 of Coleman (1981), and (b) Run 22 of Coleman (1981)]

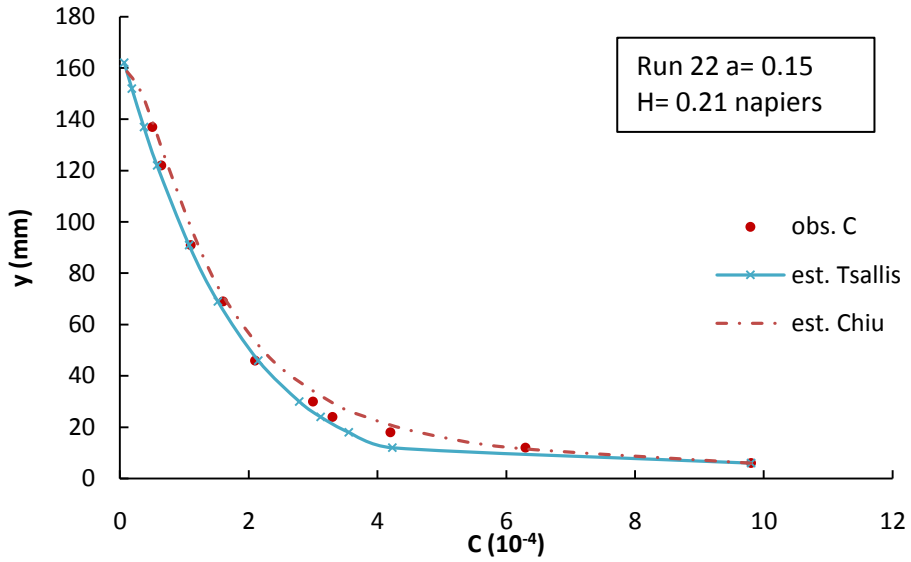

(b)

Figure 7.8 Continued

7.3.4 Choo's entropy based equation

Choo (2000) has derived entropy based method to estimate the sediment concentration distribution, which is similar to that of Chiu's (1987) velocity. Consider the time-averaged sediment concentration as a random variable, the Shannon entropy of the sediment concentration can be written as:

$$H(c) = \int_{c_0}^{c_D} f(c) ln f(c) dc \qquad (7\text{-}25)$$

Using the Lagrange multiplier method as Section 7.1, maximize the Shannon entropy subject to equations (7-2) and (7-3), and obtain the probability distribution as:

$$f(c) = \exp(\lambda_* + \lambda_1 c) \qquad (7\text{-}26)$$

To obtain the expression of the sediment concentration distribution, Choo (2000) assumed the cumulative distribution as:

$$F(c) = 1 - y/D \tag{7-27}$$

Substituting equation (7-22) in equation (7-23), the sediment concentration distribution can be obtained as

$$\mathrm{c} = \frac{\mathrm{C_0}}{\mathrm{N'}} \ln\left(\exp(\mathrm{N'}) - \left(\exp(\mathrm{N'}) - \exp\left(\frac{\mathrm{N'}}{\mathrm{K}}\right)\right)\frac{\mathrm{y}}{\mathrm{D}}\right. \tag{7-28}$$

where $\mathrm{N'} = \lambda_1 \mathrm{c_0}$ and $K = \frac{c_0}{c_D}$, in which c_D is the sediment concentration at the water surface, which can be considered as 0. Thus, $k \approx \infty$. Equation (7-24) reduces to

$$\mathrm{c} = \frac{\mathrm{c_0}}{\mathrm{N}} \ln\left(\exp(\mathrm{N'}) - (\exp(\mathrm{N'}) - 1)\frac{\mathrm{y}}{\mathrm{D}}\right) \tag{7-29}$$

Table 7.5 shows the comparison between equation (7-11) and equation (7-29). It is seen that it is hard to tell which method is better, since the estimation is close for these two methods. The root mean square error is 0.187 for the Tsallis entropy based method and is 0.195 for Choo's method.

Table 7.5 Computed sediment concentration distribution for Run 35 of Coleman (1981)

y mm	*obs. c* 10^{-4}	*est. Tsallis* 10^{-4}	*error*	*est. Choo* 10^{-4}	*error*
6.000	9.300	9.300	0.000	9.300	0.000
12.000	4.100	2.577	-0.371	3.029	-0.261
18.000	2.200	2.122	-0.036	2.385	0.084
24.000	1.700	1.837	0.081	2.008	0.181
30.000	1.500	1.627	0.084	1.741	0.160
46.000	1.100	1.233	0.121	1.266	0.151
69.000	0.860	0.859	-0.001	0.843	-0.020
91.000	0.560	0.599	0.071	0.565	0.008
122.000	0.420	0.318	-0.243	0.276	-0.344
137.000	0.340	0.204	-0.400	0.162	-0.522
152.000	0.310	0.101	-0.675	0.062	-0.801
162.000	0.250	0.037	-0.853	0.000	-1.000

From Figure 7.9, the Tsallis entropy-based method and Choo's entropy-based method give similar curves for observed values. It can be seen from the figures that the two estimated curves are mostly intertwined, though slight changes can be found. Both sediment concentrations decreases from the channel bed to higher depth, while Choo's curve goes faster from depth 20mm to 40mm, then slower from depth 40mm to the water surface. Overall the simulation is similar for both methods; however, it seems that for lower values of sediment concentration near the water surface the Tsallis entropy based method is slightly better than Choo's.

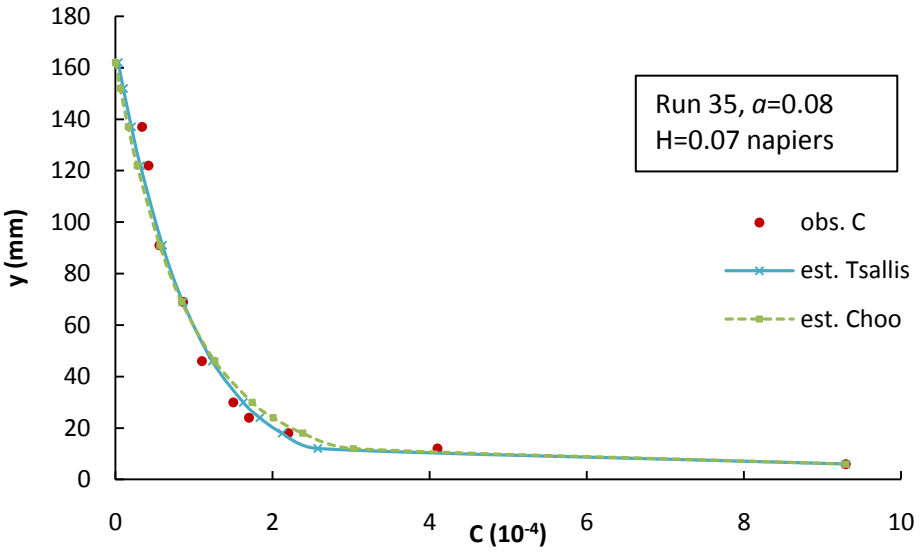

(a)

Figure 7.9 Comparison between equation (7-11) and equation (7-29) for (a).Run 35 of Coleman (1981), and (b) Run 7 of Coleman (1981)

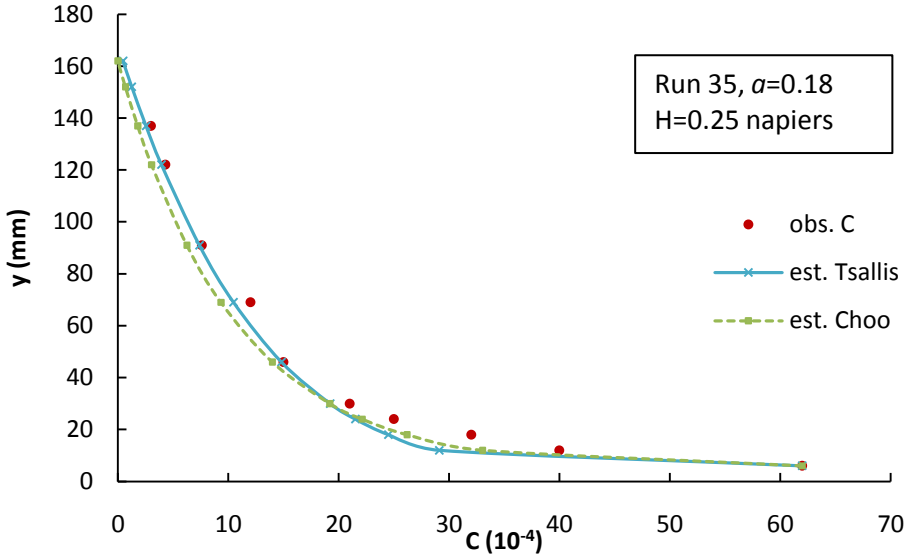

(b)

Figure 7.9 Continued

8. SUSPENDED SEDIMENT DISCHARGE

Usually, the sediment discharge is computed by integration of sediment concentration and velocity for the channel section. The suspended sediment discharge can be estimated from

$$q_s = \int_0^D cudy \tag{8-1}$$

where q_s is the specific sediment discharge, c is the sediment concentration at depth y, and u is the velocity distribution at depth y.

Equation (8-1) can also be simplified as

$$q_s = \bar{u}\bar{c}D \tag{8-2}$$

The problem of getting sediment discharge then can change with the velocity distribution and sediment concentration distribution. As discussed in Chapters 5, 6 and 7, there are both entropy methods and empirical methods to obtain velocity and sediment concentration distributions. In this chapter, different combinations of velocity distribution and sediment concentration distribution for sediment discharge will be obtained.

8.1 First combination

There are two entropy based estimation methods for the velocity distribution: Chiu's velocity distribution and the Tsallis entropy-based velocity distribution. These two methods combined with the Rouse equation can be used to compute the suspended sediment discharge.

Substituting equations (5-29) and (7-22) into equation (8-1), the sediment discharge (designated as first) is obtained as:

$$q_s1 = u_{max}c_0 \int_0^D \left(\frac{(y_0-y)}{y}\right)^{\omega_s/\beta\kappa u_*} [1 - \frac{1}{G}\left(1 - \left((1 + 0.5lnG)F(u) - 0.5lnG\right)^{\frac{2}{3}}\right)]dy \qquad (8\text{-}3)$$

Equation (8-3) can be simplified like equation (8-2), replacing the velocity term with the equation (5-31) which reduces to

$$q_s1 = c_0u_{max}(0.554G^2 - 0.077G + 0.568\,) \int_0^D \left(\frac{(y_0-y)}{y}\right)^{\omega_s/\beta\kappa u_*} dy \qquad (8\text{-}4)$$

Substituting equations (6-8) and (7-22) into Equation (8-1), the sediment discharge (designated as second) is obtained as:

$$q_s2 = \frac{\mathrm{u_{max}}c_0}{\mathrm{M}} \int_0^D \left(\frac{(y_0-y)}{y}\right)^{\omega_s/\beta\kappa u_*} \ln\,(1 + (\exp(\mathrm{M}) - 1)\mathrm{y/D})dy \qquad (8\text{-}5)$$

which can also be simplified with the mean velocity equation (6-11). Thus q_s2 changes to

$$q_s2 = c_0u_{max}[e^M(e^M - 1)^{-1} - \frac{1}{M}\,] \int_0^D \left(\frac{(y_0-y)}{y}\right)^{\omega_s/\beta\kappa u_*} dy \qquad (8\text{-}6)$$

Equations (8-4) and (8-6) can be solved numerically for the whole cross-section, and the results are shown in Table 8.1 for Einstein and Chien's (1955) sediment discharge data. Rather than q_s, *Qs* was computed by integrating the whole cross-section by *dA* not *dy* in equations (8-4) and (8-6). It is found that the computed errors are bigger in *Qs2* than in *Qs1*.

Table 8.1 Computed sediment discharge Qs for Einstein and Chien's (1955) data

obs. Qs (g/s)	Qs1 (g/s)	error	Qs2 (g/s)	error
1.713	0.553	-0.677	0.542	-0.684
3.903	1.124	-0.712	1.160	-0.703
5.025	1.509	-0.700	1.490	-0.704
5.659	1.559	-0.725	1.563	-0.724

Table 8.1 continued

obs. Qs (g/s)	Qs1 (g/s)	error	Qs2 (g/s)	error
10.887	3.057	-0.719	3.082	-0.717
0.920	0.502	-0.455	0.487	-0.471
1.874	1.008	-0.462	0.944	-0.496
2.322	0.948	-0.592	0.916	-0.605
4.109	1.875	-0.544	1.827	-0.555
5.706	2.441	-0.572	2.354	-0.587
1.165	1.006	-0.136	0.991	-0.149
5.048	3.592	-0.288	3.494	-0.308
7.924	6.059	-0.235	5.795	-0.269
9.628	6.709	-0.303	6.651	-0.309
15.665	8.348	-0.467	8.424	-0.462
14.379	8.239	-0.427	7.965	-0.446

It is seen from the results from both Figures 8.1 and 8.2 that the estimated sediment discharge is much smaller than the observed, especially for larger Qs values. The points are far from the 1:1 line. This might be due to the sediment concentration being estimated by the Rouse equation, which is often lower than expected. Due to the shortcoming of the Rouse equation, the first two methods are not preferred.

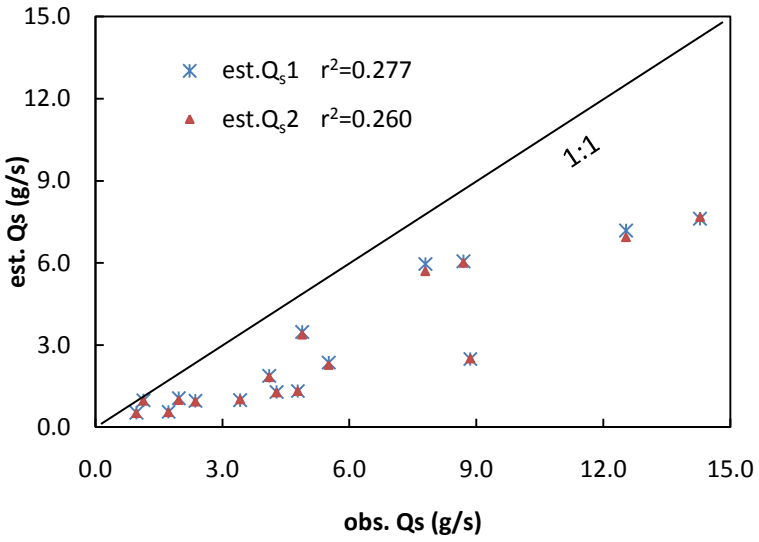

Figure 8.1 Comparison of sediment discharge for Einstein and Chien's (1955) data

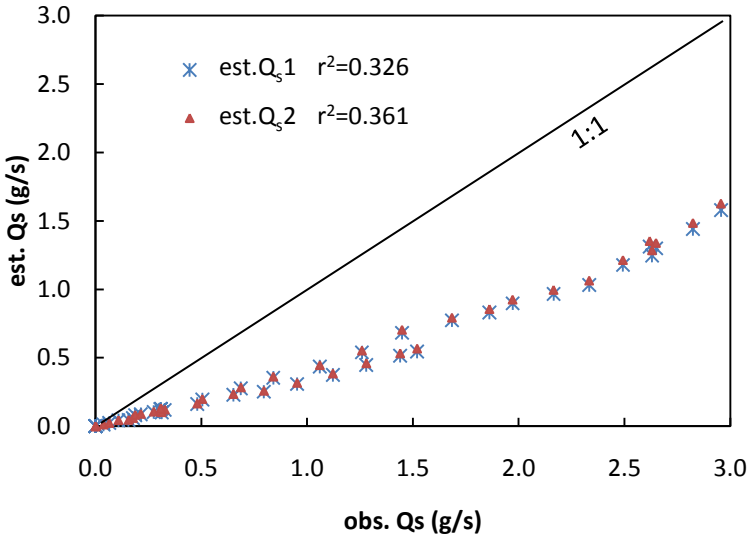

Figure 8.2 Comparison of sediment discharge from Coleman (1981)

To modify the results, which is smaller than the observation, the correction factor ω is introduced as an amplifying coefficient. It is seen from Figure 8.3, the modified discharge is now distributed nearer to the 1:1 line than before.

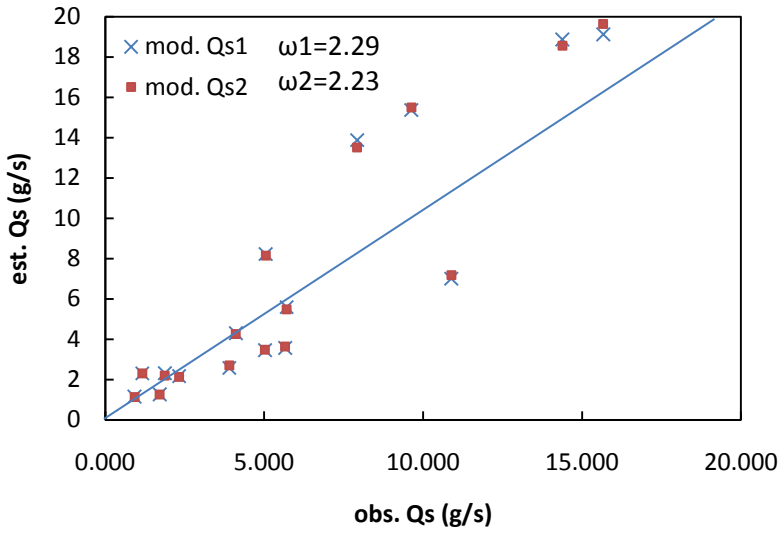

Figure 8.3 Modified sediment discharge for Einstein and Chien's (1955) data

8.2 Second combination

In this section, the suspended sediment discharge is obtained with the Prandtl-von Karman velocity distribution and entropy-based sediment concentration obtained from Chiu's (2000), Choo's (2000) methods and the method derived in this thesis. Substituting equations (6-3) and (7-24) into equation (8-1), the sediment discharge (designated as third) equation is obtained as:

$$q_s 3 = \frac{u_* c_0}{k} \int_0^D \left(\frac{1-\frac{y}{D}}{1+(e^M-1)\frac{y}{D}} \right)^{z'} \ln \frac{y}{y_0} dy \tag{8-7}$$

where $z' = \frac{\omega_s u_{max}(1-e^{-M})}{\beta u_*^2 M}$.

Substituting equations (6-3) and (7-29) into equation (8-1), the sediment discharge (designated as fourth) equation as:

$$q_s 4 = \frac{c_0}{N}\frac{u_*}{k} \int_0^D \ln\left(\exp(N') - (\exp(N') - 1)\frac{y}{D}\right) \ln \frac{y}{y_0} dy \tag{8-8}$$

Equation (8-6) can be simplified by substituting the mean sediment concentration. According to Choo's (2000) derivation, the mean sediment concentration can be written as

$$\frac{\bar{c}}{c_0} = \frac{\exp(N') - \frac{1}{NN'}[\exp(N') - 1]}{\exp(N') - 1} \tag{8-9}$$

Inputting equation (8-9) into equation (8-2) instead of equation (7-29), one obtains

$$q_s 4 = \frac{u_*}{k} c_0 \frac{exp(N') - \frac{1}{NN'}[exp(N') - 1]}{exp(N') - 1} \int_0^D ln\frac{y}{y_0} dy = \frac{u_*}{k} c_0 \frac{exp(N') - \frac{1}{NN'}[exp(N') - 1]}{exp(N') - 1} (DlnD - D) \tag{8-10}$$

Substituting equations (6-3) and (7-11) into equation (8-1), the sediment discharge (designated as fifth) equation is obtained as:

$$q_s 5 = c_0 \frac{u_*}{k} \int_0^D [1 - \frac{1}{N}(1 - \left((1-N)^{\frac{m}{m-1}} + \left(1 - (1-N)^{\frac{m}{m-1}}\right) F(c)\right)^{\frac{m-1}{m}})] \ln\frac{y}{y_0} dy \tag{8-11}$$

which also can be simplified like the fourth equation. Using equation (7-13), one obtains

$$q_s 5 = \frac{u_*}{k} c_0 (0.554N^2 - 0.077N + 0.568)(DlnD - D) \tag{8-12}$$

Table 8.2 shows the numerical solution of equations (8-7), (8-10) and (8-12) , which are also integrated by *dA* for the whole cross-section. The errors computed in these three methods are much smaller than that of *Qs1* and *Qs2*, with root mean square error for each as 0.212, 0.207 and 0.176.

Table 8.2 Computed sediment discharge for Einstein and Chien's (1955) data

obs. Qs g/s	Qs3 g/s	error	Qs4 g/s	error	Qs5 g/s	error
1.713	1.551	-0.094	1.609	-0.061	1.789	0.045
3.903	3.315	-0.151	3.291	-0.157	3.956	0.014
5.025	3.952	-0.213	3.999	-0.204	4.421	-0.120

Table 8.2 continued

obs. Qs g/s	Qs3 g/s	error	Qs4 g/s	error	Qs5 g/s	error
10.887	9.322	-0.144	8.413	-0.227	8.488	-0.220
0.920	0.772	-0.161	0.751	-0.183	0.796	-0.134
1.874	1.832	-0.022	1.783	-0.048	1.691	-0.098
2.322	1.792	-0.228	1.778	-0.234	1.844	-0.206
4.109	3.116	-0.242	3.081	-0.250	3.343	-0.186
5.706	4.569	-0.199	4.076	-0.286	5.123	-0.102
1.165	0.959	-0.176	1.020	-0.124	1.082	-0.070
5.048	4.229	-0.162	4.298	-0.149	4.062	-0.195
7.924	5.086	-0.358	5.077	-0.359	4.456	-0.438
9.628	7.552	-0.216	8.148	-0.154	7.438	-0.227
15.665	10.374	-0.338	11.365	-0.274	10.389	-0.337
14.379	9.486	-0.340	9.858	-0.314	10.215	-0.290

Comparing Figures 8.4 and 8.5, the fourth equation, which is equation (8-10) derived with Choo's (2000) sediment concentration, yields the best estimation of the suspended sediment discharge, since it is the most closely distributed to the 1:1 line. It is found that the fifth method, which is derived from the Tsallis entropy method leads to more accurate results for smaller values of sediment discharge. This might be because the Tsallis entropy-based method has an advantage in describing lower values of sediment concentration near the water surface.

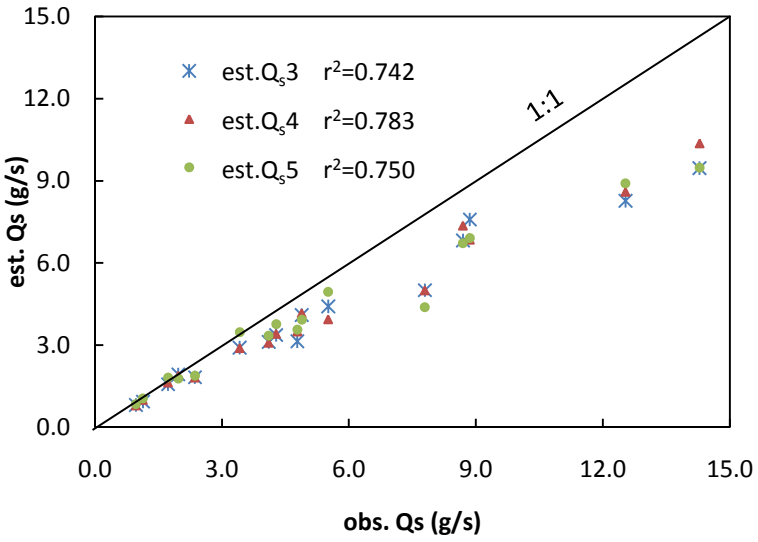

l

Figure 8.4 Comparison of sediment discharge values from Einstein and Chien (1955)

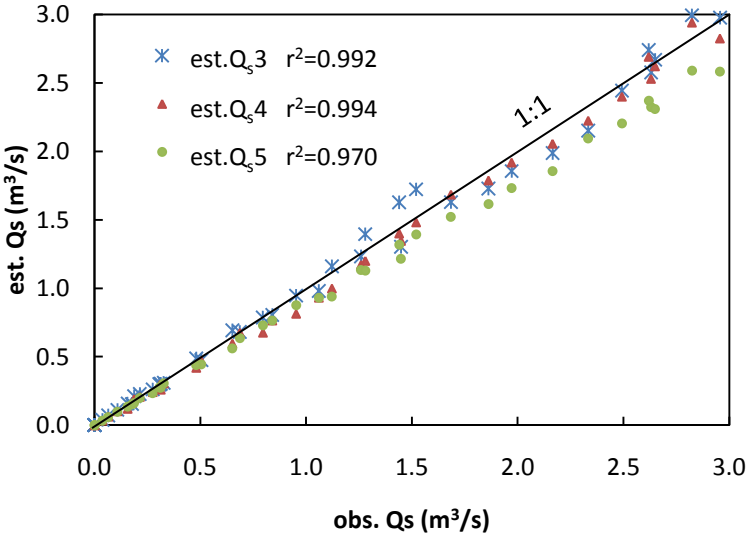

Figure 8.5 Comparison of sediment discharge values from Coleman (1981)

The estimated suspended sediment discharge is still smaller than observation for Einstein and Chien's (1955) experiment. As done in Section 8.2, the correction factor ω is applied. It is seen from Figure 8.6, after the modified the estimation is close to the

observation. However the value of correction factor is closer to 1 than that of Section 8.2, which implies the methods applied in this section are better than that in previous section.

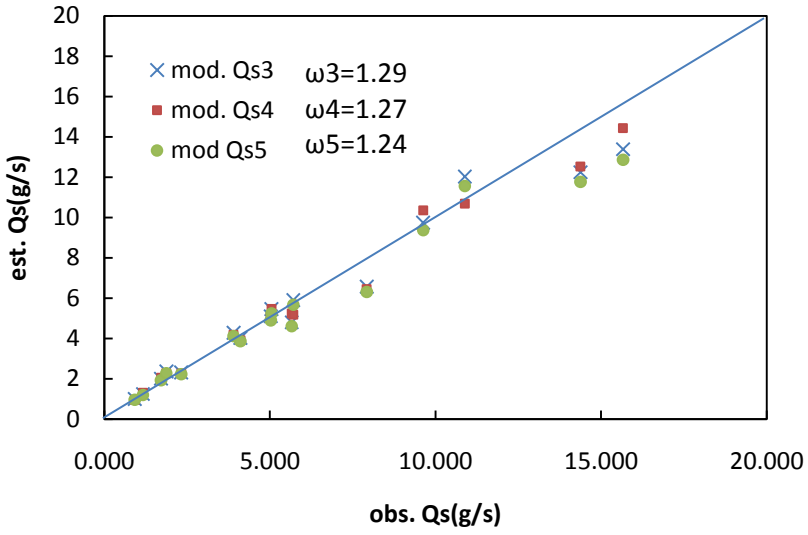

Figure 8.6 Modified sediment discharge values from Einstein and Chien (1955)

8.3 Third combination

Entropy based sediment discharge will be derived in this section, with both velocity and sediment concentration derived fully using the Tsallis entropy. The sixth equation is obtained from the Shannon entropy by substituting Chiu's velocity [equations (6-8)] and Choo's sediment concentration [equation (7-29)] into equation (8-1).

$$q_s 6 = \frac{c_0}{N}\frac{u_{max}}{M}\int_0^D \ln\left(\exp(N) - (\exp(N)-1)\frac{y}{D}\right)\ln\left(1 + (\exp(M)-1)y/D\right)dy \quad (8\text{-}13)$$

or the sediment discharge can be obtained by inputting equations (6-11) and (8-9) into equation (8-2), which is

$$q_s 6 = Dc_0 u_{max}[e^M(e^M-1)^{-1} - \frac{1}{M}]\frac{\exp(\mathrm{N}') - \frac{1}{\mathrm{NN}'}[\exp(\mathrm{N}')-1]}{\exp(\mathrm{N}')-1} \quad (8\text{-}14)$$

The last equation is the Tsallis entropy-based equation obtained from the velocity distribution and sediment concentration distribution derived in this thesis:

$$q_s 7 = \mathrm{c}_0 u_{max} \int_0^D [1 - \frac{1}{N}\left(1 - \left((1+0.5lnN)F(u) - 0.5lnN\right)^{\frac{2}{3}}\right)][1 -$$

$$1G1-1+0.5lnGFu-0.5lnG23]\mathrm{dy} \quad (8\text{-}15)$$

Equation (8-15) can also be simplified by substituting equations (5-31) and (7-13) into equation (8-2).

$$q_s 7 = Dc_0 u_{max}(0.554N^2 - 0.077N + 0.568)(0.554G^2 - 0.077G + 0.568) \quad (8\text{-}16)$$

The last two equations (8-14) and (8-16) are computed as shown in Table 8.3. *Qs* for the whole cross-sectional sediment discharge is computed instead of the specific discharge q_s. It is seen from the error values that both sets of computed values are slightly smaller than observed values.

Table 8.3 Computed sediment discharge values for Einstein and Chien's (1955) data

obs. Qs g/s	Qs6 g/s	error	Qs7 g/s	error
1.713	1.553	-0.094	1.828	0.068
3.903	3.420	-0.124	3.957	0.014
5.025	3.995	-0.205	4.526	-0.099
5.659	3.830	-0.323	4.338	-0.234
10.887	9.770	-0.103	8.823	-0.190
0.920	0.761	-0.172	0.809	-0.120
1.874	1.797	-0.041	1.771	-0.055
2.322	1.823	-0.215	1.940	-0.165
4.109	3.265	-0.205	3.594	-0.125
5.706	4.651	-0.185	5.408	-0.052
1.165	0.937	-0.196	1.073	-0.078

Table 8.3 continued

obs. Qs g/s	Qs6 g/s	error	Qs7 g/s	error
5.048	4.290	-0.150	4.235	-0.161
7.924	6.655	-0.160	6.097	-0.231
9.628	7.908	-0.179	7.857	-0.184
15.665	11.748	-0.250	11.660	-0.256
14.379	10.697	-0.256	11.916	-0.171

The Shannon entropy based discharge and the Tsallis entropy based discharge are competitive in these cases. It is seen from the Figure 8.7 that the two methods give similar results in estimating sediment discharge which is that the estimated sediment discharge is smaller than observed discharge. In Figure 8.8, the Shannon entropy based sediment discharge is distributed around the 1:1 line, while the Tsallis entropy based estimation is still a little smaller than observed values. However, since the Tsallis entropy based velocity distribution and the sediment concentration distribution did not show any trend of smaller estimation, the reason is yet to be discovered.

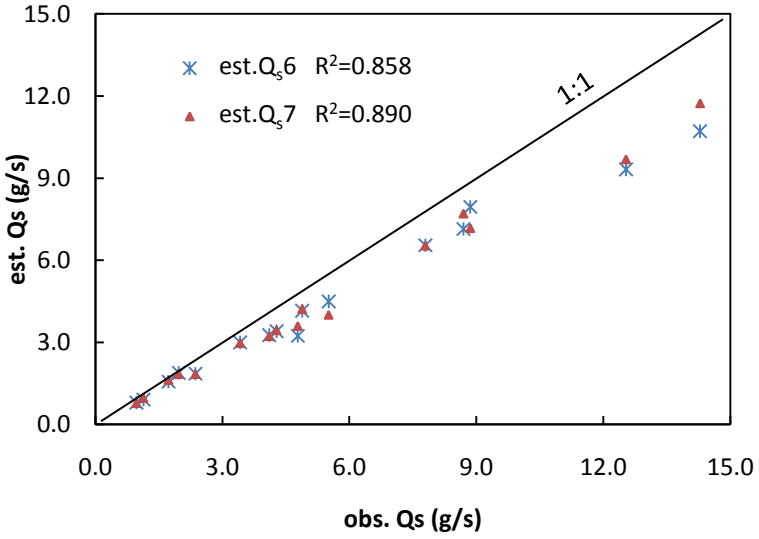

Figure 8.7 Comparison of sediment discharge for Einstein and Chien (1955)

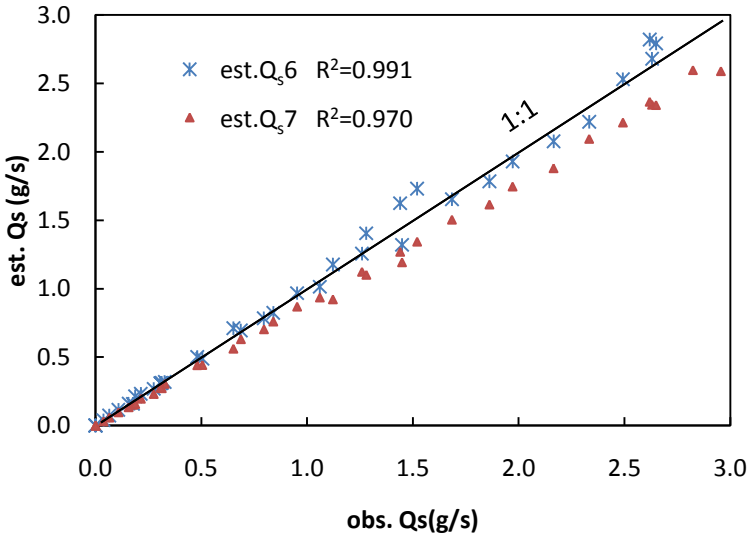

Figure 8.8 Comparison of sediment discharge values for Coleman (1981)

Figure 8.9 shows the modified suspended sediment discharge for the last two methods. Since the accuracy of the last two methods is higher than those discussed in Sections 8.2 and 8.3, the correction factor are most close to the value of 1.

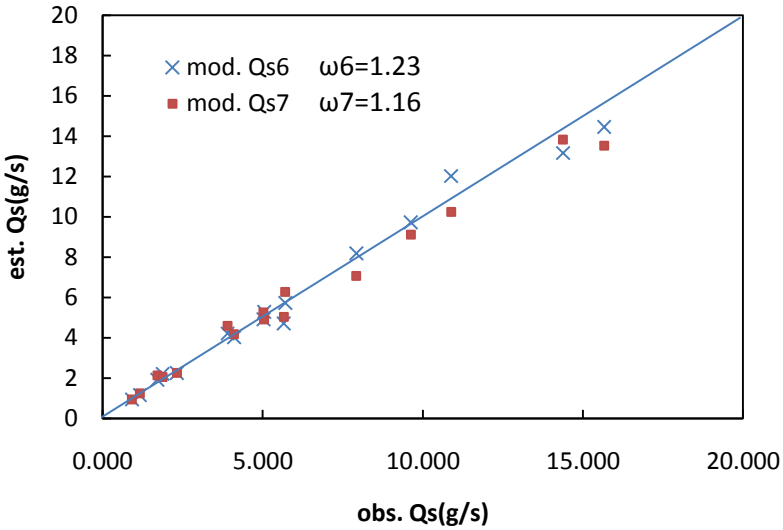

Figure 8.9 Modified sediment discharge values for Einstein and Chien (1955)

Comparing all Figures 8.1 to 8.6, the results shown in Figures 8.7 and 8.8 with both entropy methods for velocity and sediment concentration give highest value of R^2 compared to previous cases, which means the entropy-based methods give the most accurate predictions. It can be concluded that the entropy-based distribution does have an advantage over traditional methods.

9. CONCLUSIONS

Entropy-based methods are developed to compute the velocity distribution, sediment concentration and suspended sediment discharge, which are shown to be more accurate than traditional methods. The following conclusions can be drawn:

1. A hypothesis on the cumulative distribution function for the Cartesian coordinate system is verified with observed values. The exponent values in the cumulative distribution are shown to be related to the width-depth ratio for the velocity distribution, while it is shown to be related to the particle size for the sediment concentration.
2. A velocity distribution equation is derived with the Tsallis entropy and verified using experimental data. The exponent m value is proved to equal 3 as the best choice.
3. A dimensionless parameter G is introduced, which can be obtained from the maximum and mean velocities of a channel-section. Vice versa, for a known cross-section, the mean velocity can be obtained from the G value, whose accuracy is supported by observations.
4. The location of maximum velocity is discussed and an analytical solution is derived. However, lacking observed values, the computed values are not convincing.

5. Comparison with other velocity distributions, the Tsallis entropy based velocity distribution seems most accurate. This distribution is also better in capturing low velocities near the channel bed.
6. The sediment concentration distribution equation is derived with the Tsallis entropy and verified with experimental data.
7. A dimensionless parameter N is introduced like parameter G. The mean sediment concentration value is simply computed with known N value.
8. The Tsallis entropy-based sediment concentration has an advantage over other methods, especially for the sediment concentration near the water surface.
9. Suspended sediment discharge is computed with estimated velocity and sediment concentration for 7 different methods. From comparison of computed values, the entropy based methods show more advantages over traditional methods.

However, the research provided in this thesis has the following limitations:

1. The mathematical model developed in this project is proposed to be capable of describing the velocity and sediment concentration for all circumstances. However, the model itself contains parameters which need to be specified by observed data, which limits this method only applicable for the known channel sections with historical data. The validity of the data itself is also uncertain.

2. The entropy-based model is based on the probabilistic theory, which is not based on the physical process; hence it may lack relationships with physical factors, such as the characteristics of channel system and flow patterns.

REFERENCES

Afzalimehr, H. and Anctil, F. (1999), "Velocity distribution and shear velocity behavior of decelerating flows over a gravel bed", *Can J. Civil Eng.*, 26(4), 468-475.

Afzalimehr, H. and Anctil, F. (2000), "Accelerating shear velocity in gravel-bed channels", *Hydrolog Sci J*, 45(1), 113-124.

Afzalimehr, H. and Rennie, C. D. (2009), "Determination of bed shear stress in gravel-bed rivers using boundary-layer parameters", *Hydrolog Sci. J.*, 54(1), 13.

Barbe, D. E. (1990), "Probabilistic analysis of bridge scour using the principle of maximum entropy", Ph.D. dissertation, *Louisiana State University*, Baton Rouge, LA.

Barbe, D. E., Cruise, J. F. and Singh, V. P. (1991), "Solution of 3-constraint entropy-based velocity distribution", *J. Hydraul. Eng.,* 117(10), 1389-1396.

Blasius, H. (1913), "Das Ahnlichkeitsgesetz bei Ribungsvorgangen in Flussigkeiten", *Forsch Gebiete Ingeieurw*., 131.

Chien, N. and Wan, Z. (2003), "*Mechanics of sediment transport*", Science Press, Beijing.

Chiu, C. L. (1987), "Entropy and probability concepts in hydraulics", *J. Hydraul. Eng.,* 113(5), 583-600.

Chiu, C. L. (1988), "Entropy and 2-D velocity distribution in open channels", *J. Hydraul. Eng.,* 114(7), 738-756.

Chiu, C. L. (1989), "Velocity distribution in open channel flow", *J. Hydraul. Eng.,* 115(5), 576-594.

Chiu, C. L. (1991), "Application of entropy concept in open-channel flow", *J. Hydraul. Eng.*,117(5), 615-628.

Chiu, C. L., and Hsu, S. M. (2006), "Probabilistic approach to modeling of velocity distributions in fluid flows", *J. Hydrol.*, 316(1-4), 28-42.

Chiu, C. L., and Lin, G. F. (1983), "Computation of 3-D flow and shear in open channels", *J. Hydraul. Eng.*, 112(11), 1424-1440.

Chiu, C. L. and Chiou J. (1986), "Structure of 3-D flow in rectangular open channels", *J. Hydraul. Eng.*, 109(11), 1050-1068.

Chiu, C. L., and Murray, D. W. (1992), "Variation of velocity distribution along nonuniform open-channel flow", *J. Hydraul. Eng.,* 118(7), 989-1001.

Chiu, C. L., and Said, C. A. A. (1995), "Maximum and mean velocities and entropy in open-channel flow", *J. Hydraul. Eng.,* 121(1), 26-35.

Chiu, C. L., and Tung, N. C. (2002), "Maximum velocity and regularities in open-channel flow", *J. Hydraul. Eng.,* 128(8), 803-803.

Chiu, C. L., Jin, W. and Chen, Y. C. (2000), "Mathmatical models of distribution of sediment concentration", *J. Hydraul. Eng.,* 126(1).

Chiu, C. L., Lin, G. F. and Lu, J. M. (1993), "Application of probability and entropy concepts in pipe-flow study", *J. Hydraul. Eng.,* 119(6), 742-756.

Choo, T. H. (2000), "An efficient method of the suspended sediment-discharge measurement using entropy concept", *Water Engineering Research*, *1*(2), 95-105.

Coleman, N. L. (1981), "Velocity profiles with suspended sediment", *J. Hydraul. Res.*, 19(3), 211-229.

Coleman, N. L. (1986), “Effects of suspended sediment on the open-channel velocity distribution”, *Water Resour. Res.*, 22(10), 1377-1384.

Daugherty, R. L. and Franzini, J. B. (1977), “*Fluid Mechanics with Engineering Applications*”, McGraw-Hill Book Co., New York.

Einstein, H. A. (1950), “The bed load function for sediment transportation in open channels”, *Technical Bulletin 1026.* Washington, DC: USDA, Soil Conservation Service,1950.

Einstein, H. A. and Chien, N. (1955), “Effects of heavy sediment concentration near the bed on velocity and sediment distribution”, *MRD Series Report No.8.University of California at Berkeley and Missouri River Division*, U.S. Army Corps of Engineers, Omaha, NE.

Francis, J. B. (1878), “On the cause of the maximum velocity of water flowing in open channels being below the surface”, *Trans.,* May.

Jaynes, E. T. (1957a), “Information theory and statistical mechanics 1.”, *Phys. Rev.*, 106(4), 620-630.

Jaynes, E. T. (1957b), “Information theory and statistical mechanics 2.”, *Phys. Rev.*, 108(2), 171-190.

Keulegan, G. H. (1938), “Laws of turbulent flow in open channels”, *J. Res. Nat. Bur. Stand*, 21(6), 707-741.

Krarim, M. F. and Kennedy, J. F. (1987). "Velocity and sediment concentration profiles in river flows." *J. Hydraul. Eng.*, 113, 159-178.

Luo, H. (2009), "Tsallis entropy based velocity distributions in open channel flows", M.S. thesis, *Texas A&M University*, College Station, TX.

Luo, H. and Singh, V. P. (2011), "Entropy theory for two-dimensional velocity distribution", *J. Hydrologic Eng, in press*.

Marini, G., Martino, G. D., Fontana, N., Fiorentino, M. and Singh, V.P. (2010), "Derivation of 2D velocity distribution in open channel flow using entropy", *J. Hydraulic Research*, *under review*.

Moramarco, T., Saltalippi, C. and Singh, V. P. (2004), "Estimation of mean velocity in natural channels based on Chiu's velocity distribution equation", *J. Hydrol. Eng.*, 9(1), 42-50.

Murphy, C. (1904), "Accuracy of stream measurements", *Water Supply and Irrigation* Paper, 95, 2.

Nezu, I. and Nakagawa, H. (1993), "*Turbulence in open-channel flows*", Balkema, Rotterdam, The Netherlands.

Rouse, H. (1937), "Modern conceptions of the mechanics of turbulence", *Trans.,* 102, 463-543.

Rubey, W. W. (1933), "Settling velocities of gravel, sand, and silt particles", *American Journal of Science*, 5th series, 25(148), 38.

Sarma, K. V. N., Lakshminarayana, P. and Rao, N. S. L., (1983), "Velocity distribution in smooth rectangular open channels", *J. Hydraul. Eng., ASCE*, 109(2), 270-289.

Shannon, C. E. (1948), "A mathematical theory of communication", *At&t Tech J*, *27*(3), 379-423.

Singh, V. P. (1997), "The use of entropy in hydrology and water resources", *Hydrol. Process*, 11(6), 587-626.

Singh, V. P. and Luo, H. (2009), "Derivation of velocity distribution using entropy", *Proc., IAHR Congress,* Vancouver, Canada, 31-38.

Singh, V. P. and Luo, H. (2011), "Entropy theory for distribution of one-dimensional velocity in open channels", *J. of Hydrologic Eng., in press.*

Singh, V. P. and Rajagopal, A. K. (1987), "Some recent advances in the application of the principle of maximum entropy (POME) in hydrology", *Proc. of the Water for the Future: Hydrology in perspective*, IAHS Publ., Rome, 353-364.

Singh, V. P., Rajagopal, A. K. and Singh, K. (1986), "Derivation of some frequency distributions using the principle of maximum entropy (POME)", *Adv. Water Resources*, 9(June), 91-106.

Sonuga, J. O. (1972), "Principle of maximum entropy in hydrological frequency analysis", *J. of Hydrol.,* 17, 177-191.

Sonuga, J. O. (1976), "Entropy principle applied to rainfall-runoff process", *J. of Hydrol.*, 30, 81-94.

Stearns, F. P. (1883). "On the currentmeter, together with a reason why the maximum velocity of water flowing in open channel is below the surface." *Trans.,* Aug.

Stokes, G. G. (1851), "On the effect of the internal friction of fluids on the motion of pendulums", *Trans. Camb. Phil. Soc*., 9, 8-106.

Sturm, T. W. (2010), "*Open Channel Hydraulics*", McGraw-Hill, New York.

Tsallis, C. (1988), "Possible generalization of Boltzmann-Gibbs statistics", *J. Stat. Phys.*, 52(1-2), 479-487.

Van Rijn, L. C. (1984), "Sediment transport, part 2: suspended load transport", *J. of Hydraulic Engineering,* 110(11), 1733-1754.

Vanoni, V. A. (1941), "Velocity distribution in open channels", *Civil Eng. Syst.*, 11, 356-357.

von Karman, T. (1935), "Some aspects of the turbulence problem", *Mech. Eng*., July, 407-412.

Xia, R. J. (1997), "Relation between mean and maximum velocities in a natural river", *J. Hydraul. Eng.,* 123(8), 720-723.

Yang, S. Q., Tan, S. K. and Lim, S. Y., (2004), "Velocity distribution and dip-phenomenon in smooth uniform open channel flows", *J. Hydraul. Eng.,* 130(12), 1179-1186.

Zanke, U. (1977), "Berechnung der Sinkgeschwindigkeiten von sedimenten", *Mitt. des Franzius instituts fuer Wasserbau*, Heft 46, Seite 243, Technical University, Hannover, Germany.

APPENDIX A

VELOCITY DATA OBSERVED FROM ITALIAN RIVERS

Table A1 Measured velocity data for May 28, 1984, at Santa Lucia on Tiber River, Italy. (LS means the left side, RS is the right side)

vertical n.	z (m)	depth (m)	u obs. (m/s)
LS	-11.89	0	0
1	-7.24	0	1.68
1	-7.24	0.06	1.68
1	-7.24	0.2	1.70
1	-7.24	0.8	2.10
1	-7.24	1.5	2.00
1	-7.24	2.45	1.45
1	-7.24	2.95	0.71
1	-7.24	3.1	0.00
2	-4.13	0	2.24
2	-4.13	0.06	2.24
2	-4.13	0.2	2.24
2	-4.13	0.8	2.34
2	-4.13	1.38	2.39
2	-4.13	2.29	2.29
2	-4.13	3.14	1.50
2	-4.13	3.29	0.00
3	0	0	2.39
3	0	0.06	2.39
3	0	0.2	2.44
3	0	0.8	2.44
3	0	1.34	2.35
3	0	2.33	2.29
3	0	2.78	1.90
3	0	2.93	0.00
4	3.11	0	1.75
4	3.11	0.06	1.75
4	3.11	0.2	1.85
4	3.11	0.8	2.29
4	3.11	1.5	2.29
4	3.11	2.36	1.75
4	3.11	2.83	1.55
4	3.11	2.98	0.00

Table A1 continued

vertical n.	z (m)	depth (m)	u obs. (m/s)
5	6.21	0	1.28
5	6.21	0.06	1.28
5	6.21	0.2	1.23
5	6.21	0.8	1.33
5	6.21	1.5	1.13
5	6.21	2	1.06
5	6.21	2.35	1.13
5	6.21	2.5	0.00
RS	9.3	0	0

Table A2 Measured velocity data for May 28, 1984, at Rosciano on Chiascino River, Italy. (LS means the left side, RS is the right side)

vertical n.	z (m)	depth (m)	U obs. (m/s)
LS	-16.32	0	0
1	-10.34	0	1.126
1	-10.34	0.06	1.126
1	-10.34	0.26	1.261
1	-10.34	0.86	1.461
1	-10.34	1.56	1.177
1	-10.34	2.36	0.922
1	-10.34	2.56	0.294
1	-10.34	2.81	0
2	-7.25	0	1.695
2	-7.25	0.06	1.695
2	-7.25	0.26	1.762
2	-7.25	1.06	1.762
2	-7.25	2.06	1.561
2	-7.25	2.76	1.244
2	-7.25	2.96	1.244
2	-7.25	3.11	0
3	-4.14	0	2.008
3	-4.14	0.06	2.008
3	-4.14	0.26	2.133
3	-4.14	1.06	1.966
3	-4.14	2.06	1.674
3	-4.14	2.76	1.319
3	-4.14	2.96	1.277
3	-4.14	3.11	0
4	0	0	2.447
4	0	0.06	2.447
4	0	0.26	2.175
4	0	1.06	2.071
4	0	2.06	1.758
4	0	2.76	1.34
4	0	2.96	1.236
4	0	3.11	0
5	4.13	0	2.112
5	4.13	0.06	2.112
5	4.13	0.26	2.112
5	4.13	1.06	2.029

Table A2 continued

vertical n.	z (m)	depth (m)	U obs. (m/s)
5	4.13	1.86	1.82
5	4.13	2.46	1.57
5	4.13	2.66	1.34
5	4.13	2.81	0
6	8.27	0	1.883
6	8.27	0.6	1.883
6	8.27	0.26	1.862
6	8.27	1.06	1.883
6	8.27	1.86	1.674
6	8.27	2.21	1.465
6	8.27	2.46	1.236
6	8.27	2.66	1.109
6	8.27	2.81	0
7	11.37	0	1.486
7	11.37	0.06	1.486
7	11.37	0.26	1.549
7	11.37	0.86	1.632
7	11.37	1.56	1.444
7	11.37	2.16	1.298
7	11.37	2.36	1.067
7	11.37	2.51	0
8	14.47	0	0.82
8	14.47	0.06	0.82
8	14.47	0.26	0.956
8	14.47	0.86	1.261
8	14.47	1.56	1.177
8	14.47	2.06	0.939
8	14.47	2.26	0.837
8	14.47	2.41	0
RS	19.62	0	0

Table A3 Measured velocity data for April 21, 1997, at Ponte Felcino on Tiber River, Italy. (LS means the left side, RS is the right side)

vertical n.	z (m)	depth (m)	U obs. (m/s)
LS	-25.58	0	0
1	-18.86	0	0.83
1	-18.86	0.06	0.83
1	-18.86	0.2	0.74
1	-18.86	1	0.64
1	-18.86	2	1.15
1	-18.86	3	0.96
1	-18.86	3.9	0.74
1	-18.86	4.1	0.71
1	-18.86	4.25	0.00
2	-14.66	0	1.21
2	-14.66	0.06	1.21
2	-14.66	0.2	1.21
2	-14.66	1	1.18
2	-14.66	2	1.56
2	-14.66	3	1.09
2	-14.66	3.8	0.83
2	-14.66	4	0.71
2	-14.66	4.15	0.00
3	-10.46	0	2.06
3	-10.46	0.06	2.06
3	-10.46	0.2	2.34
3	-10.46	1	2.31
3	-10.46	1.93	2.44
3	-10.46	2.88	2.19
3	-10.46	3.88	2.06
3	-10.46	4.28	1.65
3	-10.46	4.48	1.59
3	-10.46	4.63	0.00
4	-6.29	0	2.99
4	-6.29	0.06	2.99
4	-6.29	0.2	2.66
4	-6.29	0.8	2.82
4	-6.29	1.71	2.66
4	-6.29	3	2.61
4	-6.29	4	2.36
4	-6.29	5	1.95

Table A3 continued

vertical n.	z (m)	depth (m)	U obs. (m/s)
4	-6.29	5.2	1.60
4	-6.29	5.45	1.46
4	-6.29	5.6	0.00
5	0	0	3.36
5	0	0.06	3.36
5	0	0.2	3.16
5	0	1	3.20
5	0	2	3.28
5	0	3	2.91
5	0	4	2.78
5	0	5	2.32
5	0	5.8	2.03
5	0	6	1.86
5	0	6.15	0.00
6	3.78	0	3.16
6	3.78	0.06	3.16
6	3.78	0.2	3.11
6	3.78	1	3.28
6	3.78	2	3.20
6	3.78	2.88	2.61
6	3.78	3.88	2.57
6	3.78	4.88	2.53
6	3.78	5.7	2.03
6	3.78	5.94	1.86
6	3.78	6.09	0.00
7	7.34	0	2.36
7	7.34	0.06	2.36
7	7.34	0.2	2.61
7	7.34	1	2.70
7	7.34	2	2.74
7	7.34	2.93	2.61
7	7.34	3.88	2.53
7	7.34	4.88	2.32
7	7.34	5.38	0.98
7	7.34	5.7	1.19
7	7.34	5.85	0.00
8	10.49	0	1.78

Table A3 continued

vertical n.	z (m)	depth (m)	U obs. (m/s)
8	10.49	0.06	1.78
8	10.49	0.2	1.44
8	10.49	1	2.15
8	10.49	2	2.32
8	10.49	3	2.57
8	10.49	3.5	2.32
8	10.49	4.6	1.95
8	10.49	5	1.61
8	10.49	5.7	0.00
RS	16.47	0	0

Table A4. Maximum and mean velocities collected at P. Felcino gauged section during 20 years

u_{max} (m/s)	u_{mean} (m/s)	u_{max} (m/s)	u_{mean} (m/s)
0.274	0.186	2.405	1.594
0.771	0.492	3.320	2.163
0.794	0.471	3.181	2.074
1.678	1.110	2.660	1.815
0.594	0.409	3.365	2.120
1.130	0.820	0.206	0.123
0.082	0.041	3.410	2.097
0.146	0.111	1.102	0.726
1.902	1.292	2.164	1.449
2.608	1.802	1.810	1.190
3.362	2.296	2.079	1.373
0.868	0.604	2.680	1.874
1.122	0.777	1.461	0.957
2.547	1.734	2.637	1.687
2.924	2.025	2.906	1.858
3.118	2.154	2.580	1.900
1.421	1.026	1.340	0.885
0.061	0.023	1.394	1.060

Table A5. Maximum and mean velocities collected at S. Lucia gauged section during 20 years

u_{max} (m/s)	u_{mean} (m/s)	u_{max} (m/s)	u_{mean} (m/s)
0.088	0.047	3.094	1.945
0.269	0.182	3.062	2.109
1.208	0.948	0.496	0.305
1.467	1.072	0.234	0.147
1.773	1.135	1.603	0.996
1.631	1.179	1.678	1.062
2.760	1.478	2.816	1.816
2.243	1.648	2.781	1.882
0.129	0.067	2.781	1.803
0.495	0.324	0.888	0.570
0.644	0.401	0.270	0.153
1.155	0.736	1.511	1.040
2.194	1.497	0.453	0.262
2.437	1.873	2.948	1.984
0.107	0.052	2.989	2.020
0.482	0.315	2.781	1.819
0.735	0.497	2.580	1.707
1.022	0.672	0.228	0.152
1.678	1.151	2.739	1.836
0.209	0.123	2.581	1.750
2.625	1.736	1.453	0.979
2.778	1.910	0.268	0.154
0.781	0.541	1.227	0.697
1.462	0.926	2.555	1.604
2.182	1.397	1.403	0.870

Table A6. Maximum and mean velocities collected at P. Nuovo gauged section during 20 years

u_{max} (m/s)	u_{mean} (m/s)	u_{max} (m/s)	u_{mean} (m/s)
0.978	0.620	2.097	1.463
2.243	1.373	2.405	1.669
2.384	1.593	0.884	0.566
2.023	1.085	1.954	1.257
0.42	0.262	1.904	1.276
1.803	1.186	1.202	0.825
2.097	1.464	1.221	0.828
0.694	0.471	0.387	0.207
2.972	1.833	1.261	0.854
2.194	1.487	0.349	0.232
0.69	0.448	2.054	1.339
1.288	0.923	0.357	0.249
2.048	1.406	2.597	1.736
0.673	0.442	2.48	1.798
1.578	1.136	1.925	1.33
0.209	0.117	2.719	1.82
2.024	1.324	1.779	1.151
2.048	1.331	1.777	1.211
2.972	1.946	0.736	0.507
2.924	1.966	0.221	0.146
2.521	1.712	1.777	1.173
0.965	0.615	2.169	1.391
2.827	1.791	2.029	1.255
0.346	0.201	1.05	0.71
2.48	1.627	2.28	1.64
2.73	1.623	2.387	1.634
1.954	1.157	2.699	1.847
1.85	1.106	2.778	1.825

APPENDIX B

VELOCITY DATA FROM IRANIAN RIVERS

Table B1. Velocity data of Run A0-2 from Ghamasiab River in Iran (d_{50}=14.5mm)

Profile 1		Profile 2		Profile 3		Profile 4		Profile 5	
Depth	Velocity	Depth	Velocity	Depth	Velocity	Depth	Velocity	Depth	Velocity
m	m/s	m	m/s	m	m/s	m	m/s	m	m/s
0.000	0.000	0.000	0.000	0.000	0.000	0.000	0.000	0.000	0.000
0.050	0.196	0.050	0.196	0.050	0.218	0.050	0.178	0.050	0.185
0.060	0.318	0.060	0.303	0.060	0.229	0.060	0.270	0.060	0.189
0.070	0.273	0.070	0.285	0.070	0.270	0.070	0.321	0.070	0.167
0.080	0.303	0.080	0.325	0.080	0.303	0.080	0.321	0.080	0.196
0.090	0.189	0.090	0.299	0.090	0.388	0.090	0.296	0.090	0.203
0.100	0.237	0.110	0.292	0.110	0.395	0.110	0.273	0.100	0.259
0.120	0.310	0.130	0.347	0.130	0.421	0.130	0.292	0.120	0.273
0.140	0.417	0.160	0.384	0.160	0.406	0.160	0.296	0.140	0.266
0.170	0.487	0.190	0.325	0.190	0.366	0.190	0.292	0.160	0.255
0.200	0.439	0.230	0.424	0.230	0.410	0.230	0.277	0.190	0.299
0.230	0.351	0.280	0.347	0.280	0.395	0.280	0.325	0.230	0.292
0.280	0.413	0.390	0.413	0.330	0.421	0.330	0.303	0.280	0.314
0.330	0.413	0.450	0.399	0.380	0.421	0.380	0.310	0.330	0.314
0.380	0.388	0.510	0.424	0.440	0.277	0.450	0.318	0.380	0.310
0.410	0.388	0.540	0.413	0.500	0.399	0.520	0.303	0.420	0.237
0.440	0.292	0.570	0.421	0.540	0.491	0.560	0.358	0.450	0.222
				0.580	0.450	0.590	0.347		

Table B2. Velocity data of Run A2-1 from Ghamasiab River in Iran (d_{50}=14.4mm)

Profile 1		Profile 2		Profile 3		Profile 4		Profile 5	
Depth	Velocity	Depth	Velocity	Depth	Velocity	Depth	Velocity	Depth	Velocity
m	m/s	m	m/s	m	m/s	m	m/s	m	m/s
0.000	0.000	0.000	0.000	0.000	0.000	0.000	0.000	0.000	0.000
0.050	0.399	0.050	0.373	0.050	0.642	0.050	0.539	0.050	0.351
0.060	0.424	0.060	0.406	0.060	0.721	0.060	0.582	0.060	0.355
0.070	0.443	0.070	0.517	0.070	0.735	0.070	0.685	0.070	0.399
0.080	0.465	0.080	0.469	0.080	0.692	0.080	0.807	0.080	0.410
0.090	0.458	0.090	0.557	0.090	0.746	0.090	0.817	0.090	0.417
0.100	0.553	0.100	0.603	0.100	0.792	0.100	0.846	0.100	0.428
0.110	0.589	0.110	0.635	0.110	0.807	0.110	0.821	0.110	0.469
0.120	0.575	0.130	0.614	0.130	0.882	0.130	0.874	0.130	0.443
0.130	0.571	0.150	0.728	0.150	0.885	0.150	0.939	0.150	0.480
0.140	0.567	0.170	0.824	0.170	0.946	0.170	1.006	0.170	0.476
0.150	0.550	0.200	0.796	0.200	0.960	0.200	1.071	0.200	0.469
0.160	0.567	0.230	0.867	0.230	0.989	0.230	1.071	0.230	0.487
0.170	0.599	0.260	0.903	0.260	1.003	0.260	1.060	0.260	0.480
0.180	0.603	0.290	0.903	0.290	1.017	0.290	1.056	0.290	0.487
0.190	0.639	0.320	0.939	0.320	1.039	0.310	1.046	0.320	0.498
0.200	0.624	0.340	0.932	0.340	1.046	0.330	1.042		
0.210	0.617								

Table B3. Velocity data of Run B9-1 from Ghamasiab River in Iran (d_{50}=16.9mm)

Profile 1		Profile 2		Profile 3		Profile 4		Profile 5	
Depth	Velocity	Depth	Velocity	Depth	Velocity	Depth	Velocity	Depth	Velocity
m	m/s	m	m/s	m	m/s	m	m/s	m	m/s
0.000	0.000	0.000	0.000	0.000	0.000	0.000	0.000	0.000	0.000
0.050	0.159	0.050	0.123	0.050	0.251	0.050	0.314	0.050	0.200
0.060	0.207	0.060	0.170	0.060	0.288	0.060	0.318	0.060	0.192
0.070	0.170	0.070	0.178	0.070	0.303	0.070	0.366	0.070	0.229
0.080	0.203	0.080	0.203	0.080	0.292	0.080	0.391	0.080	0.203
0.090	0.192	0.090	0.207	0.090	0.343	0.090	0.373	0.090	0.229
0.100	0.233	0.100	0.281	0.100	0.318	0.100	0.366	0.100	0.240
0.120	0.255	0.120	0.310	0.120	0.340	0.120	0.384	0.120	0.222
0.140	0.270	0.140	0.277	0.140	0.332	0.140	0.402	0.140	0.255
0.170	0.292	0.170	0.358	0.170	0.399	0.170	0.432	0.170	0.273
0.200	0.248	0.200	0.384	0.200	0.391	0.200	0.480	0.200	0.299
0.240	0.277	0.240	0.391	0.240	0.443	0.240	0.480	0.240	0.318
0.280	0.321	0.280	0.443	0.280	0.439	0.280	0.491	0.280	0.340
0.320	0.329	0.330	0.443	0.330	0.517	0.330	0.494	0.330	0.343
0.370	0.347	0.380	0.469	0.380	0.491	0.380	0.546	0.380	0.310
0.420	0.340	0.440	0.454	0.440	0.531	0.440	0.535	0.440	0.310
0.470	0.332	0.500	0.480	0.500	0.539	0.500	0.528	0.490	0.303
		0.540	0.498	0.540	0.524	0.530	0.550	0.540	0.296
		0.580	0.502	0.580	0.546	0.560	0.546		

APPENDIX C

DATA FROM EINSTEIN AND CHIEN (1955)

Table C1. Velocity data of C1 from Einstein and Chien (1955) (h=0.46ft, u_*=0.391ft/s)

y/h	u/u_*
0.013	7.02
0.013	6.27
0.0152	6.42
0.0174	7.24
0.0174	6.76
0.01955	7.31
0.0217	7.57
0.0261	8.02
0.0304	8.1
0.0435	9.12
0.0521	9.9
0.0609	10.06
0.0826	10.75
0.0956	11.55
0.115	11.72
0.161	12.54
0.1825	13.2
0.215	13.4
0.248	13.74
0.302	14.33
0.354	15.05
0.465	16.1

Table C2. Velocity data of S2 from Einstein and Chien (1955) (h=0.392ft, u_*=0.422ft/s)

y/h	u/u_*
0.0153	7.15
0.0204	7.88
0.0255	8.64
0.0332	9.47
0.0383	9.82
0.046	10.68
0.0587	11.5
0.0715	12.23
0.0842	12.84
0.097	13.6
0.11	14.05
0.122	14.7
0.135	15.15
0.148	15.5
0.161	15.85
0.174	16.2
0.186	16.27
0.199	16.68
0.212	16.77
0.224	17.1
0.25	17.34
0.288	17.9

Table C3. Sediment of S2 from Einstein and Chien (1955)

(h-y)/y	total c g/l
17.66	121
16.05	106
14.1	99
12.05	78.5
9.9	58
7.91	36.2
6.54	21
5.33	12.3
4.45	7.35
3.51	3.73

Table C4. Velocity data of C5 from Einstein and Chien (1955) ($h=0.582ft$, $u_*=0.246ft/s$)

y/h	u/u_*
0.00774	8.78
0.0103	9.47
0.01545	11.06
0.0189	11.38
0.0275	12.65
0.0361	13.25
0.0447	13.9
0.0533	14.23
0.0705	15.07
0.0877	15.65
0.105	16.2
0.122	16.65
0.148	17.25
0.1735	17.7
0.1995	18.15
0.225	18.4
0.26	19
0.294	19.25
0.328	19.85
0.363	20.2
0.415	20.6
0.467	20.9
0.638	21.1

Table C5. Velocity data of S4 from Einstein and Chien (1955) (h=0.476 ft, u_*=0.36 ft/s)

y/h	u (ft/s)
0.0165	2.37048
0.0206	2.4038
0.0261	2.62752
0.0316	2.80364
0.0371	3.094
0.0508	3.5938
0.0645	4.0698
0.0783	4.522
0.092	4.9504
0.106	5.355
0.1195	5.67392
0.133	6.00712
0.147	6.2832
0.174	6.7592
0.202	7.1162
0.229	7.4494
0.257	7.7588
0.27	7.9254
0.284	8.0444
0.312	8.3538
0.34	8.79648

Table C6. Sediment data of S4 from Einstein and Chien (1955)

(h-y)/y	total c g/l
14.15	328
12.96	295
11.5	263
9.95	230.5
8.25	167.3
6.66	117
5.53	76.5
4.52	45.1
3.78	28.1
2.98	14.2

Table C7. Velocity data of S7 from Einstein and Chien (1955) (h=0.47 ft, u_*=0.387 ft/s)

y/h	u/u*
0.0128	6.39
0.0128	6.79
0.017	7.26
0.0213	8.15
0.0256	8.95
0.0277	9.14
0.0383	10.4
0.0468	11.46
0.0553	12
0.0872	13.75
0.1085	14.45
0.13	15
0.151	15.6
0.183	15.97
0.226	16.75
0.268	17.35
0.321	17.9
0.374	18.42
0.481	19.2

Table C8. Sediment data of S7 from Einstein and Chien (1955)

(h-y)/y	total c g/l
22.2	64.5
20.1	54.5
17.55	37.4
15	32.4
10.9	13.34
7.59	4.8
5.27	1.9

Table C9. Velocity data of S11 from Einstein and Chien (1955) (h=0.435 ft, u_*=0.347 ft/s)

y/h	u/u*
0.0092	8.7
0.01035	8.6
0.01265	9.45
0.01494	10.13
0.01955	10.53
0.0241	11.07
0.031	11.78
0.0379	12.16
0.0448	12.65
0.054	13.1
0.0632	13.31
0.0747	13.73
0.0862	14.2
0.1046	14.7
0.1252	15.05
0.148	15.5
0.171	16.04
0.199	16.35
0.229	16.86
0.2745	17.38
0.3205	17.5
0.378	18.5
0.435	19.12

Table C10. Velocity data of S16 from Einstein and Chien (1955) (h=0.39 ft, u_*=0.409 ft/s)

y/h	u/u*
0.0103	5.75
0.0154	6.23
0.0205	6.67
0.0282	7.65
0.041	8.49
0.0538	9.4
0.0667	9.75
0.0795	10.42
0.092	11.05
0.105	11.95
0.115	12.5
0.131	13.1
0.1565	14.05
0.182	14.8
0.22	16

APPENDIX D

DATA FROM COLEMAN (1986)

Table D1. 40 series of velocity data from Coleman (1986)

y	Run no. (m/s)									
mm	1	2	3	4	5	6	7	8	9	10
6	0.709	0.705	0.68	0.665	0.662	0.652	0.639	0.63	0.621	0.619
12	0.773	0.768	0.738	0.74	0.717	0.727	0.709	0.696	0.683	0.688
18	0.823	0.817	0.795	0.802	0.788	0.766	0.77	0.751	0.751	0.759
24	0.849	0.852	0.836	0.829	0.814	0.805	0.804	0.8	0.804	0.808
30	0.884	0.883	0.87	0.863	0.852	0.848	0.849	0.831	0.842	0.841
46	0.927	0.938	0.922	0.922	0.911	0.905	0.924	0.902	0.897	0.912
69	0.981	0.975	0.963	0.965	0.968	0.951	0.962	0.958	0.945	0.976
91	1.026	1.03	1.025	1.023	1.028	1.037	1.03	1.012	1.028	1.033
122	1.054	1.049	1.048	1.049	1.038	1.054	1.061	1.044	1.048	1.061
137	1.053	1.043	1.039	1.048	1.047	1.049	1.051	1.046	1.05	1.062
152	1.048	1.03	1.028	1.033	1.03	1.026	1.04	1.033	1.04	1.05
162	1.039	1.023	1.02	1.024	1.027	1.031	1.027	1.028	1.032	1.045
y	Run no. (m/s)									
mm	11	12	13	14	15	16	17	18	19	20
6	0.625	0.598	0.6	0.598	0.588	0.583	0.586	0.579	0.576	0.57
12	0.688	0.669	0.665	0.669	0.674	0.661	0.655	0.688	0.649	0.648
18	0.761	0.731	0.747	0.746	0.746	0.744	0.75	0.734	0.743	0.743
24	0.812	0.796	0.798	0.8	0.799	0.804	0.804	0.78	0.798	0.791
30	0.855	0.83	0.844	0.84	0.85	0.854	0.838	0.836	0.838	0.848
46	0.929	0.912	0.914	0.922	0.918	0.922	0.938	0.916	0.916	0.922
69	0.989	0.964	0.973	0.971	0.98	0.978	0.976	0.966	0.976	0.986
91	1.05	1.004	1.038	1.042	1.052	1.051	1.022	1.027	1.047	1.043
122	1.085	1.052	1.07	1.067	1.074	1.074	1.071	1.054	1.07	1.07
137	1.077	1.058	1.062	1.062	1.07	1.07	1.071	1.053	1.07	1.068
152	1.07	1.045	1.045	1.051	1.059	1.057	1.06	1.049	1.057	1.057
162	1.063	1.033	1.039	1.048	1.05	1.046	1.053	1.024	1.048	1.048
y	Run no. (m/s)									
mm	21	22	23	24	25	26	27	28	29	30
6	0.734	0.738	0.717	0.684	0.66	0.649	0.662	0.638	0.648	0.661
12	0.789	0.775	0.764	0.742	0.737	0.713	0.72	0.714	0.701	0.713
18	0.827	0.814	0.816	0.794	0.79	0.775	0.775	0.771	0.776	0.772

Table D1 continued

y	Run no. (m/s)									
mm	21	22	23	24	25	26	27	28	29	30
24	0.867	0.841	0.839	0.844	0.844	0.809	0.801	0.811	0.823	0.822
30	0.891	0.855	0.866	0.872	0.872	0.843	0.863	0.848	0.853	0.876
46	0.936	0.916	0.918	0.922	0.934	0.899	0.925	0.91	0.93	0.932
69	0.987	0.953	0.971	0.959	0.984	0.96	0.984	0.967	0.991	0.999
91	1.03	1.015	1.03	1.03	1.051	1.02	1.042	1.04	1.055	1.064
122	1.048	1.026	1.052	1.056	1.073	1.045	1.075	1.065	1.084	1.089
137	1.046	1.024	1.039	1.049	1.063	1.041	1.064	1.06	1.082	1.093
152	1.033	1.012	1.027	1.034	1.048	1.032	1.052	1.043	1.066	1.076
162	1.028	1.008	1.021	1.024	1.04	1.027	1.044	1.044	1.064	1.074
y	Run no. (m/s)									
mm	31	32	33	34	35	36	37	38	39	40
6	0.598	0.689	0.69	0.709	0.688	0.698	0.674	0.716	0.677	0.678
12	0.679	0.746	0.746	0.745	0.733	0.74	0.724	0.735	0.745	0.71
18	0.743	0.786	0.791	0.788	0.788	0.804	0.796	0.81	0.798	0.792
24	0.791	0.821	0.832	0.82	0.826	0.841	0.835	0.847	0.826	0.836
30	0.828	0.838	0.853	0.861	0.863	0.881	0.871	0.884	0.871	0.879
46	0.899	0.887	0.903	0.906	0.917	0.942	0.92	0.952	0.936	0.936
69	0.96	0.994	0.948	0.952	0.96	0.988	0.985	0.998	0.989	0.985
91	1.026	0.999	1.027	1.019	1.019	1.055	1.05	1.091	1.068	1.069
122	1.063	1.024	1.018	1.046	1.065	1.09	1.086	1.118	1.099	1.107
137	1.058	1.025	1.042	1.05	1.06	1.08	1.077	1.11	1.096	1.101
152	1.048	1.012	1.027	1.029	1.045	1.068	1.067	1.098	1.084	1.086
162	1.042	1.004	1.018	1.012	1.028	1.062	1.058	1.092	1.072	1.08

Table D2. 40 series of sediment data from Coleman (1986)

y	Run no. (10^{-4})									
mm	1	2	3	4	5	6	7	8	9	10
6	0	8.5	17	28	40	51	62	77	90	110
12	0	6.4	12	19	26	32	40	49	60	66
18	0	5.2	9.7	15	19	24	32	36	42	49
24	0	4.2	7.6	12	16	20	25	30	34	39
30	0	3.7	6.8	10	14	17	21	24	27	32
46	0	2.8	5.3	7.5	11	12	15	17	19	21
69	0	2.4	3.9	5.9	7.8	9.6	12	14	15	17
91	0	1.4	2.5	3.7	5	6.2	7.6	8.6	9.6	11
122	0	0.81	1.5	2.2	2.8	3.4	4.3	5	5.4	5.5
137	0	0.65	1.1	1.4	2	2.3	3	3.4	3.5	3.4
152	0	0.5	0.73	1	1.3	1.4	1.8	2	1.9	2
162	0	0.3	0.48	0.56	0.86	0.77	1.1	1.2	1.2	1
y	Run no. (10^{-4})									
mm	11	12	13	14	15	16	17	18	19	20
6	120	130	140	150	170	180	190	190	210	230
12	78	82	90	98	100	110	110	110	120	120
18	54	56	63	68	71	74	64	74	77	82
24	41	44	49	52	54	56	58	56	59	61
30	35	36	40	44	44	47	47	46	48	48
46	24	25	28	30	31	32	31	32	32	33
69	18	19	21	23	24	25	24	24	25	26
91	12	12	14	14	16	16	15	15	16	16
122	5.9	7	7.4	8	8.2	7.9	7.6	8	8	7.6
137	3.2	4	4.4	4.6	4.5	4.6	4.7	5.2	4.4	4
152	1.8	2.3	2.4	2.4	2.3	2.2	2.1	2.5	2.2	2
162	0.7	1.3	1.3	1.2	1.3	1.2	1.4	1.3	1.6	1.1
y	Run no. (10^{-4})									
mm	21	22	23	24	25	26	27	28	29	30
6	0	9.8	21	34	48	54	66	80	95	110
12	0	6.3	12	18	26	32	40	48	52	57
18	0	4.2	8.6	13	18	22	26	31	34	39
24	0	3.3	6.8	11	13	18	21	23	26	28
30	0	3	5.6	8.6	11	14	17	19	21	24
46	0	2.1	3.9	6	7.6	9.7	12	13	17	16
69	0	1.6	2.9	4.5	5.9	7.8	8.9	9.8	11	12
91	0	1.1	1.9	2.7	3.6	4.8	5.3	5.9	6.4	7.1
122	0	0.64	1.1	1.6	2.2	2.8	2.8	3.3	3.4	3.7

Table D2 continued

y	Run no. (10^{-4})									
mm	21	22	23	24	25	26	27	28	29	30
137	0	0.5	0.9	1.2	1.5	2.1	2	2.3	2.6	2.7
152	0	0.42	0.63	0.89	1.1	1.5	1.4	1.7	1.6	1.8
162	0	0.32	0.64	0.63	0.68	1.1	0.88	1.2	0.98	1.1
y	Run no. (10^{-4})									
mm	31	32	33	34	35	36	37	38	39	40
6	120	0	2.7	5.1	9.3	17	19	22	27	26
12	63	0	1.4	2.4	4.1	6.8	7.8	11	11	11
18	40	0	0.86	1.5	2.2	3.8	4.7	6	6.2	6.4
24	30	0	0.66	1.2	1.7	3	3.6	4.6	4.9	4.6
30	24	0	0.57	0.97	1.5	2.3	2.9	4	4	4.2
46	16	0	0.43	0.7	1.1	1.7	2.2	2.7	3	3
69	12	0	0.34	0.56	0.86	1.2	1.7	2.2	2.3	2.5
91	7.7	0	0.23	0.32	0.56	0.88	1.1	1.4	1.6	1.6
122	4.1	0	0.19	0.27	0.42	0.61	0.8	0.96	1	1.2
137	3	0	0.16	0.24	0.34	0.48	0.63	0.79	0.88	0.97
152	2	0	0.14	0.19	0.31	0.4	0.54	0.64	0.8	0.8
162	1.5	0	0.12	0.18	0.25	0.32	0.43	0.55	0.64	0.69

APPENDIX E

COMPUTED RESULTS

Table E1. CDF of velocity distribution for Rosciano River (Italy)

x (m)	y′ (m)	obs. CDF	est. CDF	error	x (m)	y′ (m)	obs. CDF	est. CDF	error
-10.34	0	0.323	0.542	0.679	4.13	0	0.969	0.951	-0.019
-10.34	0.06	0.323	0.548	0.695	4.13	0.06	0.969	0.955	-0.014
-10.34	0.26	0.446	0.565	0.265	4.13	0.26	0.969	0.942	-0.028
-10.34	0.86	0.569	0.601	0.055	4.13	1.06	0.892	0.874	-0.021
-10.34	1.56	0.323	0.550	0.701	4.13	1.86	0.815	0.773	-0.051
-10.34	2.36	0.231	0.448	0.941	4.13	2.46	0.615	0.633	0.029
-10.34	2.56	0.138	0.398	1.877	4.13	2.66	0.492	0.535	0.086
-10.34	2.81	0.000	0.000	0.000	4.13	2.81	0.000	0.000	0.000
-7.25	0	0.692	0.789	0.140	8.27	0	0.815	0.806	-0.011
-7.25	0.06	0.692	0.793	0.145	8.27	0.06	0.815	0.810	-0.006
-7.25	0.26	0.738	0.805	0.090	8.27	0.26	0.815	0.824	0.010
-7.25	1.06	0.738	0.757	0.025	8.27	1.06	0.815	0.764	-0.063
-7.25	2.06	0.615	0.662	0.075	8.27	1.86	0.692	0.676	-0.024
-7.25	2.76	0.446	0.531	0.191	8.27	2.46	0.446	0.554	0.241
-7.25	2.96	0.446	0.448	0.005	8.27	2.66	0.323	0.467	0.447
-7.25	3.11	0.000	0.000	0.000	8.27	2.81	0.000	0.000	0.000
-4.14	0	0.892	0.932	0.044	11.37	0	0.569	0.627	0.101
-4.14	0.06	0.892	0.936	0.049	11.37	0.06	0.569	0.632	0.110
-4.14	0.26	0.969	0.927	-0.044	11.37	0.26	0.615	0.647	0.051
-4.14	1.06	0.831	0.868	0.044	11.37	0.86	0.692	0.638	-0.079
-4.14	2.06	0.692	0.759	0.096	11.37	1.56	0.569	0.571	0.004
-4.14	2.76	0.492	0.609	0.238	11.37	2.16	0.446	0.468	0.049
-4.14	2.96	0.446	0.514	0.153	11.37	2.36	0.246	0.395	0.604
-4.14	3.11	0.000	0.000	0.000	11.37	2.51	0.000	0.000	0.000
0.00	0	1.000	1.000	0.000	14.47	0	0.184615	0.391328	1.120
0.00	0.06	1.000	0.996	-0.004	14.47	0.06	0.184615	0.397245	1.152
0.00	0.26	0.969231	0.982691	0.014	14.47	0.26	0.230769	0.414773	0.797
0.00	1.06	0.892308	0.920023	0.031	14.47	0.86	0.446154	0.450101	0.009
0.00	2.06	0.738462	0.804796	0.090	14.47	1.56	0.323077	0.399142	0.235
0.00	2.76	0.492308	0.646043	0.312	14.47	2.06	0.230769	0.334239	0.448
0.00	3.11	0	0	0.000	14.47	2.41	0	0	0.000

Table E2. CDF of velocity distribution for Santa Lucia River (Italy)

x (m)	y′ (m)	obs. CDF	est. CDF	error	x (m)	y′ (m)	obs. CDF	est. CDF	error
-7.24	0	0.450	0.576	0.281	3.11	0	0.550	0.747	0.359
-7.24	0.06	0.450	0.581	0.291	3.11	0.06	0.550	0.758	0.379
-7.24	0.2	0.550	0.591	0.075	3.11	0.2	0.575	0.782	0.360
-7.24	0.8	0.650	0.628	-0.034	3.11	0.8	0.825	0.861	0.043
-7.24	1.5	0.625	0.584	-0.066	3.11	1.5	0.825	0.849	0.030
-7.24	2.45	0.350	0.488	0.393	3.11	2.36	0.550	0.714	0.298
-7.24	2.95	0.150	0.364	1.425	3.11	2.83	0.400	0.537	0.344
-7.24	3.1	0.000	0.000	0.000	3.11	2.98	0.000	0.000	0.000
-4.13	0	0.825	0.815	-0.012	6.21	0	0.300	0.267	-0.109
-4.13	0.06	0.825	0.824	-0.001	6.21	0.06	0.300	0.271	-0.097
-4.13	0.2	0.825	0.843	0.022	6.21	0.2	0.300	0.278	-0.072
-4.13	0.8	0.950	0.910	-0.042	6.21	0.8	0.325	0.304	-0.066
-4.13	1.38	0.950	0.912	-0.040	6.21	1.5	0.225	0.273	0.000
-4.13	2.29	0.825	0.801	-0.029	6.21	2	0.175	0.238	0.359
-4.13	3.14	0.400	0.548	0.000	6.21	2.35	0.225	0.187	-0.169
-4.13	3.29	0.000	0.000	0.000	6.21	2.5	0.000	0.000	0.000
0.00	0	0.950	0.985	0.037					
0.00	0.06	0.950	0.990	0.042					
0.00	0.2	1.000	1.000	0.000					
0.00	0.8	1.000	0.952	-0.048					
0.00	1.34	0.950	0.898	-0.055					
0.00	2.33	0.825	0.739	0.000					
0.00	2.78	0.600	0.560	-0.067					
0.00	2.93	0.000	0.000	0.000					

Table E3. CDF of velocity distribution of Run A2 (Iranian River)

Profile	y′ (m)	obs. CDF	est. CDF	error	Profile	y′ (m)	obs. CDF	est. CDF	error
1	0.000	0.000	0.001	0.000	3	0.000	0.000	0.001	0.000
1	0.050	0.381	0.363	-0.049	3	0.050	0.381	0.363	-0.049
1	0.060	0.406	0.388	-0.044	3	0.060	0.406	0.388	-0.044
1	0.070	0.424	0.411	-0.030	3	0.070	0.424	0.411	-0.030
1	0.080	0.445	0.432	-0.029	3	0.080	0.445	0.432	-0.029
1	0.090	0.438	0.451	0.030	3	0.090	0.438	0.451	0.030
1	0.100	0.529	0.468	-0.114	3	0.100	0.529	0.468	-0.114
1	0.110	0.563	0.485	0.000	3	0.110	0.563	0.485	-0.138
1	0.120	0.549	0.501	-0.089	3	0.120	0.549	0.501	-0.089
1	0.130	0.546	0.516	-0.056	3	0.130	0.546	0.516	-0.056
1	0.140	0.543	0.530	-0.024	3	0.140	0.543	0.530	-0.024
1	0.150	0.525	0.543	0.033	3	0.150	0.525	0.543	0.033
1	0.160	0.543	0.556	0.025	3	0.160	0.543	0.556	0.025
1	0.170	0.573	0.568	-0.009	3	0.170	0.573	0.568	-0.009
1	0.180	0.577	0.580	0.000	3	0.180	0.577	0.580	0.006
1	0.190	0.611	0.591	0.000	3	0.190	0.611	0.591	-0.032
1	0.200	0.597	0.602	0.009	3	0.200	0.597	0.602	0.009
1	0.210	0.590	0.591	0.002	3	0.210	0.590	0.591	0.002
2	0.000	0.000	0.001	0.000	4	0.000	0.000	0.001	0.000
2	0.050	0.357	0.442	0.241	4	0.050	0.335	0.373	0.112
2	0.060	0.388	0.475	0.224	4	0.060	0.339	0.383	0.129
2	0.070	0.494	0.505	0.022	4	0.070	0.381	0.391	0.025
2	0.080	0.448	0.532	0.187	4	0.080	0.392	0.398	0.016
2	0.090	0.532	0.557	0.047	4	0.090	0.399	0.405	0.015
2	0.100	0.577	0.580	0.006	4	0.100	0.409	0.411	0.003
2	0.110	0.607	0.602	-0.009	4	0.110	0.448	0.416	-0.072
2	0.130	0.587	0.642	0.094	4	0.130	0.424	0.426	0.005
2	0.150	0.696	0.679	-0.025	4	0.150	0.459	0.434	-0.053
2	0.170	0.788	0.712	-0.097	4	0.170	0.455	0.442	-0.029
2	0.200	0.761	0.757	-0.005	4	0.200	0.448	0.452	0.008
2	0.230	0.829	0.798	-0.037	4	0.230	0.466	0.461	-0.011
2	0.260	0.863	0.836	-0.031	4	0.260	0.459	0.468	0.021
2	0.290	0.863	0.871	0.009	4	0.290	0.466	0.476	0.021
2	0.320	0.898	0.904	0.007		0.320	0.476	0.482	0.012
2	0.340	0.891	0.883	-0.009					

Table E4. Computed *G* values for Iranian data

u_{max}	u_{mean}	λ_1	λ_*	G
0.524	0.348	6.778	3.736	0.487
0.491	0.335	9.129	4.049	0.525
0.582	0.421	6.676	2.558	0.603
0.578	0.424	7.114	2.514	0.621
0.575	0.345	3.145	3.648	0.331
0.607	0.378	3.275	3.098	0.391
1.071	0.708	0.779	0.907	0.479
0.885	0.584	1.371	1.325	0.478
0.774	0.516	2.135	1.701	0.493
0.682	0.493	4.532	1.743	0.639
0.824	0.614	2.572	1.193	0.640
0.778	0.598	3.333	1.240	0.677
0.746	0.574	3.791	1.345	0.678
0.642	0.435	3.981	2.399	0.516
0.585	0.393	5.094	2.936	0.504
0.502	0.370	11.015	3.297	0.626
0.450	0.347	17.374	3.675	0.680
0.469	0.374	16.741	3.088	0.718
0.657	0.519	5.947	1.616	0.707
0.743	0.561	3.643	1.421	0.656
0.735	0.539	3.457	1.556	0.620
0.660	0.543	6.478	1.420	0.751
0.660	0.488	4.893	1.893	0.630
0.550	0.366	5.908	3.379	0.490
0.480	0.302	6.966	4.879	0.407
0.635	0.426	3.962	2.498	0.502
0.710	0.522	3.864	1.658	0.623
0.739	0.441	1.434	2.225	0.323
0.592	0.506	9.782	1.555	0.788
0.899	0.579	1.181	1.338	0.442
0.971	0.683	1.313	0.975	0.567
0.810	0.675	3.610	0.951	0.755
0.899	0.663	1.921	1.027	0.627

Table E5. Velocity profile for Rosciano River (Italy)

x (m)	y′ (m)	obs. v (m/s)	est. v (m/s)	error	x (m)	y′ (m)	obs. v (m/s)	est. v (m/s)	error
-10.34	0	1.126	1.155	0.026	4.13	0	2.112	2.154	0.020
-10.34	0.06	1.126	1.179	0.047	4.13	0.06	2.112	2.147	0.017
-10.34	0.26	1.261	1.253	-0.007	4.13	0.26	2.112	2.125	0.006
-10.34	0.86	1.461	1.438	-0.016	4.13	1.06	2.029	2.019	-0.005
-10.34	1.56	1.177	1.217	0.034	4.13	1.86	1.820	1.856	0.020
-10.34	2.36	0.922	0.823	-0.107	4.13	2.46	1.570	1.617	0.030
-10.34	2.56	0.294	0.655	1.227	4.13	2.66	1.340	1.436	0.072
-10.34	2.81	0.000	-0.012	0.000	4.13	2.81	0.000	-0.012	0.000
-7.25	0	1.695	1.754	0.035	8.27	0	1.883	1.872	-0.006
-7.25	0.06	1.695	1.760	0.038	8.27	0.06	1.883	1.891	0.004
-7.25	0.26	1.762	1.778	0.009	8.27	0.26	1.862	1.952	0.048
-7.25	1.06	1.762	1.698	-0.036	8.27	1.06	1.883	1.930	0.025
-7.25	2.06	1.561	1.548	-0.009	8.27	1.86	1.674	1.630	-0.026
-7.25	2.76	1.244	1.326	0.066	8.27	2.46	1.236	1.232	-0.004
-7.25	2.96	1.244	1.177	-0.054	8.27	2.66	1.109	0.967	0.000
-7.25	3.11	0.000	-0.012	0.000	8.27	2.81	0.000	-0.012	0.000
-4.14	0	2.008	2.084	0.038	11.37	0	1.486	1.450	-0.024
-4.14	0.06	2.008	2.093	0.042	11.37	0.06	1.486	1.468	-0.012
-4.14	0.26	2.133	2.120	-0.006	11.37	0.26	1.549	1.521	-0.018
-4.14	1.06	1.966	1.997	0.016	11.37	0.86	1.632	1.641	0.005
-4.14	2.06	1.674	1.766	0.055	11.37	1.56	1.444	1.496	0.036
-4.14	2.76	1.319	1.440	0.092	11.37	2.16	1.298	1.264	-0.026
-4.14	2.96	1.277	1.228	-0.038	11.37	2.36	1.067	1.094	0.000
-4.14	3.11	0.000	-0.012	0.000	11.37	2.51	0	-0.01206	0.000
0.00	0	2.447	2.447	0.000	14.47	0	0.82	0.697298	-0.150
0.00	0.06	2.447	2.434181	-0.005	14.47	0.06	0.82	0.78657	-0.041
0.00	0.26	2.175	2.39003	0.099	14.47	0.26	0.956	0.941508	-0.015
0.00	1.06	2.071	2.185828	0.055	14.47	0.86	1.261	1.26388	0.002
0.00	2.06	1.758	1.819724	0.035	14.47	1.56	1.177	1.12801	-0.042
0.00	2.76	1.34	1.339437	0.000	14.47	2.06	0.939	0.952203	0.014
0.00	2.96	1.236	1.052933	-0.148	14.47	2.26	0.837	0.808693	-0.034
0.00	3.11	0	-0.01206	0.000	14.47	2.41	0	-0.01206	0.000

Table E6. Velocity profile for Santa Lucia River (Italy)

x (m)	y′ (m)	obs. v (m/s)	est. v (m/s)	error	x (m)	y′ (m)	obs. v (m/s)	est. v (m/s)	error
-7.24	0	1.680	1.650	-0.018	3.11	0	1.750	1.790	0.023
-7.24	0.06	1.680	1.677	-0.002	3.11	0.06	1.750	1.824	0.042
-7.24	0.2	1.700	1.738	0.022	3.11	0.2	1.850	1.895	0.024
-7.24	0.8	2.100	2.081	-0.009	3.11	0.8	2.290	2.310	0.009
-7.24	1.5	2.000	1.873	-0.064	3.11	1.5	2.290	2.113	-0.077
-7.24	2.45	1.450	1.434	-0.011	3.11	2.36	1.750	1.725	-0.014
-7.24	2.95	0.710	0.917	0.291	3.11	2.83	1.550	1.228	-0.208
-7.24	3.1	0.000	0.002	0.000	3.11	2.98	0.000	0.002	0.000
-4.13	0	2.240	2.202	-0.017	6.21	0	1.280	1.205	-0.058
-4.13	0.06	2.240	2.217	-0.010	6.21	0.06	1.280	1.215	-0.050
-4.13	0.2	2.240	2.248	0.004	6.21	0.2	1.230	1.237	0.006
-4.13	0.8	2.340	2.355	0.006	6.21	0.8	1.330	1.309	-0.016
-4.13	1.38	2.390	2.356	-0.014	6.21	1.5	1.130	1.222	0.000
-4.13	2.29	2.290	2.176	-0.050	6.21	2	1.060	1.116	0.053
-4.13	3.14	1.500	1.717	0.000	6.21	2.35	1.130	0.952	-0.157
-4.13	3.29	0.000	0.002	0.000	6.21	2.5	0.000	0.002	0.000
0.00	0	2.390	2.425	0.015					
0.00	0.06	2.390	2.430	0.017					
0.00	0.2	2.440	2.440	0.000					
0.00	0.8	2.440	2.391	-0.020					
0.00	1.34	2.350	2.335	-0.007					
0.00	2.33	2.290	2.155	0.000					
0.00	2.78	1.900	1.921	0.011					
0.00	2.93	0.000	0.002	0.000					

Table E7. Velocity profile for Iranian river (Run A2-1)

Profile	y′ (m)	obs. v (m/s)	est. v (m/s)	error	Profile	y′ (m)	obs. v (m/s)	est. v (m/s)	error
1	0.000	0.000	0.001	0.000	3	0.000	0.000	0.001	0.000
1	0.050	0.399	0.381	-0.045	3	0.050	0.642	0.746	0.161
1	0.060	0.424	0.408	-0.040	3	0.060	0.721	0.770	0.068
1	0.070	0.443	0.431	-0.026	3	0.070	0.735	0.791	0.077
1	0.080	0.465	0.453	-0.025	3	0.080	0.692	0.810	0.171
1	0.090	0.458	0.473	0.034	3	0.090	0.746	0.827	0.109
1	0.100	0.553	0.492	-0.111	3	0.100	0.792	0.843	0.064
1	0.110	0.589	0.509	-0.135	3	0.110	0.807	0.857	0.063
1	0.120	0.575	0.526	-0.085	3	0.120	0.882	0.883	0.001
1	0.130	0.571	0.541	-0.052	3	0.130	0.885	0.905	0.022
1	0.140	0.567	0.556	-0.020	3	0.140	0.946	0.925	-0.022
1	0.160	0.567	0.584	0.029	3	0.150	0.960	0.952	-0.009
1	0.170	0.599	0.597	-0.005	3	0.160	0.989	0.975	-0.014
1	0.180	0.603	0.609	0.010	3	0.170	1.003	0.996	-0.007
1	0.190	0.639	0.621	-0.028	3	0.180	1.017	1.015	-0.002
1	0.200	0.624	0.633	0.013	3	0.190	1.039	1.032	-0.006
1	0.210	0.617	0.621	0.006	3	0.200	1.046	1.043	-0.002
2	0.000	0.000	0.001	0.000	4	0.210	0.000	0.001	0.000
2	0.050	0.373	0.465	0.246	4	0.000	0.351	0.392	0.116
2	0.060	0.406	0.499	0.229	4	0.050	0.355	0.402	0.133
2	0.070	0.517	0.530	0.027	4	0.060	0.399	0.410	0.029
2	0.080	0.469	0.559	0.192	4	0.070	0.410	0.418	0.020
2	0.090	0.557	0.585	0.051	4	0.080	0.417	0.425	0.019
2	0.100	0.603	0.609	0.010	4	0.090	0.428	0.431	0.007
2	0.110	0.635	0.632	-0.005	4	0.100	0.469	0.437	-0.068
2	0.130	0.614	0.674	0.099	4	0.110	0.443	0.447	0.010
2	0.150	0.728	0.712	-0.021	4	0.130	0.480	0.456	-0.049
2	0.170	0.824	0.747	-0.093	4	0.150	0.476	0.464	-0.025
2	0.200	0.796	0.795	-0.001	4	0.170	0.469	0.474	0.012
2	0.230	0.867	0.838	-0.033	4	0.200	0.487	0.484	-0.007
2	0.260	0.903	0.878	-0.027	4	0.230	0.480	0.492	0.025
2	0.290	0.903	0.915	0.013	4	0.260	0.487	0.499	0.025
2	0.320	0.939	0.949	0.011	4	0.290	0.498	0.506	0.016

Table E8. Velocity profile for Iranian river (Run B9-1)

Profile	y′ (m)	obs. v (m/s)	est. v (m/s)	error	Profile	y′ (m)	obs. v (m/s)	est. v (m/s)	error
1	0	0	0.000	0.000	5	0	0	0.000	0.000
1	0.05	0.159283	0.214	0.347	5	0.05	0.1998	0.227	0.137
1	0.06	0.207167	0.224	0.080	5	0.06	0.192433	0.237	0.231
1	0.07	0.170333	0.232	0.361	5	0.07	0.229267	0.245	0.071
1	0.08	0.203483	0.239	0.175	5	0.08	0.203483	0.253	0.244
1	0.09	0.192433	0.246	0.276	5	0.09	0.229267	0.260	0.134
1	0.1	0.23295	0.252	0.080	5	0.1	0.240317	0.266	0.108
1	0.12	0.25505	0.262	0.028	5	0.12	0.2219	0.278	0.251
1	0.14	0.269783	0.272	0.007	5	0.14	0.25505	0.287	0.127
1	0.17	0.291883	0.284	-0.027	5	0.17	0.273467	0.300	0.098
1	0.2	0.247683	0.295	0.189	5	0.2	0.29925	0.312	0.041
1	0.24	0.27715	0.307	0.107	5	0.28	0.339767	0.336	-0.011
1	0.28	0.32135	0.318	-0.011	5	0.33	0.34345	0.349	0.015
1	0.32	0.328717	0.327	-0.004	5	0.38	0.3103	0.336	0.083
1	0.37	0.347133	0.338	-0.026	5	0.44	0.3103	0.318	0.026
1	0.42	0.339767	0.327	-0.036	5	0.49	0.302933	0.300	-0.008
1	0.47	0.3324	0.315	-0.052	5	0.54	0.295567	0.278	-0.061
3	0	0	0.000	0.000					
3	0.05	0.251367	0.285	0.133					
3	0.06	0.2882	0.299	0.039					
3	0.07	0.302933	0.312	0.030					
3	0.08	0.291883	0.324	0.108					
3	0.09	0.34345	0.334	-0.028					
3	0.1	0.317667	0.344	0.082					
3	0.12	0.339767	0.361	0.062					
3	0.14	0.3324	0.376	0.131					
3	0.17	0.3987	0.396	-0.007					
3	0.2	0.391333	0.413	0.056					
3	0.28	0.439217	0.452	0.028					
3	0.33	0.516567	0.472	-0.087					
3	0.38	0.490783	0.489	-0.003					
3	0.44	0.5313	0.508	-0.043					
3	0.5	0.538667	0.525422	-0.025					
3	0.54	0.523933	0.536	0.023					
3	0.58	0.54594	0.546	0.000					

Table E9. Computed mean velocity for Santa Lucia gauges for the last 20 years.

u_{max} (m/s)	obs. u_{mean} (m/s)	est. u_{mean} (m/s)	error
0.088	0.047	0.057	0.217
0.269	0.182	0.175	-0.039
1.208	0.948	0.785	-0.172
1.467	1.072	0.954	-0.110
1.773	1.135	1.152	0.015
1.631	1.179	1.060	-0.101
2.760	1.478	1.794	0.214
2.243	1.648	1.458	-0.115
0.129	0.067	0.084	0.251
0.495	0.324	0.322	-0.007
0.644	0.401	0.419	0.044
1.155	0.736	0.751	0.020
2.194	1.497	1.426	-0.047
2.437	1.873	1.584	-0.154
0.107	0.052	0.070	0.338
0.482	0.315	0.313	-0.005
0.735	0.497	0.478	-0.039
1.022	0.672	0.664	-0.011
1.678	1.151	1.091	-0.052
0.209	0.123	0.136	0.104
2.625	1.736	1.706	-0.017
2.778	1.910	1.806	-0.055
0.781	0.541	0.508	-0.062
1.462	0.926	0.950	0.026
2.182	1.397	1.418	0.015
0.268	0.154	0.174	0.131
1.227	0.697	0.798	0.144
2.555	1.604	1.661	0.035
1.403	0.870	0.912	0.048
2.436	1.543	1.583	0.026
3.094	1.945	2.011	0.034
3.062	2.109	1.990	-0.056
0.496	0.305	0.322	0.057
0.234	0.147	0.152	0.035
1.603	0.996	1.042	0.046
1.678	1.062	1.091	0.027
2.816	1.816	1.830	0.008

Table E9 continued

u_{max} (m/s)	obs. u_{mean} (m/s)	est. u_{mean} (m/s)	error
2.781	1.882	1.808	-0.040
2.781	1.803	1.808	0.003
0.888	0.570	0.577	0.013
0.270	0.153	0.176	0.147
1.511	1.040	0.982	-0.056
0.453	0.262	0.294	0.124
2.948	1.984	1.916	-0.034
2.989	2.020	1.943	-0.038
2.781	1.819	1.808	-0.006
2.580	1.707	1.677	-0.018
0.228	0.152	0.148	-0.025
2.739	1.836	1.780	-0.030
2.581	1.750	1.678	-0.041
1.453	0.979	0.944	-0.035

Table E10. Computed mean velocity for Ponte Nuovo gauges for the last 20 years

u_{max} (m/s)	obs. u_{mean} (m/s)	est. u_{mean} (m/s)	error
0.978	0.620	0.636	0.025
2.243	1.373	1.458	0.062
2.384	1.593	1.550	-0.027
2.023	1.085	1.315	0.212
0.42	0.262	0.273	0.042
1.803	1.186	1.172	-0.012
2.097	1.464	1.363	-0.069
0.694	0.471	0.451	-0.042
2.972	1.833	1.932	0.054
2.194	1.487	1.426	-0.041
0.69	0.448	0.449	0.001
1.288	0.923	0.837	-0.093
2.048	1.406	1.331	-0.053
0.673	0.442	0.437	-0.010
1.578	1.136	1.026	-0.097
0.209	0.117	0.136	0.161
2.024	1.324	1.316	-0.006
2.048	1.331	1.331	0.000
2.972	1.946	1.932	-0.007
2.924	1.966	1.901	-0.033
2.521	1.712	1.639	-0.043
0.965	0.615	0.627	0.020
2.827	1.791	1.838	0.026
0.346	0.201	0.225	0.119
2.48	1.627	1.612	-0.009
2.73	1.623	1.775	0.093
1.954	1.157	1.270	0.098
1.85	1.106	1.203	0.087
2.029	1.255	1.319	0.051
1.05	0.71	0.683	-0.039
2.28	1.64	1.482	-0.096
2.387	1.634	1.552	-0.050
2.699	1.847	1.754	-0.050
2.778	1.825	1.806	-0.011
2.097	1.463	1.363	-0.068
2.405	1.669	1.563	-0.063

Table E10 continued

u_{max} (m/s)	obs. u_{mean} (m/s)	est. u_{mean} (m/s)	error
0.884	0.566	0.575	0.015
1.954	1.257	1.270	0.010
1.904	1.276	1.238	-0.030
1.202	0.825	0.781	-0.053
1.221	0.828	0.794	-0.041
0.387	0.207	0.252	0.215
1.261	0.854	0.820	-0.040
0.349	0.232	0.227	-0.022
2.054	1.339	1.335	-0.003
0.357	0.249	0.232	-0.068
2.597	1.736	1.688	-0.028
2.48	1.798	1.612	-0.103
1.925	1.33	1.251	-0.059
2.719	1.82	1.767	-0.029
1.779	1.151	1.156	0.005
1.777	1.211	1.155	-0.046
0.736	0.507	0.478	-0.056
0.221	0.146	0.144	-0.016
1.777	1.173	1.155	-0.015
2.169	1.391	1.410	0.014

Table E11. Computation of velocity profile between Tsallis entropy-based method and simple power law [Run S1, Coleman(1981)]

y (ft)	obs. u (ft/s)	est. Tsallis (ft/s)	error	est. power n=6 (ft/s)	error	est. power n=7 (ft/s)	error
0.006	2.442	2.894	0.185	3.679	0.506	3.983	0.631
0.007	1.455	3.005	1.065	3.774	1.593	4.071	1.798
0.008	2.755	3.105	0.127	3.858	0.400	4.149	0.506
0.009	2.899	3.199	0.104	3.938	0.358	4.222	0.457
0.011	3.154	3.358	0.065	4.070	0.290	4.344	0.377
0.013	3.286	3.496	0.064	4.184	0.274	4.448	0.354
0.015	3.433	3.618	0.054	4.285	0.248	4.539	0.322
0.018	3.560	3.783	0.062	4.418	0.241	4.660	0.309
0.021	3.804	3.925	0.032	4.532	0.191	4.763	0.252
0.025	4.079	4.094	0.004	4.666	0.144	4.884	0.197
0.029	4.226	4.242	0.004	4.784	0.132	4.989	0.180
0.030	4.249	4.276	0.006	4.811	0.132	5.013	0.180
0.034	4.470	4.407	-0.014	4.912	0.099	5.103	0.142
0.039	4.636	4.553	-0.018	5.026	0.084	5.204	0.123
0.046	4.857	4.735	-0.025	5.166	0.064	5.328	0.097
0.054	5.039	4.920	-0.024	5.308	0.053	5.454	0.082
0.064	5.252	5.119	-0.025	5.459	0.039	5.586	0.064
0.074	5.395	5.296	-0.018	5.591	0.036	5.703	0.057
0.086	5.592	5.486	-0.019	5.734	0.025	5.827	0.042
0.099	5.712	5.666	-0.008	5.868	0.027	5.943	0.040
0.114	5.952	5.857	-0.016	6.008	0.009	6.065	0.019
0.130	6.084	6.029	-0.009	6.135	0.008	6.174	0.015
0.149	6.308	6.232	-0.012	6.283	-0.004	6.302	-0.001
0.170	6.416	6.417	0.000	6.416	0.000	6.416	0.000

Table E12. Computation of velocity profile between Tsallis entropy-based method and simple power law [Run 15, Coleman(1981)]

y (m)	obs. u (m/s)	est. Tsallis (m/s)	error	est. power (m/s)	error
0	0	0.000	0.000	0.000	0.000
6	0.588	0.660	0.123	0.706	0.201
12	0.674	0.749	0.111	0.766	0.136
18	0.746	0.803	0.076	0.803	0.076
24	0.799	0.842	0.053	0.831	0.039
30	0.85	0.872	0.026	0.853	0.003
46	0.918	0.932	0.015	0.896	-0.024
69	0.98	0.990	0.010	0.940	-0.041
91	1.052	1.030	-0.021	0.971	-0.077
122	1.074	1.074	0.000	1.005	-0.064
137	1.07	1.056	-0.013	1.019	-0.048
152	1.059	1.040	-0.018	1.031	-0.026
162	1.05	1.030	-0.019	1.039	-0.010

Table E13. 2D velocity profile at Ponte Felcino (Italy)

x	y′	obs. V	est. Tsallis	error	est. Chiu	error
m	m	m/s	m/s		m/s	
-18.860	0.000	0.830	0.746	-0.101	1.097	0.322
-18.860	0.060	0.830	0.779	-0.061	1.101	0.326
-18.860	0.200	0.740	0.840	0.135	1.109	0.498
-18.860	1.000	0.640	1.031	0.610	1.143	0.786
-18.860	2.000	1.150	1.158	0.007	1.141	-0.008
-18.860	3.000	0.960	1.031	0.074	1.034	0.077
-18.860	3.900	0.740	0.799	0.079	0.631	-0.147
-18.860	4.100	0.710	0.672	-0.053	0.378	-0.467
-18.860	4.250	0.000	0.000	0.000	0.000	0.000
-14.660	0.000	1.210	1.205	-0.004	1.483	0.226
-14.660	0.060	1.210	1.225	0.013	1.489	0.230
-14.660	0.200	1.210	1.271	0.050	1.500	0.240
-14.660	1.000	1.180	1.474	0.249	1.550	0.313
-14.660	2.000	1.560	1.503	-0.036	1.547	-0.009
-14.660	3.000	1.090	1.252	0.148	1.387	0.272
-14.660	3.800	0.830	0.878	0.058	0.873	0.051
-14.660	4.000	0.710	0.679	-0.044	0.526	-0.259
-14.660	4.150	0.000	0.000	0.000	0.000	0.000
-10.460	0.000	2.060	1.937	-0.060	2.350	0.141
-10.460	0.060	2.060	1.965	-0.046	2.357	0.144
-10.460	0.200	2.340	2.025	-0.135	2.370	0.013
-10.460	1.000	2.310	2.269	-0.018	2.428	0.051
-10.460	1.930	2.440	2.457	0.007	2.429	-0.004
-10.460	2.880	2.190	2.264	0.034	2.297	0.049
-10.460	3.880	2.060	1.928	-0.064	1.787	-0.132
-10.460	4.280	1.650	1.665	0.009	1.250	-0.243
-10.460	4.480	1.590	1.413	-0.111	0.733	-0.539
-10.460	4.630	0.000	0.000	0.000	0.000	0.000
-6.290	0.000	2.990	2.980	-0.003	2.922	-0.023
-6.290	0.060	2.990	2.974	-0.005	2.927	-0.021
-6.290	0.200	2.660	2.960	0.113	2.938	0.104
-6.290	0.800	2.820	2.896	0.027	2.974	0.054
-6.290	1.710	2.660	2.785	0.047	2.988	0.123
-6.290	3.000	2.610	2.583	-0.010	2.878	0.103
-6.290	4.000	2.360	2.358	-0.001	2.582	0.094

Table E13 continued

x m	y′ m	obs. V m/s	est. Tsallis m/s	error	est. Chiu m/s	error
-6.290	5.000	1.950	1.958	0.004	1.761	-0.097
-6.290	5.200	1.600	1.812	0.132	1.419	-0.113
-6.290	5.450	1.460	1.499	0.027	0.738	-0.495
-6.290	5.600	0.000	0.000	0.000	0.000	0.000
0.000	0.000	3.360	3.360	0.000	3.299	-0.018
0.000	0.060	3.360	3.354	-0.002	3.304	-0.017
0.000	0.200	3.160	3.340	0.057	3.313	0.049
0.000	1.000	3.200	3.252	0.016	3.352	0.048
0.000	2.000	3.280	3.125	-0.047	3.351	0.022
0.000	3.000	2.910	2.970	0.021	3.266	0.122
0.000	4.000	2.780	2.766	-0.005	3.034	0.091
0.000	5.000	2.320	2.461	0.061	2.491	0.074
0.000	5.800	2.030	1.964	-0.032	1.365	-0.328
0.000	6.000	1.860	1.670	-0.102	0.753	-0.595
0.000	6.150	0.000	0.000	0.000	0.000	0.000
3.780	0.000	3.160	3.197	0.012	3.219	0.019
3.780	0.060	3.160	3.191	0.010	3.224	0.020
3.780	0.200	3.110	3.177	0.022	3.233	0.040
3.780	1.000	3.280	3.093	-0.057	3.272	-0.002
3.780	2.000	3.200	2.970	-0.072	3.271	0.022
3.780	2.880	2.610	2.839	0.088	3.202	0.227
3.780	3.880	2.570	2.649	0.031	2.991	0.164
3.780	4.880	2.530	2.365	-0.065	2.491	-0.015
3.780	5.700	2.030	1.908	-0.060	1.435	-0.293
3.780	5.940	1.860	1.587	-0.147	0.742	-0.601
3.780	6.090	0.000	0.000	0.000	0.000	0.000
7.340	0.000	2.360	2.504	0.061	2.684	0.137
7.340	0.060	2.360	2.514	0.065	2.688	0.139
7.340	0.200	2.610	2.536	-0.028	2.697	0.033
7.340	1.000	2.700	2.640	-0.022	2.733	0.012
7.340	2.000	2.740	2.738	-0.001	2.732	-0.003
7.340	2.930	2.610	2.647	0.014	2.660	0.019
7.340	3.880	2.530	2.523	-0.003	2.462	-0.027
7.340	4.880	2.320	2.314	-0.003	1.950	-0.159
7.340	5.380	0.980	2.117	1.160	1.377	0.405

Table E13 continued

x m	y′ m	obs. V m/s	est. Tsallis m/s	error	est. Chiu m/s	error
7.340	5.700	1.190	1.837	0.544	0.646	-0.457
7.340	5.850	0.000	0.000	0.000	0.000	0.000
10.490	0.000	1.780	1.269	-0.287	2.514	0.412
10.490	0.060	1.780	1.355	-0.239	2.518	0.415
10.490	0.200	1.440	1.515	0.052	2.527	0.755
10.490	1.000	2.150	2.042	-0.050	2.563	0.192
10.490	2.000	2.320	2.416	0.041	2.562	0.104
10.490	3.000	2.570	2.546	-0.009	2.479	-0.035
10.490	3.500	2.320	2.404	0.036	2.388	0.029
10.490	4.600	1.950	1.974	0.012	1.947	-0.001
10.490	5.000	1.610	1.733	0.077	1.611	0.001
10.490	5.700	0.000	0.000	0.000	0.000	0.000

Table E14. 2D velocity profile at Santa Lucia (Italy)

x	y′	obs. V	est. Tsallis	error	est. Chiu	error
m	m	m/s	m/s		m/s	
-7.240	0.000	1.680	1.650	-0.018	2.057	0.224
-7.240	0.060	1.680	1.677	-0.002	2.062	0.228
-7.240	0.200	1.700	1.738	0.022	2.074	0.220
-7.240	0.800	2.100	2.081	-0.009	2.100	0.000
-7.240	1.500	2.000	1.873	-0.064	2.048	0.024
-7.240	2.450	1.450	1.434	-0.011	1.636	0.128
-7.240	2.950	0.710	0.917	0.291	0.778	0.096
-7.240	3.100	0.000	0.002	0.000	0.000	0.000
-4.130	0.000	2.240	2.202	0.000	2.347	0.000
-4.130	0.060	2.240	2.217	-0.010	2.353	0.050
-4.130	0.200	2.240	2.248	0.004	2.365	0.056
-4.130	0.800	2.340	2.355	0.006	2.390	0.021
-4.130	1.380	2.390	2.356	-0.014	2.358	-0.014
-4.130	2.290	2.290	2.176	-0.050	2.081	-0.091
-4.130	3.140	1.500	1.717	0.145	0.841	-0.440
-4.130	3.290	0.000	0.002	0.000	0.000	0.000
0.000	0.000	2.390	2.425	0.015	2.382	-0.003
0.000	0.060	2.390	2.430	0.000	2.390	0.000
0.000	0.200	2.440	2.440	0.000	2.406	-0.014
0.000	0.800	2.440	2.391	-0.020	2.440	0.000
0.000	1.340	2.350	2.335	-0.007	2.400	0.021
0.000	2.330	2.290	2.155	-0.059	1.898	-0.171
0.000	2.780	1.900	1.921	0.011	0.950	-0.500
0.000	2.930	0.000	0.002	0.000	0.000	0.000
3.110	0.000	1.750	1.790	0.023	2.238	0.279
3.110	0.060	1.750	1.824	0.042	2.245	0.283
3.110	0.200	1.850	1.895	0.024	2.259	0.221
3.110	0.800	2.290	2.310	0.000	2.290	0.000
3.110	1.500	2.290	2.113	-0.077	2.226	-0.028
3.110	2.360	1.750	1.725	-0.014	1.788	0.022
3.110	2.830	1.550	1.228	-0.208	0.879	-0.433
3.110	2.980	0.000	0.002	0.000	0.000	0.000
6.210	0.000	1.280	1.205	-0.058	1.283	0.002
6.210	0.060	1.280	1.215	-0.050	1.289	0.007
6.210	0.200	1.230	1.237	0.006	1.302	0.058
6.210	0.800	1.330	1.309	-0.016	1.330	0.000
6.210	1.500	1.130	1.222	0.081	1.264	0.119

Table E14 continued

x m	y′ m	obs. V m/s	est. Tsallis m/s	error	est. Chiu m/s	error
6.210	2.000	1.060	1.116	0.053	1.051	-0.009
6.210	2.350	1.130	0.952	0.000	0.595	0.000
6.210	2.500	0.000	0.002	0.000	0.000	0.000

Table E15. Comparison of velocity profile for all methods [Run S16 from Einstein and Chien (1955)]

y (ft)	obs. u (ft/s)	est. Tsallis (ft/s)	est. Chiu (ft/s)	est. Prandt (ft/s)	est. power (ft/s)
0.004	2.350	2.055	1.391	0.000	1.415
0.006	2.546	2.410	1.849	0.560	1.730
0.008	2.725	2.695	2.227	1.202	1.996
0.011	3.126	3.049	2.697	1.918	2.341
0.016	3.469	3.519	3.305	2.759	2.823
0.021	3.841	3.899	3.780	3.369	3.234
0.026	3.984	4.226	4.173	3.851	3.601
0.031	4.258	4.511	4.503	4.245	3.931
0.036	4.515	4.762	4.784	4.573	4.229
0.041	4.883	4.999	5.042	4.870	4.518
0.045	5.108	5.169	5.221	5.074	4.728
0.051	5.353	5.421	5.481	5.367	5.047
0.061	5.741	5.783	5.839	5.766	5.516
0.071	6.048	6.107	6.147	6.105	5.948
0.086	6.538	6.538	6.538	6.531	6.540

Table E16. Computation of Sediment concentration of Run 20 from Coleman (1981)

y mm	obs. C 10^{-4}	est. Tsallis 10^{-4}	error
6	230	230.00	0.000
12	120	73.17	-0.390
18	82	60.43	-0.263
24	61	52.42	-0.141
30	48	46.46	-0.032
46	33	35.28	0.069
69	26	24.62	-0.053
91	16	17.19	0.075
122	7.6	9.12	0.200
137	4	5.85	0.464
152	2	2.89	0.446
162	1.1	1.05	-0.041

Table E17. Sediment concentration for the Tsallis entropy and the Rouse equation [data from Run S11 of Einstein and Chien(1955)]

y m	obs. C g/l	est. Tsallis g/l	error	est. Rouse g/l	error
0.004	31.400	31.400	0.000	31.400	0.000
0.004	28.300	26.357	-0.069	26.784	-0.054
0.005	26.300	23.349	-0.112	21.998	-0.164
0.006	20.650	20.359	-0.014	17.607	-0.147
0.008	17.000	16.839	-0.009	13.517	-0.205
0.011	13.400	12.825	-0.043	10.190	-0.240
0.014	10.610	8.379	-0.210	7.709	-0.273
0.016	7.130	5.261	-0.262	6.484	-0.091

Table E18. Sediment concentration for the Tsallis entropy and Chiu's equation [data from Run S22 of Coleman (1955)]

y mm	obs. C 10^{-4}	est. Tsallis 10^{-4}	error	est. Chiu 10^{-4}	error
6.000	9.800	9.800	0.000	9.800	0.000
12.000	6.300	4.231	-0.328	6.094	-0.033
18.000	4.200	3.556	-0.153	4.648	0.107
24.000	3.300	3.118	-0.055	3.823	0.159
30.000	3.000	2.786	-0.071	3.270	0.090
46.000	2.100	2.147	0.022	2.372	0.129
69.000	1.600	1.520	-0.050	1.659	0.037
91.000	1.100	1.073	-0.025	1.216	0.106
122.000	0.640	0.575	-0.101	0.745	0.164
137.000	0.500	0.371	-0.258	0.535	0.071
152.000	0.420	0.184	-0.562	0.301	-0.283
162.000	0.320	0.067	-0.790	0.000	-1.000

Table E19. Sediment concentration for the Tsallis entropy and Choo's equation [data from Run S7 of Coleman (1955)]

y mm	obs. C 10^{-4}	est. Tsallis 10^{-4}	error	est. Choo 10^{-4}	error
6	62	62.000	0.000	62.000	0.000
12	40	29.113	-0.272	33.046	-0.174
18	32	24.511	-0.234	26.202	-0.181
24	25	21.508	-0.140	22.120	-0.115
30	21	19.222	-0.085	19.202	-0.086
46	15	14.814	-0.012	13.989	-0.067
69	12	10.480	-0.127	9.332	-0.222
91	7.6	7.385	-0.028	6.253	-0.177
122	4.3	3.954	-0.080	3.053	-0.290
137	3	2.548	-0.151	1.800	-0.400
152	1.8	1.263	-0.299	0.683	-0.621
162	1.1	0.462	-0.580	0.000	-1.000

Table E20. Suspended sediment discharge for different methods [data from Coleman (1981)] (m^3/s)

obs. Qs	*Qs1*	*Qs2*	*Qs3*	*Qs4*	*Qs5*	*Qs6*	*Qs7*
0.176	0.059	0.060	0.153	0.162	0.151	0.158	0.151
0.324	0.117	0.121	0.306	0.302	0.302	0.315	0.303
0.502	0.194	0.199	0.474	0.469	0.441	0.486	0.441
0.684	0.276	0.283	0.679	0.672	0.633	0.693	0.629
0.841	0.354	0.364	0.807	0.766	0.764	0.825	0.762
1.056	0.434	0.445	0.976	0.927	0.925	1.010	0.932
1.239	0.531	0.545	1.214	1.153	1.115	1.236	1.106
1.434	0.676	0.698	1.289	1.333	1.204	1.307	1.181
1.677	0.770	0.790	1.622	1.677	1.515	1.647	1.498
1.876	0.836	0.863	1.742	1.801	1.627	1.798	1.628
1.940	0.883	0.911	1.827	1.888	1.706	1.899	1.720
2.156	0.962	0.992	1.980	2.047	1.849	2.068	1.873
2.323	1.028	1.060	2.143	2.215	2.086	2.209	2.087
2.482	1.173	1.209	2.434	2.390	2.195	2.520	2.205
2.619	1.242	1.280	2.566	2.519	2.314	2.669	2.335
2.608	1.307	1.348	2.729	2.679	2.360	2.809	2.356
2.622	1.286	1.326	2.643	2.595	2.286	2.765	2.319
2.828	1.443	1.488	3.000	2.945	2.594	3.102	2.602
2.961	1.581	1.630	2.982	2.829	2.587	3.083	2.594
0.156	0.046	0.047	0.158	0.120	0.135	0.161	0.134
0.313	0.101	0.103	0.302	0.260	0.272	0.311	0.274
0.484	0.164	0.168	0.491	0.422	0.442	0.506	0.445
0.664	0.235	0.240	0.707	0.608	0.572	0.726	0.573
0.792	0.251	0.258	0.782	0.673	0.725	0.780	0.701
0.966	0.312	0.322	0.959	0.825	0.889	0.981	0.881
1.124	0.375	0.386	1.163	1.000	0.941	1.178	0.924
1.297	0.453	0.467	1.415	1.216	1.144	1.424	1.117
1.459	0.522	0.540	1.650	1.419	1.335	1.646	1.287
1.505	0.539	0.562	1.705	1.467	1.380	1.714	1.331
0.037	0.012	0.013	0.037	0.033	0.031	0.038	0.031
0.064	0.023	0.024	0.071	0.062	0.058	0.072	0.058
0.107	0.043	0.044	0.111	0.101	0.097	0.113	0.096
0.186	0.080	0.083	0.210	0.191	0.161	0.212	0.158
0.218	0.090	0.092	0.232	0.211	0.203	0.236	0.200
0.280	0.105	0.109	0.266	0.247	0.237	0.274	0.236
0.308	0.127	0.132	0.296	0.296	0.276	0.307	0.277
0.306	0.123	0.128	0.298	0.286	0.275	0.309	0.276

APPENDIX F

SYMBOLS

a = exponent in the cumulative distribution function

A = flow area

b = exponent in the cumulative distribution function

B = half of the channel width

c = sediment concentration at a specified point

c_0 = the maximum sediment concentration

c_a = the reference concentration at the distance z= $0.05y_0$ above the bed

$\bar{c}$ = the mean sediment concentration of the cross-section

C = time-averaged sediment concentration variable

D = water depth of the channel

D_H = the hydraulic diameter

d_s = particle size

$f(c)$ = the probability density function

$f(u)$ = probability density function

$F(u)$ = cumulative distribution function

g = the acceleration due to gravity

G = dimensionless parameter

h = defined as the depth from the water surface

h_y = proportional coefficient

h_ξ = metric coefficient

H = Shannon entropy or Tsallis entropy

$I(u)$ = velocity isovels

m = a real number

M = dimensionless parameter

n = exponent in simple power law

N = dimensionless parameter

N' = dimensionless parameter

p_i = probability of each random value

$p(x)$ = continuous probability density function of random variable x

q_s = the specific sediment discharge

Q = flow discharge

Qs = the suspended sediment discharge

R^2 = coefficient of determination

R_0 = the Rouse number

Re = Reynolds number

S = the channel slope.

S_f = friction slope

u = velocity value at a specified point

u_{max} = maximum velocity of the cross-section

$\bar{u}$ = cross-sectional mean velocity

u_* = the shear velocity

U = time-averaged velocity variable

w = a new random variable

x = distance from the channel center

y = depth from the channel bed

y_0 = the depth of the shear velocity

z' = a parameter derived by Chiu (2000)

α = the energy distribution coefficient

β = momentum distribution coefficient

ε= turbulent eddy viscosity

ε_s= diffusion coefficient for sediment transfer

ε_0 = momentum transfer coefficient at the channel bed

η = an coordinate by Chiu (1988), which are orthogonal to ξ

κ = von-Karman universal constant

λ_0 and λ_1 = the Lagrange multipliers

$\lambda_* = \lambda_0 + \frac{1}{m-1}$

ν = the kinematic viscosity

ξ = an coordinate by Chiu (1988), one-to-one relation with a value of velocity

ρ = the fluid density

ρ_s = the sediment density

τ = bed shear stress

ω = the correction factor

ω_s = settling velocity of sediment particle.

VITA

Name:	Huijuan Cui
Address:	Scoates Hall, 2117TAMU Texas A&M University College Station, TX77843-2117, USA
Email:	hj.cui@tamu.edu
Education:	B.En. Hydraulic Engineering, Tsinghua University 2009 M.S. Water Management and Hydrological Science, Texas A&M University, 2011